Mediators of Inflammation

Innate Immune and Inflammatory Responses to Respiratory Viruses

Lead Guest Editor: Shitao Li
Guest Editors: Bishi Fu and Chetan D. Meshram

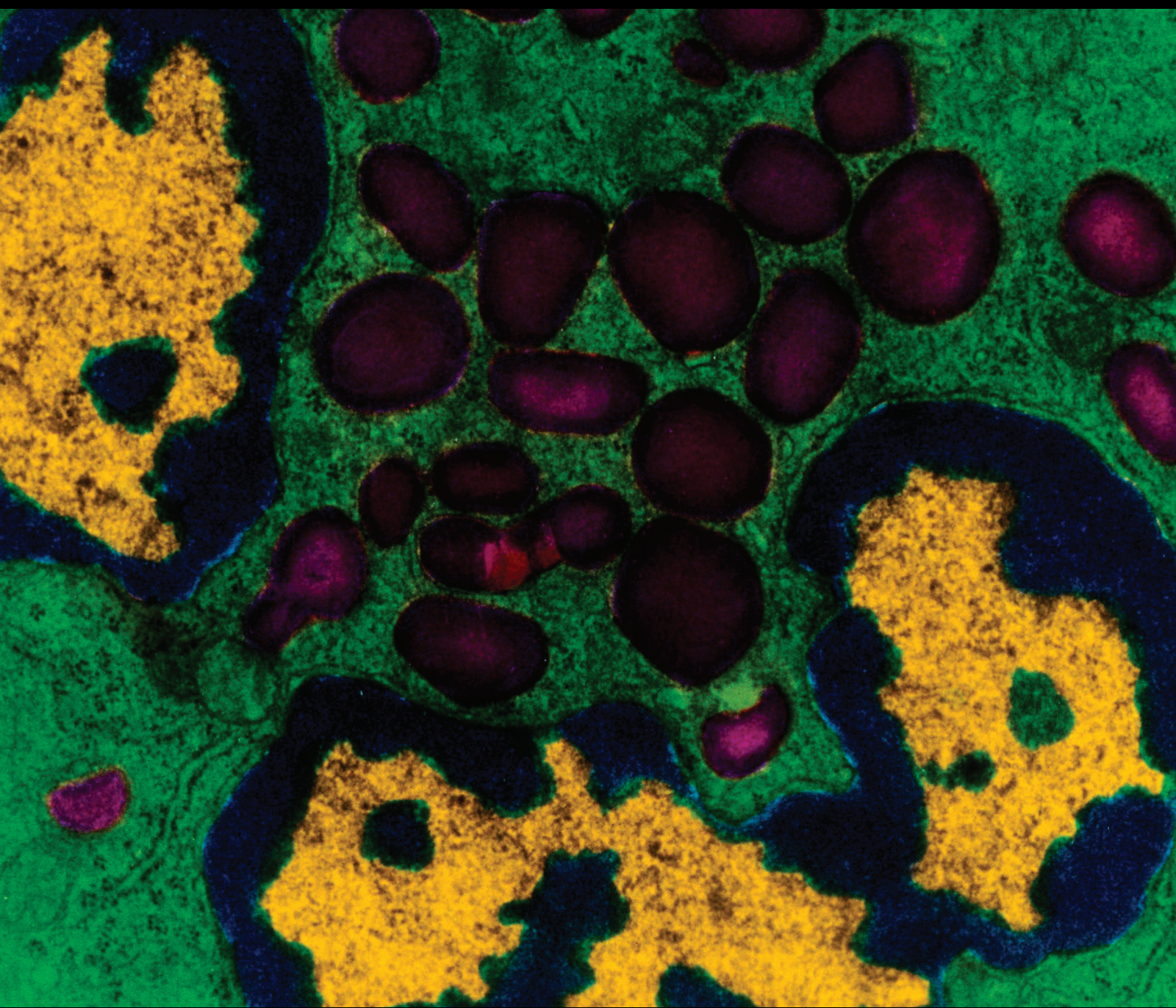

Innate Immune and Inflammatory Responses to Respiratory Viruses

Mediators of Inflammation

Innate Immune and Inflammatory Responses to Respiratory Viruses

Lead Guest Editor: Shitao Li
Guest Editors: Bishi Fu and Chetan D. Meshram

Editorial Board

Contents

Hindawi
Mediators of Inflammation
Volume 2019, Article ID 3146065, 2 pages
https://doi.org/10.1155/2019/3146065

Editorial

Innate Immune and Inflammatory Responses to Respiratory Viruses

Shitao Li[1], **Bishi Fu**[2] **and Chetan D. Meshram**[3]

[1]*Department of Physiological Sciences, Center for Veterinary Health Sciences, Oklahoma State University, Stillwater, OK, USA*
[2]*Medical Research Institute, School of Medicine, Wuhan University, Wuhan, China*
[3]*Department of Microbiology, University of Alabama at Birmingham, Birmingham, AL, USA*

Correspondence should be addressed to Shitao Li; shitao.li@okstate.edu

Received 4 April 2019; Accepted 7 April 2019; Published 14 April 2019

Respiratory viruses (RVs), including but not limited to influenza virus, respiratory syncytial virus, coronavirus, rhinovirus, parainfluenza virus, adenovirus, and human metapneumovirus, can lead to severe diseases including bronchiolitis and pneumonia or/and to exacerbations of asthma and chronic obstructive pulmonary disease. Lung airway epithelial cells and mucosal immune cells are the primary cells for RVs. Following viral infection, these cells generate a range of mediators, including type I interferon (IFN), proinflammatory cytokines, and chemokines, which not only have pivotal roles in virus control but also determine the development of inflammation and disease. Given that vaccines are not available for RVs other than influenza virus, there is a critical need for the understanding of the interactions between RV and host innate immunity and the development of effective therapies limiting the severity of inflammation caused by RV infection.

This special issue presents five original research articles on host immune responses to different RVs, including influenza A virus (IAV), adenovirus, herpesvirus, and rhinovirus. Human adenovirus causes the most community-acquired pneumonia in infants and children with significant morbidity and mortality. Viruses are known to modulate host microRNAs (miRNAs), which are critical for viral replication and host immune response. However, the profiling of miRNA in children infected with adenovirus has not been reported yet. In this issue, F. Huang et al. examined the miRNA expression in the whole blood of adenovirus-infected pneumonia children and healthy controls by RNA sequencing. Their studies showed a distinct miRNA expression profile in adenovirus-infected children highlighted with the top three unregulated miRNAs (hsa-miR-127-3p, hsa-miR-493-5p, and hsa-miR-409-3p). Analysis of the host target genes of the microRNAs revealed that most target genes are involved in the MAPK signaling pathway and innate immune response. The microRNA profiling will not only help understand the role of miRNAs in modulating the host response to adenovirus infection but also provide potential biomarkers for adenovirus-infected pneumonia.

It has been well established that retinoic acid-inducible gene I (RIG-I) is a cytosolic sensor for RNA viruses, which binds viral RNAs, such as double-stranded RNA and 5′-triphosphate RNA. Engagement of viral RNA activates RIG-I, which initiates the MAVS-TBK1-IRF3 signaling cascade and induces type I IFN expression, thereby limiting the spread of infection. W. Wu et al. presented multiple lines of evidence that deficiency of RIG-I or MAVS neither resulted in higher mortality nor reduced IAV-induced cytokine responses in mice. RIG-I knockout mice displayed comparable lung inflammation as wild-type mice after influenza infection. RNA sequencing further demonstrated that both RIG-I wild-type and knockout mice exhibited

comparable antiviral and inflammatory responses. As influenza activates multiple innate immune signaling pathways, such as TLR7 and NOD2, W. Wu et al. proposed a novel model that RIG-I serves as the primary PRR for IAV while TLR3, NOD2, MDA5, and TLR7 serve as the alternate PRRs for generating an innate response to IAV.

Acute exacerbation of idiopathic pulmonary fibrosis (AE-IPF) is a diagnosis of IPF with acute worsening of dyspnea in the preceding month and associated with high mortality. Whether pathogens can trigger AE-IPF is unknown. D. Weng et al. investigated the role of infection in AE-IPF by examining the changes in pathogen involvement during AE-IPF. They recruited 170 IPF patients (48 AE-IPF, 122 stable) and 70 controls. Their studies showed that the antiviral/bacterial IgM was higher in IPF vs. controls and in AE-IPF vs. stable IPF. Fifty-seven different viruses were detected in nasopharyngeal swabs of AE-IPF patients. AE-IPF also displayed abnormally activated inflammatory cytokines.

Recent studies show that CD4+ stem cell-like memory T cells (TSCMs) are a distinct memory T cell subset and preferentially reside in the bone marrow (BM). However, the existence and function of CD4+ TSCMs in a mouse, especially at the anatomical site of CD4+ TSCMs, were not well characterized. In this special topic issue, K. Wu et al. provided evidence that the BM acts as a hub for the relocation of most of antigen-specific CD4+ TSCMs. Furthermore, BM-resident TSCMs showed higher activity in inducing antibodies against influenza infection when compared with the spleen-resident TSCMs in mice. These findings may provide insights for future implications of immunotherapy against influenza.

Bovine herpesvirus type 1 (BoHV-1) infection causes inflammation in the respiratory tract and reproductive system in cattle of all ages and breeds. How BoHV-1 infection leads to inflammation is not well elucidated. X. Fu et al. found that BoHV-1 infection induces overproduction of reactive oxidative species (ROS), which are inflammatory mediators. Their studies further showed that interruption of the mitochondrial respiratory chain (RC) complexes by different chemicals reduced virus productive infection, suggesting that the integrity of RC complexes is critical for BoHV-1 replication. The virus infection significantly regulated the expression of various genes involved in the mitochondrial respiratory chain, antioxidant enzymes, and mitochondrial biogenesis-related signalings, such as MTCO1 SOD1/2, TFAM, and NRF1/2. These findings will advance the understanding of the mechanisms of BoHV-1 infection-induced ROS production and mitochondrial damage.

Overall, these original research articles will improve our knowledge of immune responses to RV infection, provide insights into the future design of effective antivirals, and pave the avenues for a rational basis for the development of potential therapeutic strategies.

Conflicts of Interest

The authors declare no conflict of interest.

Acknowledgments

We thank the authors for their contribution to this special research topic. We also express our gratitude to all the reviewers for their valuable comments.

Shitao Li
Bishi Fu
Chetan D. Meshram

Hindawi
Mediators of Inflammation
Volume 2019, Article ID 7072917, 10 pages
https://doi.org/10.1155/2019/7072917

Research Article

The Differential Expression of Mitochondrial Function-Associated Proteins and Antioxidant Enzymes during Bovine Herpesvirus 1 Infection: A Potential Mechanism for Virus Infection-Induced Oxidative Mitochondrial Dysfunction

Xiaotian Fu,[1,2,3] Xinyi Jiang,[2,3] Xinye Chen,[1,2,3] Liqian Zhu,[2,3] and Gaiping Zhang[1,3,4]

[1]*Key Laboratory for Animal Immunology of the Ministry of Agriculture, Henan Provincial Key Laboratory of Animal Immunology, Henan Academy of Agricultural Sciences, Zhengzhou, Henan Province 450002, China*
[2]*College of Veterinary Medicine, Yangzhou University, Yangzhou 225009, China*
[3]*Jiangsu Co-Innovation Center for Prevention and Control of Important Animal Infectious Diseases and Zoonoses, Yangzhou 225009, China*
[4]*College of Animal Science and Veterinary Medicine, Henan Agricultural University, Zhengzhou, Henan Province 450000, China*

Correspondence should be addressed to Liqian Zhu; lzhu3596@163.com and Gaiping Zhang; zhanggaip@126.com

Received 17 September 2018; Revised 20 December 2018; Accepted 1 January 2019; Published 18 March 2019

Guest Editor: Bishi Fu

Reactive oxidative species (ROS) are important inflammatory mediators. Electrons escaping from the mitochondrial electron transport chain (ETC) during oxidative phosphorylation (OXPHOS) in the mitochondrial respiratory chain (RC) complexes contribute to ROS production. The cellular antioxidant enzymes are important for maintaining ROS release at the physiological levels. It has been reported that BoHV-1 infection induces overproduction of ROS and oxidative mitochondrial dysfunction in cell cultures. In this study, we found that chemical interruption of RC complexes by TTFA (an inhibitor of RC complex II), NaN_3 (an inhibitor of RC complex IV), and oligomycin A (an inhibitor of ATP synthase) consistently decreased virus productive infection, suggesting that the integral processes of RC complexes are important for the virus replication. The virus infection significantly increased the expression of subunit SDHB (succinate dehydrogenase) and MTCO1 (cytochrome c oxidase subunit I), critical components of RC complexes II and IV, respectively. The expression of antioxidant enzymes including superoxide dismutase 1 (SOD1), SOD2, catalase (CAT), and glutathione peroxidase 4 (GPX4) was differentially affected following the virus infection. The protein TFAM (transcription factor A, mitochondrial) stimulated by either nuclear respiratory factor 1 (NRF1) or NRF2 is a key regulator of mitochondrial biogenesis. Interestingly, the virus infection at the late stage (at 16 h after infection) stimulated TFAM expression but decreased the levels of both NRF1 and NRF2, indicating that virus infection activated TFAM signaling independent of either NRF1 or NRF2. Overall, this study provided evidence that BoHV-1 infection altered the expression of molecules associated with RC complexes, antioxidant enzymes, and mitochondrial biogenesis-related signaling NRF1/NRF2/TFAM, which correlated with the previous report that virus infection induces ROS overproduction and mitochondrial dysfunction.

1. Introduction

Bovine herpesvirus type 1 (BoHV-1) is a virus of the family *Herpesviridae* and the subfamily *Alphaherpesvirinae*. The acute virus infection causes diseases in cattle of all ages and breeds, including inflammation in the respiratory tract and reproductive system [1]. The immune suppression and mucosal damages due to the virus infection may trigger a secondary bacterial or virus infection and ultimately lead to a disease referred to as bovine respiratory disease complex (BRDC), the most important disease in cattle [2, 3]. Generally, the peak incidence of BRDC occurs in young calves of

less than 6 months old, a potential reason to cause death [4]. Both BoHV-1 infection and BRDC cause great economic loss to the cattle industry worldwide [3].

Mitochondria are important cellular organelles involved in multiple functions such as energy metabolism, programmed cell death, and innate immunity. As a "powerhouse of the cell," mitochondria play a central role in orchestrating ATP production [5]. Generally, cellular energy was provided by three metabolic pathways, that is, β-oxidation, tricarboxylic cycle, and oxidative phosphorylation (OXPHOS). The OXPHOS metabolic pathway, consisting of the multiprotein respiratory chain (RC) complexes I to IV and the ATP synthase (ATPase), produces about 90% of the cellular ATP [6, 7]. During OXPHOS, electrons are passing through the mitochondrial electron transport chain (ETC) in the RC complexes, and a proton gradient is established across the inner mitochondrial membrane as the energy source for ATP production. Concomitantly, electrons may escape from the ETC [8], especially at complex I, II, or III, and react with a molecular oxygen to form superoxide radical ($O2^{-\cdot}$), which can be converted to various components of ROS [9–11]. Therefore, electrons escaping from ETC are the main source for ROS generation. Under physiological conditions, ROS are produced at low levels and act as second messengers to regulate diverse biological processes [12], whereas excessive ROS are toxic and can damage cellular components such as lipids, proteins, nucleic acids, and carbohydrates [13, 14], while there are numerous intracellular antioxidant enzymes, such as superoxide dismutase 1 (SOD1), SOD2, glutathione peroxidase 4 (GPX4), and catalase (CAT), responsible for maintaining the redox homeostasis by disturbing ROS generation with diverse mechanisms [15].

Accumulated researches have indicated that mitochondria act as a platform for antiviral innate immune response in vertebrates, mainly depending on the activation of retinoic acid-inducible gene I- (RIG-I-) like receptor signal and the participation of the mitochondrial outer membrane adaptor protein MAVS (mitochondrial antiviral signaling protein) to protect from virus invasion [16, 17]. Therefore, in favor of viral infection or pathogenesis, mitochondria are generally damaged by the invading viruses [18]. To aid in this endeavor, viruses have developed diverse approaches to affect mitochondrial function. For example, human immunodeficiency virus-1 Tat protein reduces the mitochondria size and impairs mitochondrial fission by increasing the expression levels of fission and fusion proteins dynamin-related protein 1 (Drp1) in neurons [19], vaccinia virus inhibits OXPHOS and ETC to increase ROS production during the infection of macrophages [20], and influenza A virus can translocate viral protein PB1-F2 into the mitochondria via Tom40 channels and thereby impairs the innate immune response mediated by mitochondria [21]. For the virus HSV-1, genetically closed to BoHV-1, the viral protein US3 has been found to suppress the mitochondrial respiration by blocking ETC function [22]. BoHV-1 infection impairs mitochondria membrane potential, increases ROS levels, and reduces ATP production [23], while the mechanisms underlying these detrimental effects on the cell are not clear.

In this study, we focus on identifying the expression profiles of critical molecules in the RC complexes and antioxidant enzymes, as well as the mitochondria biogenesis-related signaling NRF1 (nuclear respiratory factor 1)/2/TFAM (mitochondrial transcription factor A signaling). Our data suggested that BoHV-1 infection increased the expression of SDHB and MTCO1, components in mitochondrial RC complexes, which is supported by the increased expression of TFAM signaling, because TFAM is a critical transcriptional regulator of mitochondrial biogenesis. In addition, we found that virus infection broadly affected the expression of the antioxidant enzymes such as SOD1, CAT, GPX4, and SOD2 at both mRNA and protein levels. The aberrant expression of certain components in the RC complexes and antioxidant enzymes as well as the NRF1/2/TFAM signaling correlated well with a previous report that virus infection stimulates excessive ROS production and mitochondrial dysfunction. These findings add our knowledge to understand the mechanisms regarding ROS production and mitochondrial damage due to the virus infection.

2. Materials and Methods

2.1. Cells and Virus. MDBK cells were maintained in DMEM (Gibco BRL) supplemented with 10% horse serum (HyClone Laboratories, Logan, UT, USA). BoHV-1 (Colorado1 stain) was propagated in MDBK cells. Aliquots of virus stocks were stored at −70°C until use. The virus was titrated in MDBK cells with results expressed as $TCID_{50}$/mL calculated using the Reed-Muench formula.

2.2. Antibodies and Chemicals. The following chemical inhibitors and antibodies were used in this study: 2-thenoyltrifluoroacetone (TTFA) (Sigma, # T27006), oligomycin A (Sigma, # O4876), nicotinamide adenine dinucleotide phosphate (NADPH) oxidase (NOX) inhibitor diphenylene iodonium (DPI) (Sigma, # D2926), SOD1 polyclonal antibody (ABclonal, # A0274, 1 : 1000), SOD2 polyclonal antibody (ABclonal, # A1340, 1 : 1000), CAT polyclonal antibody (ABclonal, # A11780, 1 : 1000), GPX4 polyclonal antibody (ABclonal, # A11309, 1 : 1000), OXPHOS antibody cocktail (Abcam, # ab110413, 1 : 2000), TFAM polyclonal antibody (Thermo Fisher Scientific, # PA5-68789, 1 : 1000), NRF1 antibody (GeneTex, # PA5-40912, 1 : 1000), NRF2 antibody (Abcam, # ab137550, 1 : 500), tubulin antibody (Abcam, # ab18251, 1 : 3000), β-actin rabbit mAb (Cell Signaling Technology, # 4970, 1 : 2000), HRP labeled anti-mouse IgG (Cell Signaling Technology, # 7076, 1 : 3000), and HRP labeled anti-rabbit IgG (Cell Signaling Technology, # 7074, 1 : 3000).

2.3. Western Blot Analysis. Monolayers of MDBK cells in 60 mm dishes were infected with BoHV-1 (MOI = 1) for 2, 4, 8, and 16 hours. Cell lysates were prepared using lysis buffer (1% Triton X-100, 50 mM sodium chloride, 1 mM EDTA, 1 mM EGTA, 20 mM sodium fluoride, 20 mM sodium pyrophosphate, 1 mM phenylmethylsulfonyl fluoride, 0.5 g/mL leupeptin, 1 mM benzamidine, and 1 mM sodium orthovanadate in 20 mM Tris–HCl, pH 8.0). The

respective samples were boiled in Laemmli sample buffer for 5 min, and all samples were separated on 8% or 10% SDS-PAGE. The antibodies used for Western blots were described as above. To analyze the effects that ROS had on the expression of detected proteins, MDBK cells in 60 mm dishes were pretreated with solvent DMSO or DPI (5 μM) for 1 h, then infected with the virus (MOI = 1) for 16 h along with DPI (5 μM) or DMSO treatment. Cell lysates prepared using the lysis buffer as described above were subjected to Western blot analysis.

2.4. Relative Quantification of mRNA by qRT-PCR. The total RNA was extracted from infected cells or uninfected cells using TRIzol LS Reagent (Ambion, cat: 10296010) following the manufacturer instructions. Freshly prepared total RNA (1 μg) was used as a template for synthesis of first-strand cDNA with commercial random hexamer primers using the ThermoScript™ RT-PCR system kit (Invitrogen, catalogue # 11146-024) following the manufacturer instructions. The cDNA products were used as templates for real-time quantitative PCR to measure mRNA levels of indicated genes with gene-specific primers. For these studies, we analyzed SOD1 (forward primer: 5′- GTTGGAGACCTGGGCAATGT -3′ and reverse primer: 5′- TCCACCCTCGC CCAAGTCAT-3′), SOD2 (forward primer: 5′- CCCATGAAGCCTTTCTAA TCCTG-3′ and reverse primer: 5′- TTCAGAGGCGCTAC TATTTCCTTC-3′), CAT (forward primer: 5′- CGCGCA GAAACCTGATGTC-3′ and reverse primer: 5′- GGAATT CTCTCCCGGTCAAAG-3′), GPX4 (forward primer: 5′- TC ACCAAG TTCCTCATTGACAAGA-3′ and reverse primer: 5′- TTCTCGGAACACAG GCAACA-3′) [24], and GAPDH (forward primer: 5′- CCATGGAGAAGGCTGGGG-3′ and reverse primer: 5′- AAGTTGTCATGGATGACC-3′) [25].

Analysis of glyceraldehyde-3-phosphate dehydrogenase (GAPDH) mRNA was used as an internal control. Real-time PCR was carried out using the ABI 7500 fast real-time system (Applied Biosystems, CA). Expression levels of the tested genes were normalized to GAPDH. The relative mRNA level of each gene was calculated using the method ($2^{-\Delta\Delta CT}$) by comparison to the control cells.

2.5. Cellular ROS Assay. MDBK cells in 24-well plates were pretreated with solvent DMSO or DPI (5 μM) for 1 h, then infected with BoHV-1 (MOI = 1) or mock infected with cell lysates from uninfected MDBK cells in the presence of inhibitor DPI or DMSO control for 1 h. After washing with PBS for three times, fresh medium containing DPI was added. At 16 hours after infection, the cells were washed with PBS and exposed to ROS fluorescence indicator H2DCFDA (50 μM) for 30 min at 37°C. The reaction mixture was then replaced with PBS, and images were acquired under a fluorescence microscope; the fluorescence intensity of cellular ROS was quantified with software Image-pro Plus 6.

3. Results

3.1. Respiratory Complexes Are Important for BoHV-1 Productive Infection. We initially investigated whether chemical interruption of certain OXPHOS complexes would affect the virus productive infection by inhibitors TTFA (inhibitor for complex II), NaN_3 (inhibitor for complex IV), and oligomycin A (inhibitor for ATP synthase, ATPase). The treatment of cells with 100 and 200 μM of TTFA resulted in approximately a 1.0 and 1.7-log reduction of the virus yield compared to that in the mock-treated control, respectively (Figure 1(a)). When the virus-infected cells were treated with 1 mM of Na_3N, the virus titer was reduced ~1.4-log compared to the mock-treated control (Figure 1(b)). Oligomycin A blocks OXPHOS by inhibition of membrane-bound mitochondrial ATPase. When the virus-infected cells were treated with oligomycin A (200 μM), the virus titer was reduced ~1.2-log relative to the mock-treated control (Figure 1(c)). Of note, all the chemicals were used at a proper concentration to ensure that they did not affect cell viability (Figure 1(d)). These results suggested that integral processes in RC complexes are essential for virus productive infection.

3.2. BoHV-1 Infection Altered the Expression of Certain Components in Mitochondrial RC Complexes. Next, we detect whether virus infection altered the protein expression of certain components in the mitochondrial RC complexes. Therefore, we measured the protein markers of five OXPHOS complexes by using a specific antibody cocktail against the following proteins: NDUFB8 (NADH dehydrogenase 1 beta subcomplex subunit 8) for complex I, SDHB (succinate dehydrogenase) for complex II, cytochrome c oxidase subunit I (MTCO1) for complex IV, UQCRC2 (ubiquinol-cytochrome c reductase complex 2) for complex III, and ATP5A (ATP synthase α subunit) for complex V. Among the detected proteins, the expressions of both SDHB and MTCO1 were significantly increased by virus infection (Figure 2(a)). Relative to the mock-infected control, the protein levels of SDHB were consistently increased ~2-fold at 2, 4, 8, and 16 hours after infection; MTCO1 was increased approximately 2-, 12-, 15-, and 14-fold at 2, 4, 8, and 16 hours after infection, respectively (Figure 2(b)), while the virus infection had no effects on the expression of NDUFB8, UQCRC2, and ATP5A (Figures 2(a) and 2(b)). These results indicated that virus infection differentially altered the expression of certain proteins in the mitochondrial RC complexes.

3.3. BoHV-1 Infection Differentially Affected the Expression of Certain Antioxidant Enzymes including SOD1, SOD2, CAT, and GPX4. Mitochondrial dysfunction is often concurrently associated with premature leaking of electrons from the ETC [26], which may ultimately lead to an increased ROS production. However, there are intracellular defense systems including the antioxidant enzymes to finely counteract ROS production [27]. Here, we initially characterized the mRNA expression of certain antioxidant enzymes including SOD1, SOD2, CAT, and GPX4 during the course of BoHV-1 infection using qRT-PCR. When MDBK cells were infected for 8 and 16 hours, the mRNA levels of SOD1, CAT, and GPX4 were unanimously decreased while SOD2 mRNA levels were significantly increased (Figures 3(a), 3(c), 3(e), and 3(g)). At 8 and 16 h after infection, relative to the uninfected control,

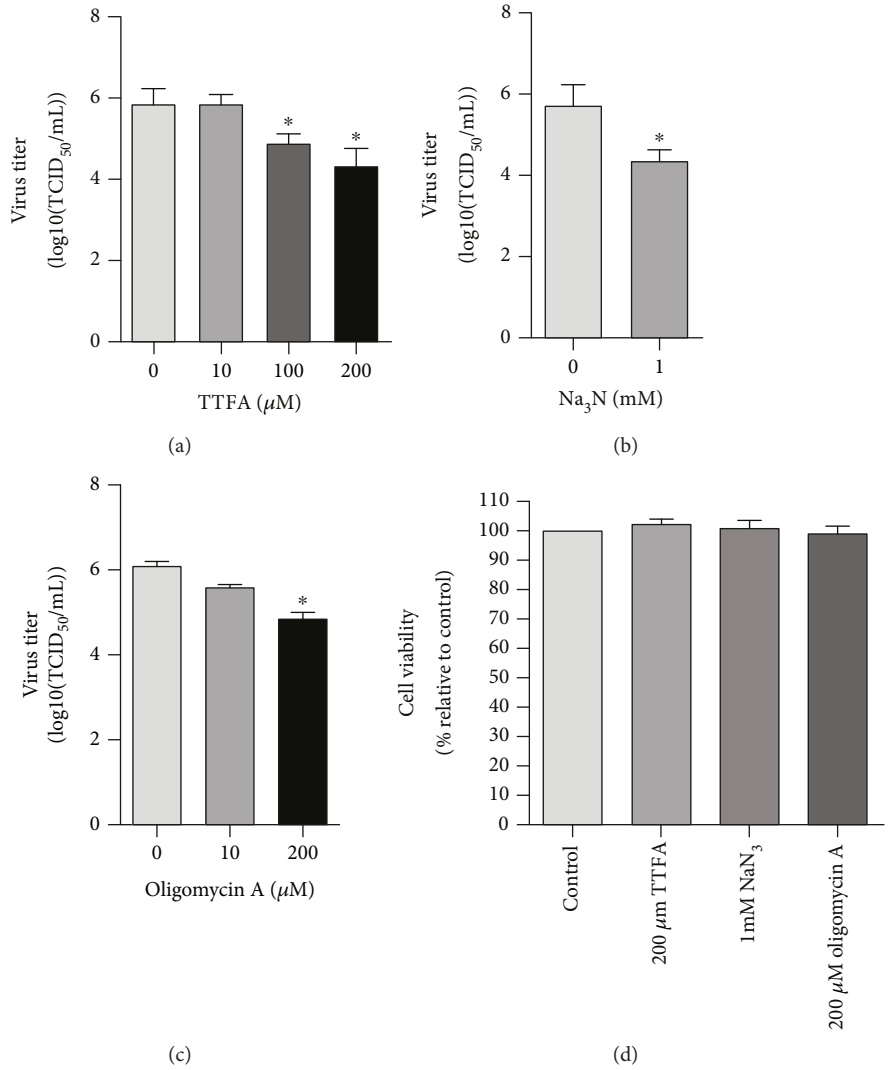

Figure 1: The effects of respiratory complex inhibitors on virus productive infection in MDBK cells. MDBK cells were infected with BoHV-1 (MOI = 1) for 24 h. Throughout infection, the cells were treated with TTFA (a), an inhibitor for mitochondrial RC complex II, NaN_3 (b), an inhibitor for mitochondrial RC complex IV, and oligomycin A (c), an inhibitor for ATP synthase, at indicated concentrations, respectively. After infection, the cell cultures were subjected to frozen-thawing twice, and the viral titer was determined in MDBK cells with the results expressed as $TCID_{50}$/mL. (d) The cytotoxicity of TTFA (200 μM), NaN_3 (1 mM), and oligomycin A (200 μM) in MDBK cells for 24 h was analyzed by the Trypan-blue exclusion test as described elsewhere [47]. Data represent means of three independent experiments. Significance was assessed with the Student t-test. $^*p < 0.05$.

SOD1 mRNA levels were decreased to approximately 39.2% ($p < 0.05$) and 52.3% ($p < 0.05$), respectively (Figure 3(a)); CAT mRNA levels were decreased to ~15.3% ($p < 0.05$) and 19.7% ($p < 0.05$), respectively (Figure 3(e)); GPX4 mRNA levels were decreased to ~34.3% ($p < 0.05$) and 33.4% ($p < 0.05$), respectively (Figure 3(g)); and SOD2 mRNA levels were increased to approximately 199.5% ($p < 0.05$) and 245% ($p < 0.05$), respectively (Figure 3(c)).

However, virus infection altered the steady state protein levels of these antioxidant enzymes with diverse manners which were different from that for the mRNA levels. Relative to the control, the SOD1 protein level was decreased to 66.18% ($p < 0.05$), at 8 h after infection, but at 16 h after infection, it was reversed to a level close to the control (Figure 3(b)); SOD2 protein level was increased to 186.9% ($p < 0.05$) at 8 h after infection, then decreased to 65.5% ($p < 0.05$) at 16 h after infection (Figure 3(d)); CAT protein level was decreased to 66.8% ($p < 0.05$) at 16 h after infection (Figure 3(f)); and GPX4 protein levels were consistently increased to 144.1% ($p < 0.05$) and 183.5% ($p < 0.05$) at 8 and 16 h after infection, respectively (Figure 3(h)).

Taken together, the alteration of the detected antioxidant enzymes in both mRNA and protein suggested that virus infection differentially regulated the expression of these antioxidant enzymes with complicated mechanisms. The decreased protein levels of both SOD2 and CAT due to virus infection indicated a decreased capability to counteract ROS production, which is in agreement with the finding that the virus infection stimulated ROS overproduction (Figure 4(a)).

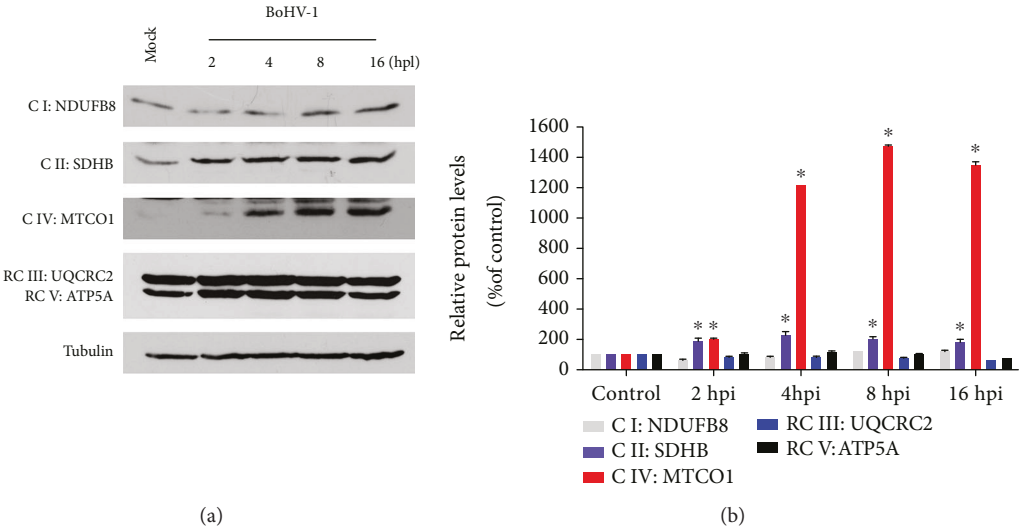

Figure 2: BoHV-1 infection affected the expression of certain components in mitochondrial RC complexes. (a) MDBK cells in 60 mm dishes were mock infected or infected with BoHV-1 at an MOI of 1 for 2, 4, 8, and 16 hours. The cell lysates were then prepared for Western blots to detect NDUFB8 for complex I, SDHB for complex II, MTCO1 for complex IV, UQCRC2 for complex III, and ATP5A for complex V, using OXPHOS antibody cocktail (Abcam; ab110413, 1 : 2000). Data shown are representative of three independent experiments. (b) The relative band intensity was analyzed with software ImageJ, and each analysis was compared with that of uninfected control which was arbitrarily set as 100%. Data are means of three independent experiments. Significance was assessed with the Student t-test ($^*p < 0.05$).

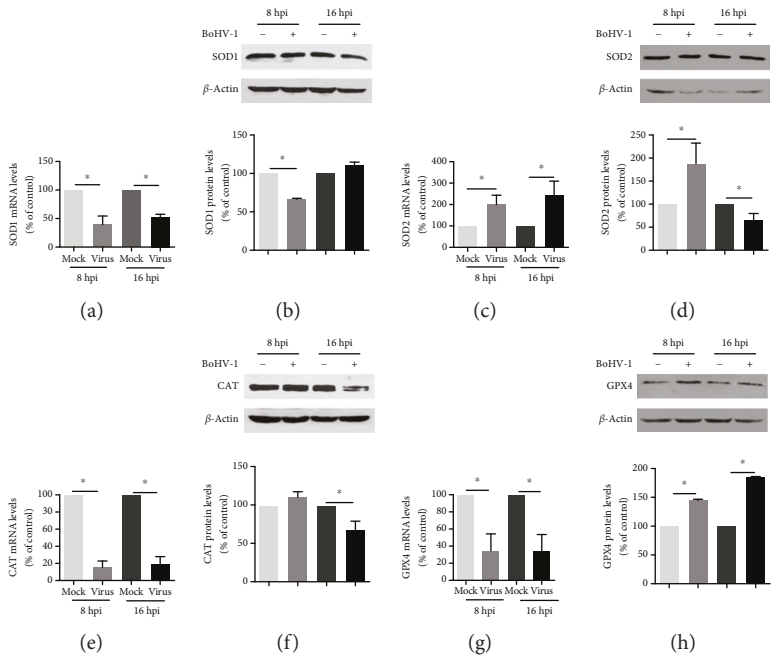

Figure 3: The effects of BoHV-1 infection on the gene expression of antioxidant enzymes. (a, c, e, and g) The total RNA was prepared at 8 and 16 h after infection in MDBK cells, and the mRNA levels of SOD1 (a), SOD2 (c), CAT (e), and GPX4 (g) were measured by qRT-PCR. Each analysis was compared with that of uninfected control which was arbitrarily set as 100%. Data represent three independent experiments. Significance was assessed with the Student t-test ($^*p < 0.05$). (b, d, f, and h) MDBK cells in 60 mm dishes were mock infected or infected with BoHV-1 at an MOI of 1 for 8 and 16 h. The cell lysates were then prepared for Western blots to detect the expression of SOD1 (b), SOD2 (d), CAT (f), and GPX4 (h) using SOD1 polyclonal antibody (ABclonal, #A0274, 1 : 1000), SOD2 polyclonal antibody (ABclonal, #A1340, 1 : 1000), CAT polyclonal antibody (ABclonal, #A11780, 1 : 1000), and GPX4 polyclonal antibody (ABclonal, #A11309, 1 : 1000). The band intensity was analyzed with software ImageJ. Each analysis was compared with that of uninfected control which was arbitrarily set as 100%. Data represent two independent experiments. Significance was assessed with the Student t-test ($^*p < 0.05$), ns: not significant.

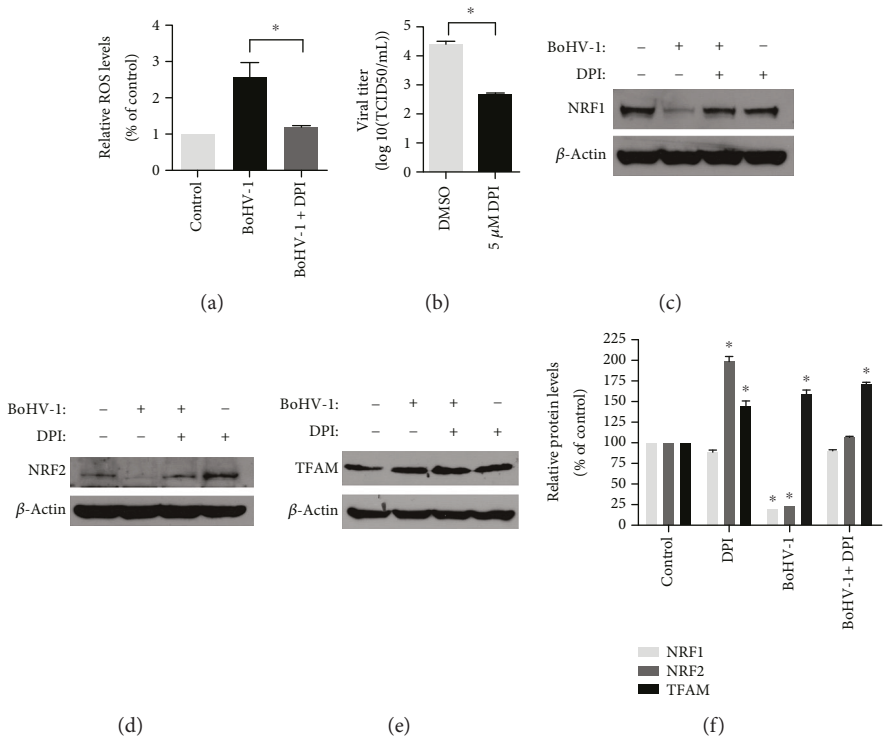

Figure 4: The effects of DPI treatment on the expression of NRF1, NRF2, and TFAM following BoHV-1 infection. (a) MDBK cells in 24-well plates pretreated with DPI (5 μM) or DMSO control for 1 h were infected with BoHV-1 (MOI = 1) along with corresponding chemical treatment. After infection for 16 h, cellular ROS levels were determined using H2DCFDA (5 μM, 30 min) (Sigma-Aldrich, St. Louis, MO, USA) and quantitatively analyzed using software Image-pro Plus 6. Data shown are means of three independent experiments. *Significant differences ($p < 0.05$), as determined by the Student t-test. (b) MDBK cells in 24-well plates were treated with DPI or MDSO control and infected by BoHV-1 (MOI = 1) at the same condition as described in (a). Finally, the cell cultures were subjected to frozen-thawing twice, and viral production was determined using MDBK cells with results expressed as TCID50/mL. (c–e) MDBK cells in 60 mm dishes pretreated with DPI (5 μM) or DMSO control for 1 h were infected with BoHV-1 (MOI = 1) in the presence of DPI or DMSO control for 16 h; the cell lysates were prepared for Western blots to detect the expression of NRF1 (c), NRF2 (d), and TFAM (e). Data shown are representative of three independent experiments. (f) The relative band intensity was analyzed with software ImageJ, and each analysis was compared with that of the uninfected control which was arbitrarily set as 100%. Data are means of three independent experiments. Significance was assessed with the Student t-test (*$p < 0.05$).

3.4. BoHV-1 Infection Stimulated TFAM Signaling Independent of Its Canonical Activator NRF1 and NRF2. TFAM signaling stimulated by transcription factor NRF1 or NRF2 is a key transcription factor regulating the expression of nuclear genes required for keeping mitochondrial respiratory function and mitochondrial DNA replication and transcription [28]. We then investigated the effects of virus infection on the expression of these transcription factors. Relative to the control, NRF1 and NRF2 were increased to approximately 114.4% ($p > 0.05$) and 136.3% ($p < 0.05$) at 2 h postinfection, then gradually decreased and peaked at 16 h after infection, which were reduced to ~19.9% ($p < 0.05$) and 19.3% ($p < 0.05$), respectively (Figures 5(a), 5(b), and 5(d)). The virus infection consistently increased the expression of TFAM from 2 h after infection and peaked at 16 h after infection, with a level increased to approximately 164.4% ($p < 0.05$) relative to the control (Figures 5(c) and 5(d)). These results indicated that the virus infection stimulated mitochondrial biogenesis-related signaling TFAM independent on its canonical upstream activators of either NRF1 or NRF2.

3.5. NADPH Oxidases Inhibitor DPI Affected the Expression of Both NRF1 and NRF2 But Not TFAM. NADPH oxidases (NOXs) are responsible for transporting electrons across biological membranes to generate ROS [29, 30]. BoHV-1 infection-induced excessive production of ROS is significantly decreased by NOX inhibitor DPI [9, 23, 31]. We initially detected whether ROS generation was stimulated in the context of the virus infection at an MOI of 1 for 16 hours. As expected, the intracellular ROS level was increased to ~2.6-fold ($p < 0.05$) relative to the control, which can be significantly inhibited by DPI (5 μM) treatment (Figure 4(a)). In addition, DPI treatment significantly inhibited virus replication, with viral titer decreased ~1.8-log relative to the control (Figure 4(b)). In view of the fact that ROS affect various transcription factors such as nuclear factor kappa-light-chain-enhancer of activated B cells (NF-κB) and activator protein-1 (AP-1) [32], we identify whether DPI treatment affected the NRF1/2/TFAM signaling at 16 h after infection. Though DPI (5 μM) treatment significantly increased the expression of NRF2 but not NRF1 in the mock-infected cells, it reversed the depletion of both NRF1

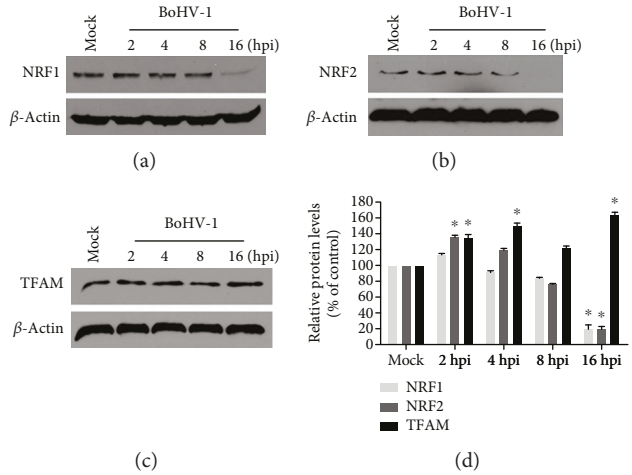

Figure 5: The effects of virus infection on the expression of NRF1, NRF2, and TFAM. MDBK cells in 60 mm dishes were mock infected or infected with BoHV-1 at an MOI of 1 for 2, 4, 8, and 16 hours. The cell lysates were then prepared for Western blots to detect the expression of NRF1 (a), NRF2 (b), and TFAM (c) using NRF1 antibody (GeneTex; # PA5-40912, 1 : 1000), NRF2 antibody (Abcam; # ab137550, 1 : 500), and TFAM polyclonal antibody (Thermo Fisher Scientific; # PA5-68789, 1 : 1000). (d) The relative band intensity was analyzed with software ImageJ, and each analysis was compared with that of uninfected control which was arbitrarily set as 100%. Data are means of three independent experiments. Significance was assessed with the Student t-test ($^*p < 0.05$).

and NRF2 in the virus-infected cells, which were rescued to a level almost the same as that in the uninfected control (Figures 4(c), 4(d), and 4(f)). It seems that DPI treatment affected the expression of NRF1 and NRF2 with different mechanisms. Mechanistically, ROS may negatively control the expression of NRF2 but not NRF1. The increased protein levels of TFAM in response to DPI (5 μM) treatment in mock-infected cells suggest that ROS may inhibit TFAM expression (Figures 4(e) and 4(f)), while DPI (5 μM) treatment did not affect the increased expression of TFAM in virus-infected cells (Figures 4(e) and 4(f)), suggesting that ROS were not involved in virus infection-induced TFAM expression.

4. Discussion

During coevolution with their hosts, viruses have developed sophisticated mechanisms to hijack some cellular functions for efficient infection. ATP mainly produced by mitochondria is essential not only for maintaining normal cell function but also for the viruses to complete their life cycles. Given that highly released ATP by virus-infected cells is regarded as a "danger signal" and extracellular ATP inhibits the replication of multiple viruses including HSV-1 [33], it does make sense why both BoHV-1 and HSV-1 infections decline ATP production via interruption of mitochondrial dysfunction at the late stage of infection [23, 34]. HSV-1 infection induces mitochondrial dysfunction through diverse mechanisms, e.g., in HSV-infected Vero cells, the mitochondria migrates to a perinuclear region in the cytoplasm and forms a ring-like structure, which is closely associated with viral tegument protein UL41 and UL46 [34]; HSV-1 viral protein US3 inhibits the mitochondrial RC by targeting a site between complexes II and III [22]; and HSV-1 viral protein UL7 associates with adenine nucleotide translocator 2 (ANT2) located on the inner mitochondrial membrane which is essential for exchange of cytosolic ADP for mitochondrial ATP [35, 36]. BoHV-1 infection reduced mitochondrial membrane potential (MMP) and intracellular ATP levels mediated by overproduced ROS [23]. In this study, for the first time, we provided evidence that the mitochondrial RC complexes are important for BoHV-1 infection because the widely used inhibitor TTFA for complex II, NaN_3 for complex IV, and oligomycin A for ATPase could significantly inhibit virus productive infection (Figure 1). In addition, we found that BoHV-1 infection significantly increased the protein expression levels of subunits SDHB and MTCO1 which are important marker proteins for mitochondrial RC complexes II and IV, respectively (Figure 2). The aberrant expression of components in the mitochondrial RC complexes may partially interrupt the function of mitochondria, which supports the report that BoHV-1 infection reduced ATP production [23]. This finding provided an evidence that BoHV-1 infection disrupted mitochondrial function by affecting the expression of certain molecules in mitochondrial RC complexes.

During OXPHOS, electrons are transferred along the ETC to produce ATP. Under stress condition, a larger number of electrons will exit the ETC and generate superoxide such as $O2^{-\cdot}$, which can be converted into hydrogen peroxide (H_2O_2) in the mitochondrial matrix by SOD2 or in the mitochondrial intermembrane space by SOD1. H_2O_2 is further detoxified by antioxidant enzymes, such as by GPX4 inside the mitochondria or by the peroxisomal enzyme CAT in the cytosol [11, 26]. So, the disruption of ETC or blocking the expression of antioxidant enzymes would tend to promote ROS production. Here, we found that the virus infection significantly decreased the protein levels of both SOD2 and CAT at the late stage of infection (16 h after infection) (Figures 3(d) and 3(f)), which may compromise their capacity of converting $O_2^{-\cdot}$ into H_2O_2 in the mitochondrial matrix as well as detoxifying H_2O_2 in the cytosol. These results

correlated well with our finding that virus infection increases ROS production (Figure 4(a)).

It is well known that GPX4 protects the cells against oxidative stress by catalyzing the reduction of hydrogen peroxide, organic hydroperoxides, and lipid peroxides to water or corresponding alcohols at the expense of glutathione (GSH) [37]. GSH constitutes a major cellular antioxidant system and provides reducing equivalents to eliminate oxidative species [38]. BoHV-1 infection leads to a significant depletion of GSH in cell culture [39]. So, it would be disadvantageous to keep GPX4 function as normal, though virus infection apparently increased GPX4 expression (Figure 3(h)), which was consistent with the fact that virus infection induces the formation of ROS (Figure 4(a)). Ferroptosis is a mode of nonapoptotic cell death involving the production of iron-dependent ROS [40]. GPX4 has been identified as a central regulator of ferroptosis, and the inactivation of GPX4 leads to an accumulation of lipid peroxides, which consequently results in ferroptotic cell death [38, 41]. We reasoned that the increased GPX4 expression due to BoHV-1 infection would be beneficial for preventing the ferroptotic cell death to facilitate viral productive infection, which needs further study in the future.

Homeostasis of mitochondrial biogenesis is required to maintain the normal function of mitochondria, which is mainly regulated by TFAM signaling. The transcription coactivator peroxisome proliferator-activated receptor gamma coactivator 1 alpha (PGC-1α) is considered as the master regulator of the mitochondrial biogenesis process via interacting with two key nuclear transcription factors NRF1 and NRF2 [28, 42]. Once activated, PGC-1α activates NRF1 and NRF2 and subsequently downstream activator TFAM which binds to promoter regions of nuclear genes encoding certain subunits of the mitochondrial RC complexes, thereby regulating the expression of the target genes [43]. In this study, we found that BoHV-1 infection at the late stage inhibited the expression of both NRF1 and NRF2 (Figures 5(a)–5(c)). While the expression levels of TFAM, an executor of the canonical PGC-1α pathway, were consistently increased from 2 to 16 h after infection (Figures 5(c) and 5(d)), suggesting that virus infection promotes TFAM expression with an unknown mechanism that is independent on either NRF1 or NRF2. However, the increased expression of TFAM corroborated well with our findings that virus infection enhanced the expression of SDHB and MTCO1 (Figure 1), components in mitochondrial RC complexes.

In contrast to BoHV-1, HSV-1 infection induces TFAM depletion and consequently triggers mtDNA stress, which further stimulates the antiviral signaling and type I interferon responses [44]. So the depletion of TFAM in response to virus infection is potentially associated with priming the antiviral innate immune response. Mechanistically, the accumulation of TFAM due to BoHV-1 infection would possibly depress the antiviral innate immune response, which is an interesting issue that needs extensive study in the future.

It has been reported that the oxidants such as tertiary butyl hydroperoxide (t-BOOH), an ROS mimic, increase cellular NRF1 and TFAM gene expression in rat liver cells and hepatoma cells [45, 46]. We therefore investigated whether ROS are involved in the regulation of NRF1/2 and TFAM expressions using the NOX inhibitor DPI, which has been confirmed to block ROS production ([31] and Figure 4(a)). The enhanced expression of NRF2 but not NRF1 by DPI treatment in the mock-infected cells (Figures 4(c), 4(d), and 4(f)) indicated that ROS may partially regulate the expression of NRF2 but not NRF1. Interestingly, DPI treatment could reverse the depletion of both NRF1 and NRF2 due to virus infection (Figures 4(c), 4(d), and 4(f)), but it had no effect on the expression of TFAM (Figures 4(e) and 4(f)), which further confirmed that the virus infection stimulated TFAM signaling independent on either NRF1 or NRF2. Furthermore, DPI treatment demonstrated minor effects on the expression of TFAM in the context of virus infection, though DPI treatment led to an increased level of TFAM protein in mock-infected cells. Therefore, we assumed that certain viral components, such as viral protein and/or DNA produced during the replication cycle, rather than ROS accounted for the promoted expression of TFAM, which needs an independent investigation in the future.

In summary, our data suggest that BoHV-1 infection leads to differential expression of certain components in mitochondrial RC complexes such as SDHB and MTCO1, mitochondrial biogenesis-associated signaling of NFR1/2/TFAM pathway, and enzymes such as SOD1, SOD2, CAT, and GPX4, which correlated well with excessive ROS production and mitochondrial dysfunction. Moreover, for the first time, we found that BoHV-1 infection stimulated TFAM signaling independent of either NRF1 and NRF2 signaling or excessive ROS. These findings add our knowledge to understand the mechanisms of virus infection-induced ROS production and mitochondrial damage.

Data Availability

The data used to support the findings of this study are available from the corresponding author upon request.

Conflicts of Interest

The authors declare that they have no conflict of interest.

Acknowledgments

This research was supported by National Key Research and Development Program of China (Grant No. 2016YFD0500704), Chinese National Science Foundation (Grant No. 31772743), Key Laboratory of Animal Immunology of the Ministry of Agriculture, and Henan Provincial Key Laboratory of Animal Immunology (KLAI20170602) and partially supported by the Priority Academic Program Development of Jiangsu Higher Education Institutions (PAPD).

References

[1] P. D. Hodgson, P. Aich, A. Manuja et al., "Effect of stress on viral-bacterial synergy in bovine respiratory disease: novel mechanisms to regulate inflammation," *Comparative and Functional Genomics*, vol. 6, no. 4, pp. 244–250, 2005.

[2] J. A. Rice, L. Carrasco-Medina, D. C. Hodgins, and P. E. Shewen, "*Mannheimia haemolytica* and bovine respiratory

disease," *Animal Health Research Reviews*, vol. 8, no. 2, pp. 117–128, 2007.

[3] C. Jones and S. Chowdhury, "A review of the biology of bovine herpesvirus type 1 (BHV-1), its role as a cofactor in the bovine respiratory disease complex and development of improved vaccines," *Animal Health Research Reviews*, vol. 8, no. 2, pp. 187–205, 2007.

[4] J. R. Patel and S. A. Didlick, "Evaluation of efficacy of an inactivated vaccine against bovine respiratory syncytial virus in calves with maternal antibodies," *American Journal of Veterinary Research*, vol. 65, no. 4, pp. 417–421, 2004.

[5] J. L. Jacobs and C. B. Coyne, "Mechanisms of MAVS regulation at the mitochondrial membrane," *Journal of Molecular Biology*, vol. 425, no. 24, pp. 5009–5019, 2013.

[6] M. Saraste, "Oxidative phosphorylation at the *fin de siècle*," *Science*, vol. 283, no. 5407, pp. 1488–1493, 1999.

[7] L. Meyer, O. Leymarie, C. Chevalier et al., "Transcriptomic profiling of a chicken lung epithelial cell line (CLEC213) reveals a mitochondrial respiratory chain activity boost during influenza virus infection," *PLoS One*, vol. 12, no. 4, article e0176355, 2017.

[8] M. Penumetcha, M. Song, N. Merchant, and S. Parthasarathy, "Pretreatment with n-6 PUFA protects against subsequent high fat diet induced atherosclerosis—potential role of oxidative stress-induced antioxidant defense," *Atherosclerosis*, vol. 220, no. 1, pp. 53–58, 2012.

[9] T. C. Cardoso, A. C. G. Rosa, H. L. Ferreira et al., "Bovine herpesviruses induce different cell death forms in neuronal and glial-derived tumor cell cultures," *Journal of Neurovirology*, vol. 22, no. 6, pp. 725–735, 2016.

[10] H. Pelicano, L. Feng, Y. Zhou et al., "Inhibition of mitochondrial respiration: a novel strategy to enhance drug-induced apoptosis in human leukemia cells by a reactive oxygen species-mediated mechanism," *The Journal of Biological Chemistry*, vol. 278, no. 39, pp. 37832–37839, 2003.

[11] L. Zhao, L. Qi, C. Li, L. Li, L. Jin, and J. Yuan, "SVCV impairs mitochondria complex III resulting in accumulation of hydrogen peroxide," *Fish & Shellfish Immunology*, vol. 75, pp. 58–65, 2018.

[12] L. A. Sena and N. S. Chandel, "Physiological roles of mitochondrial reactive oxygen species," *Molecular Cell*, vol. 48, no. 2, pp. 158–167, 2012.

[13] C. Tapeinos and A. Pandit, "Physical, chemical, and biological structures based on ROS-sensitive moieties that are able to respond to oxidative microenvironments," *Advanced Materials*, vol. 28, no. 27, pp. 5553–5585, 2016.

[14] R. L. Auten and J. M. Davis, "Oxygen toxicity and reactive oxygen species: the devil is in the details," *Pediatric Research*, vol. 66, no. 2, pp. 121–127, 2009.

[15] J. M. Matés, "Effects of antioxidant enzymes in the molecular control of reactive oxygen species toxicology," *Toxicology*, vol. 153, no. 1-3, pp. 83–104, 2000.

[16] J. L. Jacobs, J. Zhu, S. N. Sarkar, and C. B. Coyne, "Regulation of mitochondrial antiviral signaling (MAVS) expression and signaling by the mitochondria-associated endoplasmic reticulum membrane (MAM) protein Gp78," *The Journal of Biological Chemistry*, vol. 289, no. 3, pp. 1604–1616, 2014.

[17] T. Koshiba, N. Bashiruddin, and S. Kawabata, "Mitochondria and antiviral innate immunity," *International Journal of Biochemistry and Molecular Biology*, vol. 2, no. 3, pp. 257–262, 2011.

[18] S. K. Anand and S. K. Tikoo, "Viruses as modulators of mitochondrial functions," *Advances in Virology*, vol. 2013, Article ID 738794, 17 pages, 2013.

[19] S. J. Rozzi, V. Avdoshina, J. A. Fields, and I. Mocchetti, "Human immunodeficiency virus Tat impairs mitochondrial fission in neurons," *Cell Death Discovery*, vol. 4, 2018.

[20] S. Baldanta, M. Fernández-Escobar, R. Acín-Perez et al., "ISG15 governs mitochondrial function in macrophages following vaccinia virus infection," *PLoS Pathogens*, vol. 13, no. 10, article e1006651, 2017.

[21] T. Yoshizumi, T. Ichinohe, O. Sasaki et al., "Influenza A virus protein PB1-F2 translocates into mitochondria via Tom40 channels and impairs innate immunity," *Nature Communications*, vol. 5, article 4713, 2014.

[22] M. Derakhshan, M. M. Willcocks, M. A. Salako, G. E. N. Kass, and M. J. Carter, "Human herpesvirus 1 protein US3 induces an inhibition of mitochondrial electron transport," *The Journal of General Virology*, vol. 87, no. 8, pp. 2155–2159, 2006.

[23] L. Zhu, C. Yuan, D. Zhang, Y. Ma, X. Ding, and G. Zhu, "BHV-1 induced oxidative stress contributes to mitochondrial dysfunction in MDBK cells," *Veterinary Research*, vol. 47, no. 1, p. 47, 2016.

[24] R. S. Ramos, M. L. Oliveira, A. P. Izaguirry et al., "The periovulatory endocrine milieu affects the uterine redox environment in beef cows," *Reproductive Biology and Endocrinology*, vol. 13, p. 39, 2015.

[25] L. Zhu, J. Thompson, F. Ma, J. Eudy, and C. Jones, "Effects of the synthetic corticosteroid dexamethasone on bovine herpesvirus 1 productive infection," *Virology*, vol. 505, pp. 71–79, 2017.

[26] A. P. West, G. S. Shadel, and S. Ghosh, "Mitochondria in innate immune responses," *Nature Reviews Immunology*, vol. 11, no. 6, pp. 389–402, 2011.

[27] E. Birben, U. M. Sahiner, C. Sackesen, S. Erzurum, and O. Kalayci, "Oxidative stress and antioxidant defense," *World Allergy Organization Journal*, vol. 5, 2012.

[28] P. A. Li, X. Hou, and S. Hao, "Mitochondrial biogenesis in neurodegeneration," *Journal of Neuroscience Research*, vol. 95, no. 10, pp. 2025–2029, 2017.

[29] A. R. Cross and A. W. Segal, "The NADPH oxidase of professional phagocytes—prototype of the NOX electron transport chain systems," *Biochimica et Biophysica Acta (BBA) - Bioenergetics*, vol. 1657, no. 1, pp. 1–22, 2004.

[30] A. Panday, M. K. Sahoo, D. Osorio, and S. Batra, "NADPH oxidases: an overview from structure to innate immunity-associated pathologies," *Cellular and Molecular Immunology*, vol. 12, no. 1, pp. 5–23, 2015.

[31] L. Zhu, X. Fu, C. Yuan, X. Jiang, and G. Zhang, "Induction of oxidative DNA damage in bovine herpesvirus 1 infected bovine kidney cells (MDBK cells) and human tumor cells (A549 cells and U2OS cells)," *Viruses*, vol. 10, no. 8, 2018.

[32] S. C. Gupta, D. Hevia, S. Patchva, B. Park, W. Koh, and B. B. Aggarwal, "Upsides and downsides of reactive oxygen species for cancer: the roles of reactive oxygen species in tumorigenesis, prevention, and therapy," *Antioxidants & Redox Signaling*, vol. 16, no. 11, pp. 1295–1322, 2012.

[33] C. Zhang, H. He, L. Wang et al., "Virus-triggered ATP release limits viral replication through facilitating IFN-β production in a P2X7-dependent manner," *The Journal of Immunology*, vol. 199, pp. 1372–1381, 2017.

[34] T. Murata, F. Goshima, T. Daikoku et al., "Mitochondrial distribution and function in herpes simplex virus-infected cells," *Journal of General Virology*, vol. 81, no. 2, pp. 401–406, 2000.

[35] I. Marzo, C. Brenner, N. Zamzami et al., "Bax and adenine nucleotide translocator cooperate in the mitochondrial control of apoptosis," *Science*, vol. 281, no. 5385, pp. 2027–2031, 1998.

[36] M. Tanaka, T. Sata, and Y. Kawaguchi, "The product of the herpes simplex virus 1 UL7 gene interacts with a mitochondrial protein, adenine nucleotide translocator 2," *Virology Journal*, vol. 5, no. 1, article 125, 2008.

[37] R. Brigelius-Flohe and M. Maiorino, "Glutathione peroxidases," *Biochimica et Biophysica Acta (BBA) – General Subjects*, vol. 1830, no. 5, pp. 3289–3303, 2013.

[38] W. S. Yang, R. SriRamaratnam, M. E. Welsch et al., "Regulation of ferroptotic cancer cell death by GPX4," *Cell*, vol. 156, no. 1-2, pp. 317–331, 2014.

[39] C. H. Yuan, X. Fu, L. Huang et al., "The synergistic antiviral effects of GSH in combination with acyclovir against BoHV-1 infection in vitro," *Acta Virologica*, vol. 60, no. 3, pp. 328–332, 2016.

[40] S. J. Dixon, K. M. Lemberg, M. R. Lamprecht et al., "Ferroptosis: an iron-dependent form of nonapoptotic cell death," *Cell*, vol. 149, no. 5, pp. 1060–1072, 2012.

[41] J. P. Friedmann Angeli, M. Schneider, B. Proneth et al., "Inactivation of the ferroptosis regulator Gpx4 triggers acute renal failure in mice," *Nature Cell Biology*, vol. 16, no. 12, pp. 1180–1191, 2014.

[42] V. S. LeBleu, J. T. O'Connell, K. N. Gonzalez Herrera et al., "PGC-1α mediates mitochondrial biogenesis and oxidative phosphorylation in cancer cells to promote metastasis," *Nature Cell Biology*, vol. 16, no. 10, pp. 992–1003, 2014.

[43] M. Uittenbogaard and A. Chiaramello, "Mitochondrial biogenesis: a therapeutic target for neurodevelopmental disorders and neurodegenerative diseases," *Current Pharmaceutical Design*, vol. 20, no. 35, pp. 5574–5593, 2014.

[44] A. P. West, W. Khoury-Hanold, M. Staron et al., "Mitochondrial DNA stress primes the antiviral innate immune response," *Nature*, vol. 520, no. 7548, pp. 553–557, 2015.

[45] H. B. Suliman, M. S. Carraway, K. E. Welty-Wolf, A. R. Whorton, and C. A. Piantadosi, "Lipopolysaccharide stimulates mitochondrial biogenesis via activation of nuclear respiratory factor-1," *The Journal of Biological Chemistry*, vol. 278, no. 42, pp. 41510–41518, 2003.

[46] C. A. Piantadosi and H. B. Suliman, "Mitochondrial transcription factor A induction by redox activation of nuclear respiratory factor 1," *The Journal of Biological Chemistry*, vol. 281, no. 1, pp. 324–333, 2006.

[47] F. Fiorito, G. Marfè, E. de Blasio et al., "2,3,7,8-Tetrachlorodibenzo-*p*-dioxin regulates bovine herpesvirus type 1 induced apoptosis by modulating Bcl-2 family members," *Apoptosis*, vol. 13, no. 10, pp. 1243–1252, 2008.

Hindawi
Mediators of Inflammation
Volume 2019, Article ID 3231696, 10 pages
https://doi.org/10.1155/2019/3231696

Research Article

$CD4^+$ TSCMs in the Bone Marrow Assist in Maturation of Antibodies against Influenza in Mice

Kang Wu,[1,2,3] Fei Wang,[1,2] Guangwu Guo,[2] Yuqing Li,[2,3] Li-Jun Qiu,[4] and Xuefeng Li[2,3]

[1]*Zhongshan School of Medicine, Sun Yat-sen University, Guangzhou 510080, China*
[2]*Shenzhen Luohu People's Hospital, The Third Affiliated Hospital of Shenzhen University, Shenzhen 518001, China*
[3]*Key Laboratory of Regenerative Biology, Guangdong Provincial Key Laboratory of Stem Cell and Regenerative Medicine, South China Institute for Stem Cell Biology and Regenerative Medicine, Guangzhou Institutes of Biomedicine and Health, Chinese Academy of Sciences, Guangzhou 510530, China*
[4]*Department of Neurology, The Central Hospital of Wuhan, Tongji Medical College, Huazhong University of Science and Technology, Wuhan 430014, China*

Correspondence should be addressed to Li-Jun Qiu; 13476164215@163.com and Xuefeng Li; xuefengli@gzhmu.edu.cn

Received 26 August 2018; Revised 10 October 2018; Accepted 31 October 2018; Published 10 January 2019

Guest Editor: Bishi Fu

The bone marrow (BM) is not only a reservoir of hematopoietic stem cells but a repository of immunological memory cells. Further characterizing BM-resident memory T cells would be helpful to reveal the complicated relationship between the BM and immunological memory. In this study, we identified $CD122^{high}$ stem cell antigen-1 (Sca-1) ^{high} B cell lymphoma 2 (Bcl-2) ^{high} $CD4^+$ stem cell-like memory T cells (TSCMs) as a distinct memory T cell subset, which preferentially reside in the BM, where they respond vigorously to blood-borne antigens. Interestingly, the natural $CD4^+$ TSCMs homing to the BM colocalized with VCAM-1^+ IL-15^+ IL-7^+ CXCL-12^+ stromal cells. Furthermore, compared to spleen-resident $CD4^+$ TSCMs, BM-resident TSCMs induced the production of high-affinity antibodies against influenza by B lymphocytes more efficiently. Taken together, these observations indicate that the BM provides an appropriate microenvironment for the survival of $CD4^+$ TSCMs, which broadens our knowledge regarding the memory maintenance of antigen-specific $CD4^+$ T lymphocytes.

1. Introduction

$CD8^+$ stem cell-like memory T cells (TSCMs) with properties of self-renewal and multipotency have been well identified in human and mouse [1–3]. Mouse $CD8^+$ TSCMs highly express stem cell antigen-1 (Sca-1) and common interleukin- (IL-) 2 and IL-15 receptor beta chain (CD122), as well as B cell lymphoma protein-2 (Bcl-2) at high levels, and human $CD8^+$ TSCMs highly expressed CD95 (also called Fas/APO-1) and CD122 [1, 2]. Human $CD4^+$ TSCMs were isolated from peripheral blood mononuclear cells of health donors [2]. In particular, human $CD4^+$ TSCMs were considered as the HIV-1 latent reservoir [4]. In addition, Th17, as a special $CD4^+$ T cell subset-producing inflammation, exhibited a certain degree of stem cell characteristics [5, 6]. However, the existence and function of $CD4^+$ TSCMs in mouse, especially at the anatomical site of $CD4^+$ TSCMs, were not well characterized.

Previous studies have demonstrated the bone marrow (BM) functions as the major reservoir and site of recruitment for hematopoietic stem cells (HSCs) as well as memory B and T cells by means of providing appropriate niches [7–10]. A common niche that supports HSCs or leukocytes in the BM is constituted by CXCL-12^+ stromal cells. In certain circumstances, the BM can also support the homeostasis of naïve T cells and pro-B cells [11, 12]. More importantly, BM-resident $CD4^+$ T cells show a distinct function from those residing in other organs. For instance, compared with $CD4^+$ T cells in the peripheral blood, BM-resident $CD4^+$ T cells elicit more efficient activity of inducing the production of high-affinity antibodies. Accordingly, the BM is now regarded as a reservoir of Treg cells to provide an immunosuppressive

microenvironment for the maintenance of HSCs [13]. Nevertheless, it has not yet been well characterized whether $CD4^+$ TSCMs, as a distinct T cell subset with stem cell property, accumulate in the BM.

Influenza infection may cause serious damage to human health and economy [14]. Antibodies secreted by B cells play an important role in anti-influenza immunity [15]. Many subsets of B cells, including pre-pro-B cells and long-lived plasma cells and memory B cells, preferentially reside in the BM [12]. In mice immunized with T cell-dependent antigen (4-hydroxy-3-nitrophenyl)acetyl-coupled KLH (NP-KLH), the BM-derived $CD4^+$ memory T cells could help the maturation of specific antibodies [16]. Of note, human long-lived plasma cells (LLPCs) in the BM were identified to response to the influenza vaccine [17]. Although it is well known that $CD4^+$ T cells could help the maturation of antibodies, the relationship between $CD4^+$ T cells and B cells in the BM was less characterized.

In this study, we provided evidence that the BM acts as a hub where most of antigen-specific $CD4^+$ TSCMs were relocated. Importantly, BM-resident TSCMs showed higher activity in inducing antibodies against influenza when compared with the spleen- (SP-) resident TSCMs in mice. These findings may offer direct implications for immunotherapy against influenza.

2. Materials and Methods

2.1. Ethics Statement. Animal experiments were carried out following the Sun Yat-sen University Laboratory Animal Center guidelines and were approved by the Institutional Animal Care and Use Committee of Sun Yat-sen University (SYSU-2016-053). Efforts were made to minimize animal suffering.

2.2. Mice. OT-II, C57BL/6J, and CD45.1 (B6.SJL-$Ptprc^aPep3^b$/BoyJ) mice were purchased from Jackson Laboratories and were bred in SPF condition.

2.3. Virus and Infection. Infectious influenza A/Puerto Rico/8/34 (PR8) (H1N1) and PR8-OVA were provided by Dr. Zhongfang Wang in Guangzhou Medical University. Viruses were grown in the allantoic cavity of embryonated hen eggs from virus stocks. Lightly anesthetized mice were infected with influenza A virus by intranasal inoculation in 50 μl PBS. The stock of PR8 employed 2×10^4 EID50 (4LD50) and 970 PFU (approximately 2LD50) for PR8-OVA.

2.4. Viral Titers. Mice injected with influenza A virus were sacrificed by cervical dislocation at various time points. The lungs were removed, teased into single-cell suspensions in a fixed volume of 5 ml and then 1 ml aliquots frozen, and finally stored at −80°C. The lysates were thawed, and the influenza titers were determined using the Madin-Darby canine kidney (MDCK) cell plaque assay as detailed previously [18, 19].

2.5. Flow Cytometry and Sorting. Single-cell suspensions were prepared from the individual mouse spleen, mesenteric lymph nodes, blood, or bone marrow. For staining, cells were preincubated in a 0.1% bovine serum albumin (BSA)/phosphate-buffered saline (PBS) solution of 10 μg/ml anti-FcgRII/III (2.4G2) (eBioscience) for 10 min at 4°C. The cells were then stained for 20 min at 4°C with anti-CD62L (MEL-14), anti-CD45.2 (104), anti-CD44 (IM7), anti-CD3 (145-2C11), anti-Sca-1 (D7), anti-CD8 (53-6.7), anti-IFN-γ (XMG1.2), anti-CD4 (RM4-5), anti-BrdU (3D4), anti-CD69 (H1.2F3), anti-CD127 (A7R34), anti-Bcl-2 (3F11), anti-CD183 (CXCR3-173), anti-VCAM-1 (429), anti-CD140b (APB5), and anti-CD31 (MEC13.3). Finally, the cells were stained with live/dead viability (Molecular Probes) to exclude dead cells. For cell sorting, a BD FACSAria II cell sorter (BD Biosciences) was used. For intracellular cytokine staining, cells were stimulated with 100 ng/ml PMA (Sigma) and 1 μg/ml ionomycin (Sigma) in the presence of 5 μg/ml brefeldin A (Sigma) for 4 h. Cells were washed twice in PBS and fixed and permeabilized with BD Cytofix/Cytoperm™ Fixation/Permeabilization Kit. Stained samples were analyzed in a BD LSR II Fortessa (BD Biosciences). Flow cytometric data were analyzed with the FlowJo (Tree Star) software.

Table 1: Primers used in this study.

CD44 forward	AAAAAGCCATGCAGCAGCTC
CD44 reverse	TTGCCTCTTGGGTGGTGTTT
Sca-1 forward	CCACATCTGACAGAACTTGCC
Sca-1 reverse	GCTGCACAGATAAAACCTAGCAG
β-Catenin forward	CGCCGCTTATAAATCGCTCC
β-Catenin reverse	TTCACAGGACACGAGCTGAC
Klf7 forward	CGTTGAAACTGGTGGCCAAG
Klf7 reverse	ATAAACTTTCCGGCACCCGT
Tcf 7 forward	GTACATGGAGAAGCCGAGGG
Tcf 7 reverse	ACTCTGGAAGTTTGTCCGGG
Lef-1 forward	AGCACGGAAAGAGAGACAGC
Lef-1 reverse	GCTGTCATTCTGGGACCTGT
GAPDH forward	GGACCTCATGGCCTACATGG
GAPDH reverse	TAGGGCCTCTCTTGCTCAGT

2.6. Quantitative Real-Time PCR (qRT-PCR). Total RNA was isolated using TRIzol reagent (Life Technologies) and then subjected to cDNA synthesis with a PrimeScript reverse transcription (RT) reagent kit (Takara). All primers were annealed at 37°C, and RT was processed at 42°C. Quantitative real-time PCR was performed with a SYBR Premix Ex Taq II kit (Takara) following the manufacturer's instructions. The primers in our experiments are listed in Table 1.

2.7. In Vivo Activation of $CD4^+$ T Cells. The 5×10^5 three subsets T cells (naïve T cells: $CD3^+$ $CD4^+$ $CD62L^+$ $CD44^-$ Sca-1^- $CD122^-$; TCMs: $CD3^+$ $CD4^+$ $CD62L^+$ $CD44^+$; TSCMs: $CD3^+$ $CD4^+$ $CD62L^+$ $CD44^-$ Sca-1^+ $CD122^+$) from the SP or BM of OT-II mice were adoptively transferred to CD45.1 mice. Recipients were immunized with 500 μg of OVA in CFA and sacrificed after 3 days for further analysis.

2.8. Frozen Section and Immunofluorescence Staining. Femur samples were fixed in 4% paraformaldehyde (Sigma) for 4 h and equilibrated in 30% sucrose (Sigma)/PBS. After two rinses with cold PBS, samples were decalcified with 0.25 M EDTA (Acros) for 2 days and then embedded in O.C.T. (Sakura). For staining, monoclonal antibodies against VCAM-1 (BD Pharmingen) and CXCL-12 (BD Pharmingen), polyclonal antibodies against IL-7 (Abcam) and IL-15 (Abcam), and cell labeling reagents (Molecular Probes), including 5-(and-6)-carboxyfluorescein diacetate, succinimidyl ester (5(6)-CFDA, SE; CFSE), CellTracker™ Red CMTPX Dye, and DAPI (4′,6-diamidino-2-phenylindole), were used. For secondary antibodies, Alexa Fluor 488 goat anti-rabbit and Alexa Fluor 488 goat anti-rat were purchased from Abcam. Cryostat sections were carried out in Leica CM1900.

2.9. Cell Proliferation. Cell proliferation *in vitro* was determined by BrdU. The $CD44^{low}$ $CD62L^{high}$ T cells at 2×10^6/ml from the SP or BM were cultured in RPMI 1640 medium (Gibco) containing 10% FBS (Gibco), penicillin (100 U/ml) (HyClone), and streptomycin (100 μg/ml) (HyClone). For the activation of C57BL/6 J mice-derived T cells, cells were stimulated with anti-CD3 (2 μg/ml) and anti-CD28 (1 μg/ml) (BD Pharmingen) in the presence of IL-2 (10 ng/ml) (PeproTech). For the activation of OT-II mice-derived T cells, experiments were performed by following protocols as described. Briefly, the 1×10^6/ml T cells were cocultured with 2×10^7/ml irradiated T-depleted SP or BM-derived antigen-presenting cells in the presence of $OVA_{323\text{-}339}$ peptides *(ISQAVHAAHAEINEAGR)* (2 μM) (AnaSpec) and IL-2 (10 ng/ml) (PeproTech).

2.10. BrdU Labeling. For *in vivo* proliferation assay, BrdU (Sigma) was injected at 100 mg/kg with 10 mg/ml in saline intraperitoneally.

2.11. Homing Assay. Homing experiments of CMTPX-labeled $CD4^+$ TSCMs and CFSE-labeled reference cells were performed as described previously [20]. Briefly, the 2×10^6 CMTPX-labeled (10 μM) $CD4^+$ TSCMs were mixed with the same number of newly isolated and CFSE-labeled (10 μM) total spleen cells and then injected intravenously into the CD45.1 recipients. The recipients were sacrificed after 24 h, and cells from the spleen and bone marrow were obtained as described to measure $CMTPX^+/CFSE^+$ ratios by flow cytometry. An aliquot was assessed for the input ratio ($IR = (CMTPX)_{input}/(CFSE)_{input}$). The homing index (HI) was calculated as the ratio of $(CMTPX)_{tissue}/(CFSE)_{tissue}$ to $(CMTPX)_{input}/(CFSE)_{input}$. For instance, a homing index of 1 means that frequency of CMTPX-staining cells was equivalent with that of naïve T cells labeled with CFSE.

2.12. Statistical Analysis. Statistical analyses were carried out using the GraphPad 5.0. Data are representative from indicated experiments and are shown as means ± SD. Differences were calculated by one-way ANOVA or *t*-test. $^*P < 0.05$, $^{**}P < 0.01$, and $^{***}P < 0.001$.

3. Results

3.1. $CD4^+$ T Memory Stem Cells Preferentially Reside in the BM. Although $CD8^+$ TSCMs are categorized as memory cells, they display a largely naïve-like phenotype, including $CD62L^+$ $CCR7^+$ $CD45RO^-$ $CD45RA^+$ in humans and $CD44^{low}$ $CD62L^{high}$ in mice [21–23]. Given the similarity of $CD4^+$ and $CD8^+$ T cells on surface markers in most subsets of mice and the consistency of $CD4^+$ and $CD8^+$ TSCMs surface markers in humans, we sought to apply the criteria of $CD8^+$ TSCMs to explore $CD4^+$ TSCMs in mice. As expected, significant elevation of the $CD122^{high}$ $Sca\text{-}1^{high}$ subset was observed in the BM-derived naïve T cell compartment (Figure 1(a)) when compared with those from other tissues, including the SP, peripheral blood (PB), and mesenteric lymph node (LN) (Figure 1(b)). Thus, we hypothesized that the $CD122^{high}$ $Sca\text{-}1^{high}$ TSCMs preferentially reside in the BM.

The well-defined TSCMs have been shown to express not only high levels of CD122 and Sca-1 but also Bcl-2. To validate whether these natural $CD122^{high}$ $Sca\text{-}1^{high}$ TSCMs in the BM are completely consistent with the previously well-defined TSCMs, the expression level of Bcl-2 was evaluated in $CD122^{high}$ $Sca\text{-}1^{high}$ TSCMs and $CD122^{low}$ $Sca\text{-}1^{low}$ naïve T cells. As expected, the expression level of Bcl-2 was higher in $CD122^{high}$ $Sca\text{-}1^{high}$ TSCMs than in naïve $CD4^+$ T cells (Figure 1(c)), which was consistent with the previously defined TSCMs. Similar to unstimulated naïve T cells, BM-resident TSCMs expressed high levels of CD127 (IL-7Rα) (Figure 1(d)). Interestingly, the expression of CD69 in BM-resident TSCMs was slightly higher than that of naïve T cells (Figure 1(d)). Surprisingly, similar to $CD8^+$ TSCMs in mouse GVHD model, BM-resident $CD4^+$ TSCMs also highly expressed CXCR3 molecule (Figure 1(d)). Given the higher expressions of genes that involved in the regulation of stemness of cells in $CD8^+$ TSCMs, we also examined these genes referred to a previous report by qRT-PCR (Figure 1(e)). The qRT-PCR data indicated that the mRNA levels of *β-catenin*, *Klf7*, *Tcf-7*, and *Lef-1* in BM-resident TSCMs were much higher than those in naïve T cells (Figure 1(e)). It is notable that the mRNA levels of *CD44* and *Sca-1*, as a reference for the efficacy of sorting by flow cytometry, were consistent with the previous report (Figure 1(e)). Collectively, these observations supported that BM-enriched $CD122^{high}$ $Sca\text{-}1^{high}$ naïve-like $CD4^+$ T lymphocytes can be identified as TSCMs that naturally inhabit the BM.

3.2. BM-Resident $CD4^+$ TSCMs Vigorously Respond to a Blood-Borne Antigen. As previously reported, $CD4^+$ TSCMs can elicit rapid immune response upon antigen rechallenge [23]. To investigate the immune response of $CD4^+$ TSCMs in situ, purified naïve T cells ($CD4^+$ $CD44^{low}$ $CD62L^{high}$ $CD122^{low}$ $Sca\text{-}1^{low}$) and central memory T cells (TCMs) ($CD4^+$ $CD44^{high}$ $CD62L^{high}$) and TSCMs ($CD4^+$ $CD44^{low}$ $CD62L^{high}$ $CD122^{high}$ $Sca\text{-}1^{high}$) from the BM of OT-II mice ($CD45.2^+$) were adoptively transferred into congenic mice ($CD45.1^+$), followed by antigen stimulation using ovalbumin (OVA) immunization (Figure 2(a)). Flow cytometric

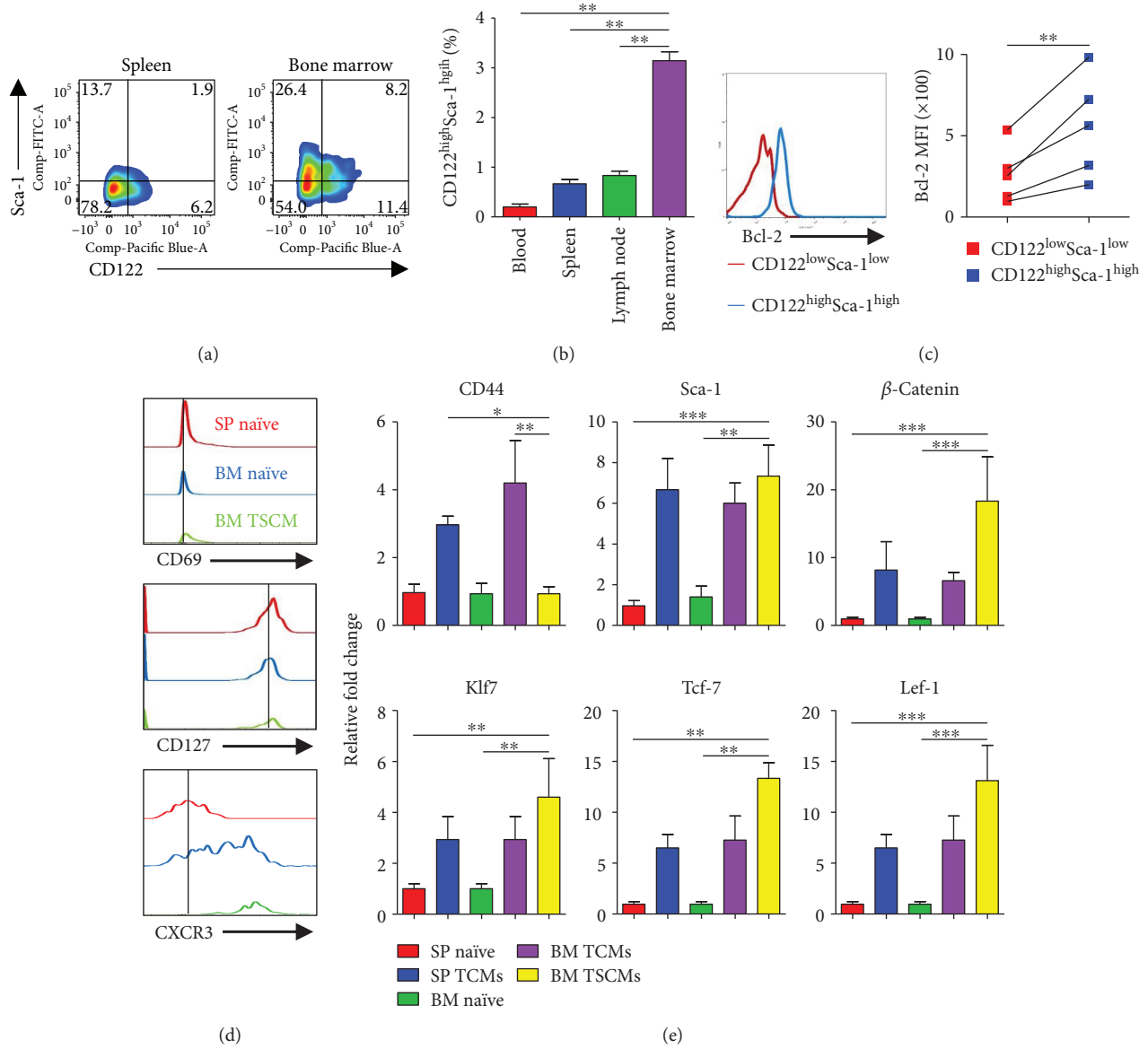

FIGURE 1: $CD4^+$ memory stem cells preferentially reside in BM. (a) Expression of CD122 and Sca-1 in SP- and BM-resident naïve-like T cell compartment. Iridescent cloud represents the frequencies of $CD122^{high}$ $Sca\text{-}1^{high}$ subset gated on $CD3^+$ $CD4^+$ $CD8^-$ $CD44^{low}$ $CD62L^{high}$ cells. Data are representative of six independent experiments. (b) TSCMs in various organs. The frequencies of TSCMs accounting for $CD44^{low}$ $CD62L^{high}$ $CD4^+$ T cells in the peripheral blood (PB), lymph node (LN), spleen (SP), and bone marrow (BM) were shown as means ± SD, one-way ANOVA. $^{**}P < 0.01$. Data are representative of four independent experiments. (c) Expression of Bcl-2 in naïve and TSCMs subsets in BM-resident T cells. Overlaid histogram plots show the levels of Bcl-2 in BM-resident $CD122^{low}$ $Sca\text{-}1^{low}$, $CD122^{low}$ $Sca\text{-}1^{high}$, $CD122^{high}$ $Sca\text{-}1^{low}$, and $CD122^{high}$ $Sca\text{-}1^{high}$ subsets gated on $CD3^+$ $CD4^+$ $CD8^-$ $CD44^{low}$ $CD62L^{high}$ cells. Data are representative of five independent experiments. The MFI of Bcl-2 in $CD122^{low}$ $Sca\text{-}1^{low}$, $CD122^{low}$ $Sca\text{-}1^{high}$, $CD122^{high}$ $Sca\text{-}1^{low}$, and $CD122^{high}$ $Sca\text{-}1^{high}$ subsets was shown as means ± SD, one-way ANOVA. $^{**}P < 0.01$. (d) Flow cytometric analysis of BM-resident TSCMs overlaid with SP- and BM-resident naïve T cells. Overlaid histogram lines show expression levels of a given molecule in different $CD4^+$ T cell subsets. $CD4^+$ T cell subsets were defined as follows: BM-resident TSCMs, $CD3^+$ $CD4^+$ $CD8^-$ $CD44^{low}$ $CD62L^{high}$ $CD122^{high}$ $Sca\text{-}1^{high}$; BM- and SP-resident naïve T cells, $CD3^+$ $CD4^+$ $CD8^-$ $CD44^{low}$ $CD62L^{high}$ $CD122^{low}$ $Sca\text{-}1^{low}$. Data are representative of five independent experiments. (e) qRT-PCR results show the expressions of *CD44*, *Sca-1*, *β*-catenin, *Klf-7*, *Tcf-7*, and *Lef-1* in different $CD4^+$ T cell subsets. $CD4^+$ T cell subsets were defined as follows: BM-resident TSCMs, $CD3^+$ $CD4^+$ $CD8^-$ $CD44^{low}$ $CD62L^{high}$ $CD122^{high}$ $Sca\text{-}1^{high}$; BM- and SP-resident naïve T cells, $CD3^+$ $CD4^+$ $CD8^-$ $CD44^{low}$ $CD62L^{high}$ $CD122^{low}$ $Sca\text{-}1^{low}$. Data are representative of 3 independent experiments ($n = 3$) and shown as means ± SD, one-way ANOVA. $^{*}P < 0.05$, $^{**}P < 0.01$, and $^{***}P < 0.001$.

analysis showed that BM TSCMs displayed much higher levels of cell proliferation and IFN-γ production when compared with those of BM TCMs and BM naïve T cells (Figures 2(b) and 2(c)). These results indicated that BM-enriched $CD122^{high}$ $Sca\text{-}1^{high}$ TSCMs respond to a blood-borne antigen efficiently.

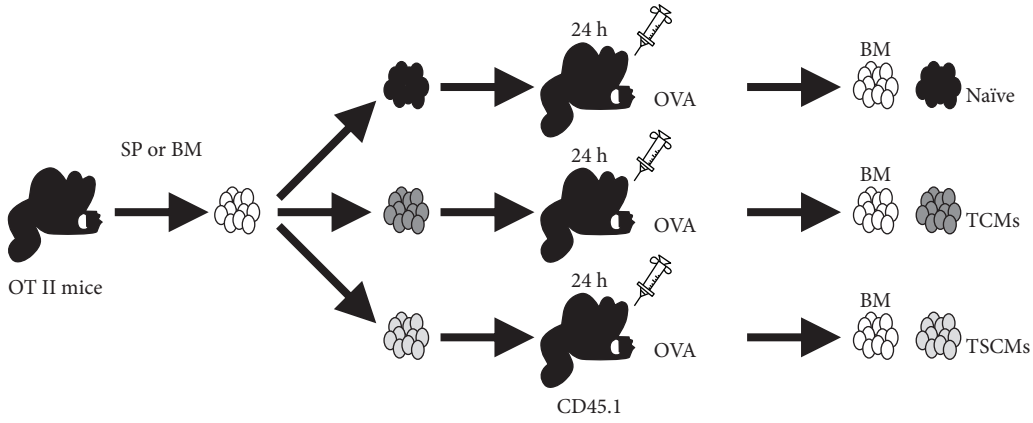

(a)

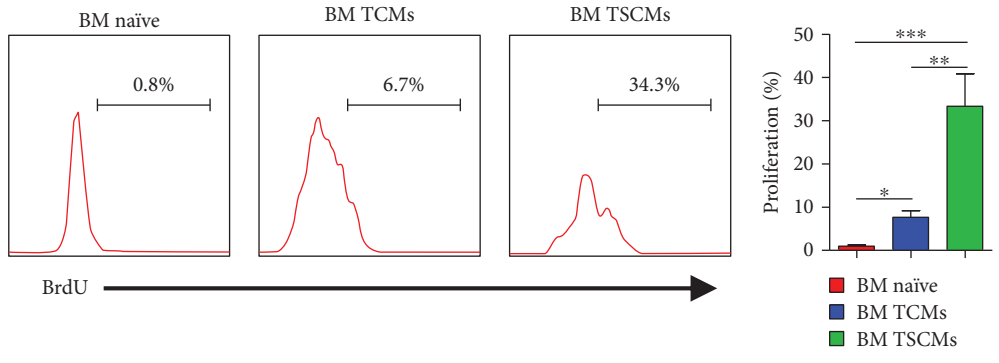

(b)

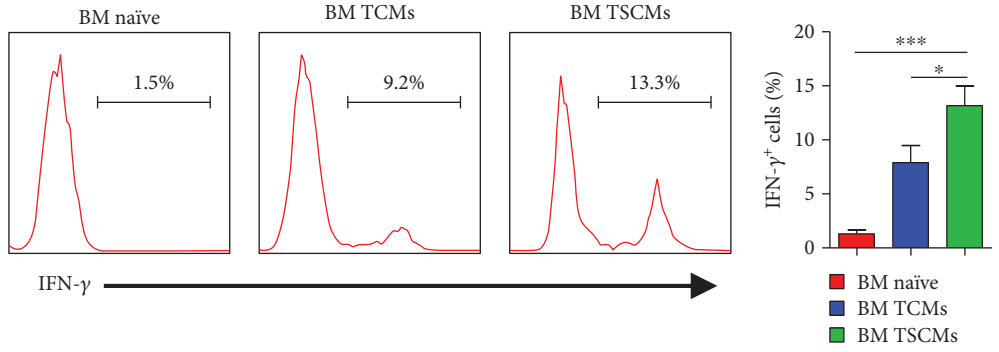

(c)

Figure 2: $CD4^+$ TSCMs from the BM respond to blood-borne antigens *in vivo*. (a) Schematic diagram of adoptive transfer. (b, c) BM-resident TSCMs possess the capacity of rapidly acquiring effector functions *in vivo*. The 5×10^5 subset of T cells from the BM of OT-II mice was adoptively transferred to CD45.1 mice, respectively. Recipients were immunized with 500 μg OVA in CFA and sacrificed after 3 days for further analysis. The T cell subsets were determined by the following FACS isolations: $CD45.2^+$ $CD4^+$ $CD44^{low}$ $CD62L^{high}$ $CD122^{low}$ $Sca\text{-}1^{low}$ for naïve T cells; $CD45.2^+$ $CD4^+$ $CD44^{low}$ $CD62L^{high}$ $CD122^{high}$ $Sca\text{-}1^{high}$ for TSCMs; $CD45.2^+$ $CD4^+$ $CD44^{high}$ $CD62L^{high}$ for TCMs. (b) Numbers in histograms represent the percentage of BrdU-positive cells in BM-resident naïve T cells, TCMs and TSCMs after OVA stimulation. (c) Intracellular cytokine staining of naïve T cells, TCMs and TSCMs in the BM. Numbers in histograms show the percentage of IFN-γ-expressing cells in the BM after OVA stimulation. Data are representative of three independent experiments ($n = 6$). Frequencies of $BrdU^+$ (b) and IFN-γ^+ cells (c) were shown as means ± SD, *t*-test. $^*P < 0.05$, $^{**}P < 0.01$, and $^{***}P < 0.001$.

3.3. Preferential Migration of $CD4^+$ TSCMs to the BM. Different from $CD8^+$ TSCMs, it was not impacted that the generation of $CD4^+$ TSCMs was dependent on β-catenin signaling pathway. It is indispensable to purify the $CD4^+$ TSCMs from the BM to perform the homing assay. The purified $CD4^+$ TSCMs were labeled with CMTPX and then mixed with CFSE-labeled total SP cells (as reference) at ratio of 1 : 1. The mixed cells were injected into recipient mice. After 12 hours, we detected the ratios of CMTPX-positive cells and CFSE-positive cells and then calculated the homing index. Obviously, the homing index of $CD4^+$ TSCMs in the BM was higher than that in the SP (Figures 3(a) and 3(b)). In

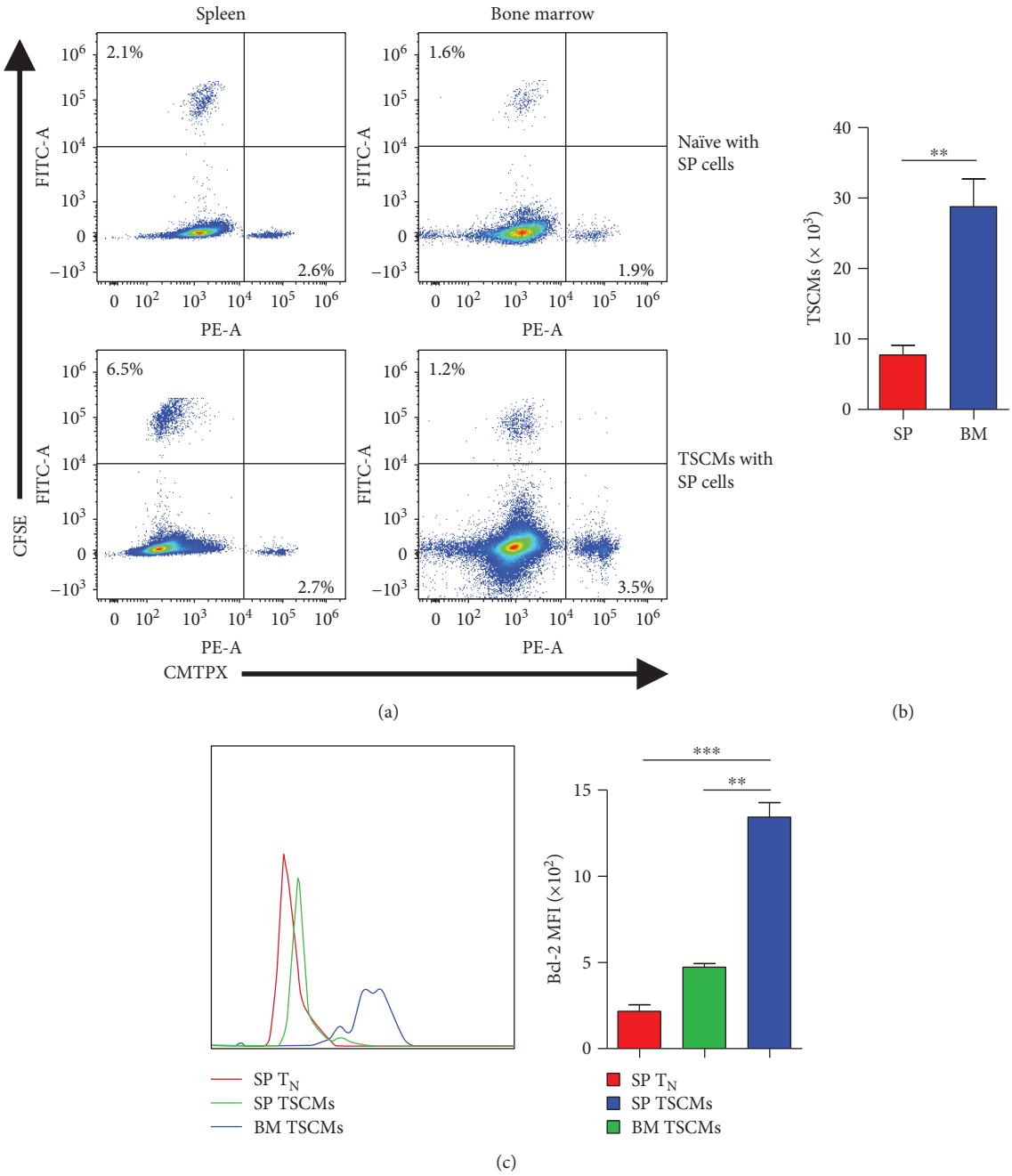

Figure 3: Homing of TSCMs to the BM. (a) Comparison of the homing index of naïve T cells and $CD4^+$ TSCMs. Data are representative of three independent experiments. (b) Numbers of transferred TSCMs in the SP and BM. Data were representative of three independent experiments ($n = 6$). The numbers of $CD45.2^+$ $CD4^+$ $CD44^{low}$ $CD62L^{high}$ $CD122^{high}$ $Sca\text{-}1^{high}$ cells were shown as means ± SD, t-test. $^{**}P < 0.01$, $^{***}P < 0.001$. (c) High expression of Bcl-2 in $CD4^+$ TSCMs relocated in the BM. The 2×10^6 $CD44^{low}$ $CD62L^{high}$ $CD4^+$ T cells sorted from the spleen or bone marrow in C57B6/J mice were adoptively transferred to CD45.1 mice. The overlaid histogram shows the expressions of Bcl-2 of CMTPX-positive cells in BM and SP cells. Data are representative from three independent experiments and shown as means ± SD ($n = 6$), one-way ANOVA. $^{**}P < 0.01$, $^{***}P < 0.001$.

addition, we also compared the protein levels of Bcl-2 in SP- and BM-resident $CD4^+$ TSCMs to validate their phenotypes. Importantly, the expression of Bcl-2 in BM-resident $CD4^+$ TSCMs was much higher than that of SP-resident $CD4^+$ TSCMs (Figure 3(c)). Taken together, these data demonstrated that the $CD122^{high}$ $Sca\text{-}1^{high}$ TSCMs preferentially homed to the BM.

3.4. $CD4^+$ TSCMs Are Attached to $VCAM\text{-}1^+$ IL-15- or IL-7-Expressing Stromal Cells in the BM. CD122 (IL-2Rβ) is also shared as the IL-15 receptor, and the persistence of TSCMs is dependent on IL-7 and IL-15, whereas IL-15 is highly expressed in stromal cells in the BM, which overlap with IL-7-expressing cells. Thus, we speculated that these cells could constitute the appropriate niches for BM-resident

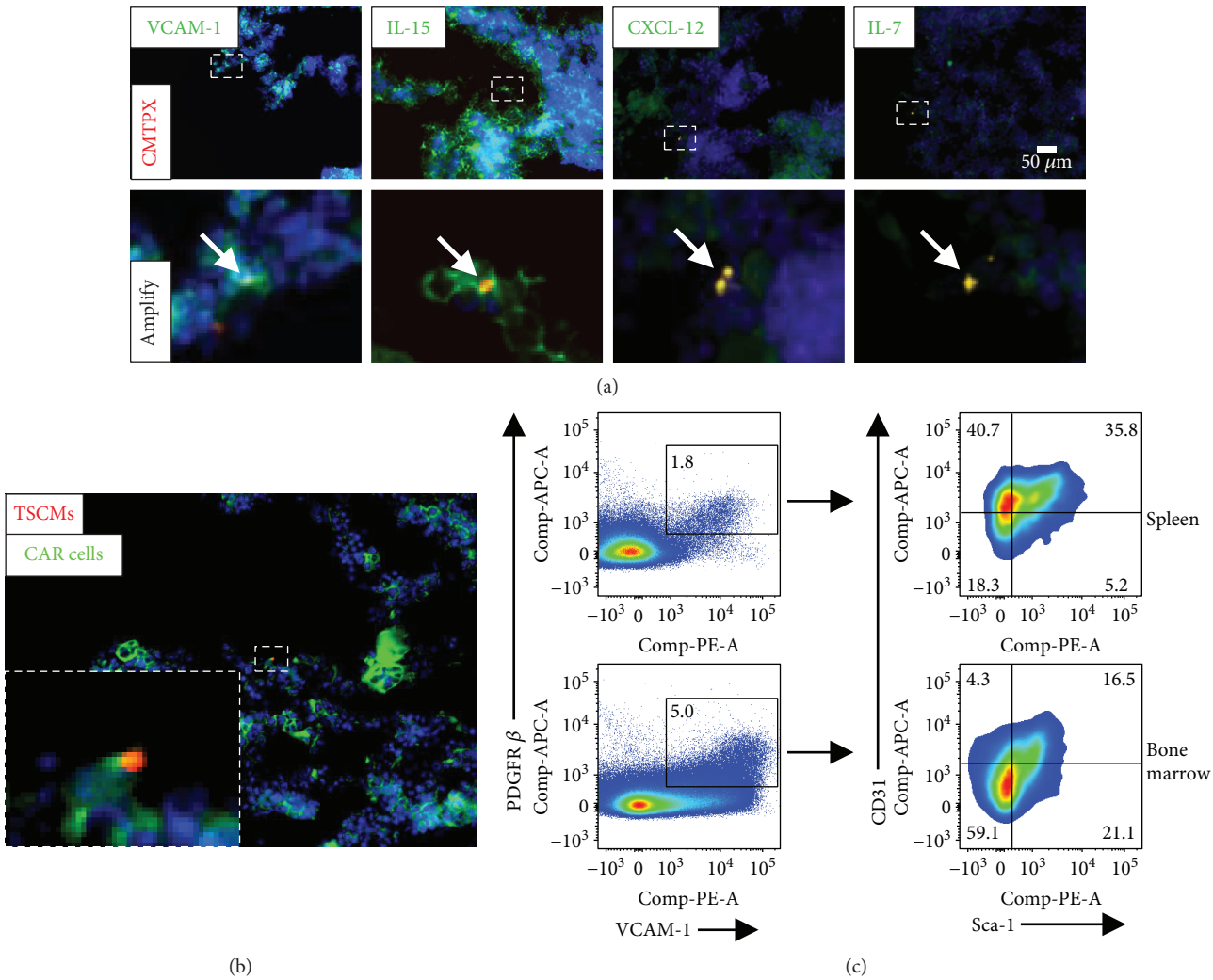

FIGURE 4: $CD4^+$ TSCMs attach to VCAM-1^+ IL-15- and IL-7-expressing stromal cells. (a) Colocalizations of $CD4^+$ TSCMs with VCAM-1^+ IL-15- and IL-7-expressing stromal cells. The 1×10^6 $CD4^+$ TSCMs isolated from the BM were labeled with CMTPX (red) and then injected to CD45.1 mice. After 24 h, the recipients were sacrificed and bone tissues were conducted for immunofluorescence staining. The immunofluorescence images show a representative picture of anti-VCAM-1 (green), IL-15 (green), CXCL-12 (green), or IL-7 (green) versus CMTPX-labeled TSCMs (red). The scale bars indicate that the actual distances on the specimen are 50 μm. Data are representative of three independent experiments. (b) Colocalizations of TSCMs with VCAM-1^+ PDGFRβ^+ $CD31^-$ Sca-1^- cells. The 5×10^5 TSCMs sorted from the C57B6/J mice BM were labeled with CMTPX (red, 5 μM) and mixed with 1×10^6 VCAM-1^+ PDGFRβ^+ $CD31^-$ Sca-1^- cells (from the BM) labeled with CFSE (green, 10 μM). Cells were injected into CD45.1 mice. After 24 h, the recipients were sacrificed and conducted frozen sections. The photo shows a representative picture of CFSE-staining VCAM-1^+ PDGFRβ^+ $CD31^-$ Sca-1^- cells (CXCL-12-abundant reticular cells, CAR cells) versus CMTPX-labeled TSCMs. The scale bar indicates that the actual distance on the specimen is *50* μm. (c) Flow cytometric analysis of VCAM-1^+ PDGFRβ^+ $CD31^-$ Sca-1^- cells in the SP and BM. Dot plots represent the frequencies of VCAM-1^+ PDGFRβ^+ cells (left) and $CD31^-$ Sca-1^- cells (right) in the SP and BM. Data are representative for three independent experiments ($n = 5$). Frequencies of VCAM-1^+ PDGFRβ^+ $CD31^-$ Sca-1^- cells were shown as means ± SD, *t*-test. $^*P < 0.05$, $^{**}P < 0.01$, and $^{***}P < 0.001$.

TSCMs [16, 24, 25]. To validate this hypothesis, the colocalization of TSCMs with stromal cells in the BM was examined by cryofluorescence. TSCMs were clearly colocalized with VCAM-1^+ IL-7- or IL-15-expressing stromal cells (Figure 4(a)). In addition, TSCMs were also located adjacent to CXCL-12^+ stromal cells (Figure 4(a)). According to the previous report, the IL-7- and IL-15-expressing cells were constituted by CXCL-12-abundant reticular (CAR) cells whose surface marker is VCAM-1^+ PDGFRβ^+ $CD31^-$ Sca-1^-. It is indispensable to investigate whether BM-resident $CD4^+$ TSCMs are colocalized with CAR cells. To test our hypothesis, the VCAM-1^+ PDGFRβ^+ $CD31^-$ Sca-1^- cells were isolated from the BM and transferred into recipient mice with BM $CD4^+$ TSCMs. As expected, the cryofluorescence results represent that $CD4^+$ TSCMs were surrounded by CAR cells in the BM (Figure 4(b)). Further flow cytometric analysis confirmed the significantly higher levels of VCAM-1^+ PDGFRβ^+ $CD31^-$ Sca-1^- stromal cells in the

BM (Figure 4(c)). These observations indicated that TSCMs are attached to CXCL-12$^+$ VCAM-1$^+$ IL-7- and IL-15-expressing stromal cells in the BM.

3.5. BM CD4$^+$ TSCMs Assist in Affinity Maturation of Antibodies against Influenza In Vivo. CD4 T cells, also known as helper T cells, assist CD8 T cell-mediated cellular immunity and B cell-mediated humoral immunity in antivirus infection. To explore the relationship between BM CD4$^+$ TSCMs and BM B cells, naïve B cells were transferred together with BM CD4$^+$ TSCMs and other T cell subsets (including naïve T cells and memory T cells) from the BM or SP of unimmunized mice into recipient mice which were then immunized with influenza A virus. Apparently, recipient mice with transferred BM CD4$^+$ TSCMs secreted more influenza antibodies in serum (Figure 5). These data demonstrated that BM CD4$^+$ TSCMs provide help for affinity maturation of antibodies against influenza *in vivo*.

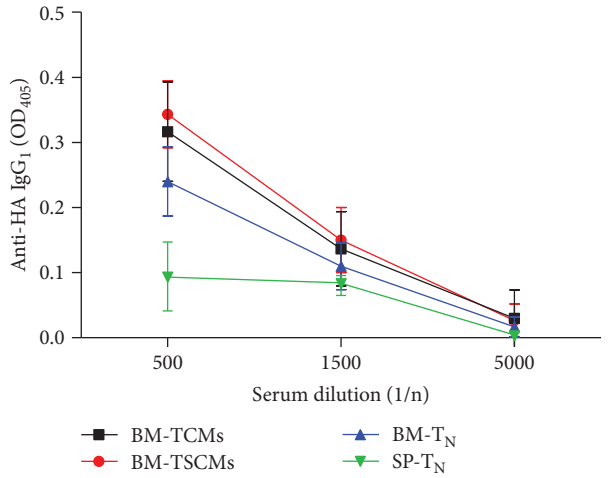

FIGURE 5: BM memory CD4$^+$ TSCMs assist in affinity maturation of antibodies *in vivo*. Transferred CD4$^+$ TSCMs from the BM provide help for affinity maturation of antibodies *in vivo*. 4×10^6 CD19$^+$ CD138$^-$ CD4$^-$ cells (naïve B cells) from OT-II mice SP were transferred with 1×10^5 CD4$^+$ CD44^{low} CD62L^{high} CD122^{high} Sca-1^{high} T cells from the BM or SP of OT-II mice, into CD45.1 mice. One day later, recipients were immunized with 2000 hemagglutination units PR8-OVA in CFA. The blood taken from transferred mice 5 days later was analyzed for anti-HA IgG$_1$ by ELISA. Data are representative of three independent experiments, means ± SD. $n = 6$.

4. Discussion

The BM is known to play an important role in controlling immune responses by influencing the generation of lymphocytes and the maintenance of immunological memory [16, 26–30]. Although CD4$^+$ TSCMs could relocate in the BM, the unambiguous anatomical sites of transition from the naïve state have not yet been determined. Of note, the specific adhesion molecules involved in the process of the relocation of CD4$^+$ TSCMs in the BM were still not determined. In this study, CD4$^+$ TSCMs that highly expressed CD122, Sca-1, and Bcl-2 were found to reside in the BM-resident naïve-like T cell compartments unambiguously. Although a small number of natural TSCMs were detected in the peripheral lymphoid organs, including the SP, PB, and LN, the frequencies of natural TSCMs in these organs were much lower than those in the BM. Notably, similar to SP-derived TSCMs, the BM-resident TSCMs were capable of acquiring effector functions more rapidly upon blood-borne antigen exposure when compared with naïve T cells. In fact, these data also suggest the significant accumulation of TSCMs in the BM rather than being simply confined to peripheral inflammatory sites. Despite the concomitant expression of numerous markers of naïve T cells on the surface of TSCMs, both bioinformatic analysis of microarray data and antigenic stimulation experiments have suggested that TSCMs are most closely related to TCMs [22, 31]. However, it remains unknown whether the other characteristics of TSCMs, especially the trafficking properties, are also similar to those of TCMs. Through the calculation of homing index of CD4$^+$ TSCMs, we found the preferential relocation of CD4$^+$ TSCMs in the BM.

An appropriate microenvironment for BM-resident TSCMs requires an architecture facilitating homeostasis of TSCMs in specific areas. These conditions seem to be met in BM stroma, which consists of a fibrous network of VCAM-1$^+$ IL-7- and IL-15-expressing stromal cells within VCAM-1$^+$ PDGFRβ^+ CD31$^-$ Sca-1$^-$ stromal cell compartments [24, 25]. Consistent with the previous report, the expression level of CD127 molecule was downregulated in BM CD4$^+$ TSCMs by IL-15 signaling from stromal cells [32, 33]. In particular, the niches in the BM could provide not only signaling of homeostatic proliferation (provided by IL-15 signaling) but also a survival signal (provided by the pair of IL-7 and CD127) through upregulating the expression of Bcl-2 for the maintenance of TSCMs. The cooperation of these two signaling pathways (IL-7 and IL-15 signaling) supported the residence of CD4$^+$ TSCMs in the bone marrow and the recalling of CD4$^+$ TSCMs in the influenza model. In contrast, we could not detect the colocalization of TSCMs with conventional APCs, including B220$^+$, CD11C$^+$, and F4/80$^+$ cells (data not shown). Strikingly, although the result of cell cycle indicated that BM-resident TSCMs were in resting status, the expression of CD69 in BM-resident TSCMs was slightly higher than that of naïve T cells. Simultaneously, BM-resident TSCMs could be reactivated rapidly upon exogenous antigen invasion, which provided a hint that active TSCMs are more likely to reside in areas close to APCs. We speculated that the antigen-specific responses might be accompanied by the confluence of TSCMs to large aggregates with several APCs, leading to the activation of TSCMs in the BM. Given that a minority of TSCMs was found in the periphery immune organs and a large number of TSCMs rapidly accumulated in inflammatory sites, we propose that these cells utilize the niches in the BM as a refuge and can be temporarily hidden from antigenic exposure before executing immunological surveillance. Of note, the CAR cells surrounded the CD4$^+$ TSCMs in the BM and the frequency of CAR cells in the BM was much higher than that in the SP, which might be a key factor affecting the dynamics of blood-borne TSCM migration *in vivo*.

The severity of influenza infection depends mainly on the type of influenza virus and the status of the patient's immune system [34], since cancer patients who receive bone marrow or stem cell transplants have decreased immune and poor responses to influenza vaccines [35, 36]. In our study, we have demonstrated that BM $CD4^+$ TSCMs that could help the maturation of antibodies against influenza were very important for anti-influenza immune. In the clinical bone marrow transplantation, T cells, including $CD4^+$ T cells and $CD8^+$ T cells, must be depleted from donor's BM cells to reduce graft-versus-host disease [37–39]. Perhaps, with the transplantation of a small amount of $CD4^+$ TSCMs from the donor BM, the anti-influenza immune of transplant recipients can be effectively improved to resist infection after BM transplantation. Although our data have demonstrated that the BM $CD4^+$ TSCMs could help the maturation of antibodies against influenza produced by B cells, it remained unknown whether BM $CD4^+$ TSCMs could help B cell-secreted antibodies against other fatal diseases.

Our data indicate that the BM-resident TSCMs exert much stronger activity of inducing production of antibodies against influenza, which could be instructive for development of anti-infection immunotherapy [40]. In melanoma patients, high frequencies of tumor-specific T cells could be detected by HLA tetramer binding; nevertheless, most of these cells were anergic or nonresponsive [41]. Compared with other subsets, TSCMs show higher immune activity. Although the expression of IFN-γ and cell proliferation of natural SP-derived TSCMs was almost equal to those of natural BM-derived TSCMs, we exploited the fact that the microenvironment in the BM could generate more functional $CD4^+$ TSCMs *in vivo*. Our data suggest that the selection of a proper microenvironment for functional $CD4^+$ TSCMs might be a novel direction to improve the efficacy of immunotherapies.

Overall, our study has revealed that TSCMs, as a distinct member of the memory cell club, exist naturally in wild-type mice and principally accumulate in the BM. In addition, these findings have revealed the relationship between BM $CD4^+$ TSCMs and anti-influenza immunity. It is intriguing that the BM might function as a type of "nest" for long-lived cells, including HSCs, conventional memory B and T cells, and TSCMs, by providing dedicated and distinct niches to each of them [42–44]. Moreover, these findings open the door to the development of a new infection disease immunotherapy strategy by driving the pathogen-specific TSCMs out from the BM of patients who suffer from malignant viral infections.

Data Availability

The data used to support the findings of this study are available from the corresponding author upon request.

Conflicts of Interest

The authors declare no conflict of interest.

Authors' Contributions

Kang Wu and Fei Wang contributed equally to this work.

Acknowledgments

This study was supported by the National Natural Science Foundation of China (81702327, 81802741, and 81502207).

References

[1] Y. Zhang, G. Joe, E. Hexner, J. Zhu, and S. G. Emerson, "Host-reactive $CD8^+$ memory stem cells in graft-versus-host disease," *Nature Medicine*, vol. 11, no. 12, pp. 1299–1305, 2005.

[2] C. J. Turtle, H. M. Swanson, N. Fujii, E. H. Estey, and S. R. Riddell, "A distinct subset of self-renewing human memory $CD8^+$ T cells survives cytotoxic chemotherapy," *Immunity*, vol. 31, no. 5, pp. 834–844, 2009.

[3] D. O'Sullivan, G. J. W. van der Windt, S. C.-C. Huang et al., "Memory $CD8^+$ T cells use cell-intrinsic lipolysis to support the metabolic programming necessary for development," *Immunity*, vol. 49, no. 2, pp. 375-376, 2018.

[4] M. J. Buzon, H. Sun, C. Li et al., "HIV-1 persistence in $CD4^+$ T cells with stem cell-like properties," *Nature Medicine*, vol. 20, no. 2, pp. 139–142, 2014.

[5] P. Muranski, Z. A. Borman, S. P. Kerkar et al., "Th17 cells are long lived and retain a stem cell-like molecular signature," *Immunity*, vol. 35, no. 6, pp. 972–985, 2011.

[6] C. J. Luckey and C. T. Weaver, "Stem-cell-like qualities of immune memory; $CD4^+$ T cells join the party," *Cell Stem Cell*, vol. 10, no. 2, pp. 107-108, 2012.

[7] D. T. Scadden, "The stem-cell niche as an entity of action," *Nature*, vol. 441, no. 7097, pp. 1075–1079, 2006.

[8] T. C. Becker, S. M. Coley, E. J. Wherry, and R. Ahmed, "Bone marrow is a preferred site for homeostatic proliferation of memory CD8 T cells," *The Journal of Immunology*, vol. 174, no. 3, pp. 1269–1273, 2005.

[9] L. L. Cavanagh, R. Bonasio, I. B. Mazo et al., "Activation of bone marrow-resident memory T cells by circulating, antigen-bearing dendritic cells," *Nature Immunology*, vol. 6, no. 10, pp. 1029–1037, 2005.

[10] I. B. Mazo, M. Honczarenko, H. Leung et al., "Bone marrow is a major reservoir and site of recruitment for central memory $CD8^+$ T cells," *Immunity*, vol. 22, no. 2, pp. 259–270, 2005.

[11] M. Feuerer, P. Beckhove, N. Garbi et al., "Bone marrow as a priming site for T-cell responses to blood-borne antigen," *Nature Medicine*, vol. 9, no. 9, pp. 1151–1157, 2003.

[12] K. Tokoyoda, T. Egawa, T. Sugiyama, B. I. Choi, and T. Nagasawa, "Cellular niches controlling B lymphocyte behavior within bone marrow during development," *Immunity*, vol. 20, no. 6, pp. 707–718, 2004.

[13] A. Pierini, H. Nishikii, J. Baker et al., "$Foxp3^+$ regulatory T cells maintain the bone marrow microenvironment for B cell lymphopoiesis," *Nature Communications*, vol. 8, article 15068, 2017.

[14] S. Sullivan, "Challenges in reducing influenza-associated mortality," *Lancet*, vol. 391, no. 10127, pp. 1242–1244, 2018.

[15] The Lancet Infectious Diseases, "Plotting a route to a universal influenza vaccine," *The Lancet Infectious Diseases*, vol. 18, no. 5, p. 475, 2018.

[16] K. Tokoyoda, S. Zehentmeier, A. N. Hegazy et al., "Professional memory CD4$^+$ T lymphocytes preferentially reside and rest in the bone marrow," *Immunity*, vol. 30, no. 5, pp. 721–730, 2009.

[17] C. T. D'Angio, C. P. Wyman, R. S. Misra et al., "Plasma cell and serum antibody responses to influenza vaccine in preterm and full-term infants," *Vaccine*, vol. 35, no. 38, pp. 5163–5171, 2017.

[18] J. Zhang, F. Huang, L. Tan et al., "Host protein Moloney leukemia virus 10 (MOV10) acts as a restriction factor of influenza A virus by inhibiting the nuclear import of the viral nucleoprotein," *Journal of Virology*, vol. 90, no. 8, pp. 3966–3980, 2016.

[19] F. Huang, J. Chen, J. Zhang et al., "Identification of a novel compound targeting the nuclear export of influenza A virus nucleoprotein," *Journal of Cellular and Molecular Medicine*, vol. 22, no. 3, pp. 1826–1839, 2018.

[20] D. L. Woodland and J. E. Kohlmeier, "Migration, maintenance and recall of memory T cells in peripheral tissues," *Nature Reviews. Immunology*, vol. 9, no. 3, pp. 153–161, 2009.

[21] L. Gattinoni, X. S. Zhong, D. C. Palmer et al., "Wnt signaling arrests effector T cell differentiation and generates CD8$^+$ memory stem cells," *Nature Medicine*, vol. 15, no. 7, pp. 808–813, 2009.

[22] M. Neuenhahn and D. H. Busch, "The quest for CD8$^+$ memory stem cells," *Immunity*, vol. 31, no. 5, pp. 702–704, 2009.

[23] L. Gattinoni, E. Lugli, Y. Ji et al., "A human memory T cell subset with stem cell-like properties," *Nature Medicine*, vol. 17, no. 10, pp. 1290–1297, 2011.

[24] G. Cui, T. Hara, S. Simmons et al., "Characterization of the IL-15 niche in primary and secondary lymphoid organs in vivo," *Proceedings of the National Academy of Sciences of the United States of America*, vol. 111, no. 5, pp. 1915–1920, 2014.

[25] Ö. Sercan Alp, S. Durlanik, D. Schulz et al., "Memory CD8$^+$ T cells colocalize with IL-7$^+$ stromal cells in bone marrow and rest in terms of proliferation and transcription," *European Journal of Immunology*, vol. 45, no. 4, pp. 975–987, 2015.

[26] F. Di Rosa and T. Gebhardt, "Bone marrow T cells and the integrated functions of recirculating and tissue-resident memory T cells," *Frontiers in Immunology*, vol. 7, p. 51, 2016.

[27] S. L. Pull, J. M. Doherty, J. C. Mills, J. I. Gordon, and T. S. Stappenbeck, "Activated macrophages are an adaptive element of the colonic epithelial progenitor niche necessary for regenerative responses to injury," *Proceedings of the National Academy of Sciences of the United States of America*, vol. 102, no. 1, pp. 99–104, 2005.

[28] F. E. Mercier, C. Ragu, and D. T. Scadden, "The bone marrow at the crossroads of blood and immunity," *Nature Reviews. Immunology*, vol. 12, no. 1, pp. 49–60, 2012.

[29] X. Li, S. He, X. Zhou et al., "Lyn delivers bacteria to lysosomes for eradication through TLR2-initiated autophagy related phagocytosis," *PLoS Pathogens*, vol. 12, no. 1, article e1005363, 2016.

[30] X. Li, S. He, R. Li et al., "*Pseudomonas aeruginosa* infection augments inflammation through miR-301b repression of c-Myb-mediated immune activation and infiltration," *Nature Microbiology*, vol. 1, no. 10, article 16132, 2016.

[31] P. Graef, V. R. Buchholz, C. Stemberger et al., "Serial transfer of single-cell-derived immunocompetence reveals stemness of CD8$^+$ central memory T cells," *Immunity*, vol. 41, no. 1, pp. 116–126, 2014.

[32] A. C. Quinci, S. Vitale, E. Parretta et al., "IL-15 inhibits IL-7Rα expression by memory-phenotype CD8$^+$T cells in the bone marrow," *European Journal of Immunology*, vol. 42, no. 5, pp. 1129–1139, 2012.

[33] E. Parretta, G. Cassese, P. Barba, A. Santoni, J. Guardiola, and F. Di Rosa, "CD8 cell division maintaining cytotoxic memory occurs predominantly in the bone marrow," *Journal of Immunology*, vol. 174, no. 12, pp. 7654–7664, 2005.

[34] M. J. Crane, Y. Xu, W. L. Henry, S. P. Gillis, J. E. Albina, and A. M. Jamieson, "Pulmonary influenza A virus infection leads to suppression of the innate immune response to dermal injury," *PLoS Pathogens*, vol. 14, no. 8, article e1007212, 2018.

[35] J. Gooskens, W. A. F. Marijt, E. H. R. van Essen, G. F. Rimmelzwaan, and A. C. M. Kroes, "Host immunity dictates influenza A(H1N1)pdm09 infection outcome in hematology-oncology patients," *Bone Marrow Transplantation*, vol. 51, no. 1, pp. 138–141, 2016.

[36] A. Zumla, M. Rao, R. S. Wallis et al., "Host-directed therapies for infectious diseases: current status, recent progress, and future prospects," *The Lancet Infectious Diseases*, vol. 16, no. 4, pp. e47–e63, 2016.

[37] L. Zhang, J. Yu, and W. Wei, "Advance in targeted immunotherapy for graft-versus-host disease," *Frontiers in Immunology*, vol. 9, p. 1087, 2018.

[38] M. M. Moutuou, G. Page, I. Zaid, S. Lesage, and M. Guimond, "Restoring T cell homeostasis after allogeneic stem cell transplantation; principal limitations and future challenges," *Frontiers in Immunology*, vol. 9, p. 1237, 2018.

[39] R. Nishimura, J. Baker, A. Beilhack et al., "In vivo trafficking and survival of cytokine-induced killer cells resulting in minimal GVHD with retention of antitumor activity," *Blood*, vol. 112, no. 6, pp. 2563–2574, 2008.

[40] J. Mateus, P. Lasso, P. Pavia et al., "Low frequency of circulating CD8$^+$ T stem cell memory cells in chronic chagasic patients with severe forms of the disease," *PLoS Neglected Tropical Diseases*, vol. 9, no. 1, article e3432, 2015.

[41] M. Feuerer, P. Beckhove, L. Bai et al., "Therapy of human tumors in NOD/SCID mice with patient-derived reactivated memory T cells from bone marrow," *Nature Medicine*, vol. 7, no. 4, pp. 452–458, 2001.

[42] L. E. Silberstein and C. P. Lin, "A new image of the hematopoietic stem cell vascular niche," *Cell Stem Cell*, vol. 13, no. 5, pp. 514–516, 2013.

[43] A. Ehninger and A. Trumpp, "The bone marrow stem cell niche grows up: mesenchymal stem cells and macrophages move in," *The Journal of Experimental Medicine*, vol. 208, no. 3, pp. 421–428, 2011.

[44] R. S. Welner and P. W. Kincade, "9-1-1: HSCs respond to emergency calls," *Cell Stem Cell*, vol. 14, no. 4, pp. 415-416, 2014.

Hindawi
Mediators of Inflammation
Volume 2019, Article ID 5160694, 10 pages
https://doi.org/10.1155/2019/5160694

Research Article

The Role of Infection in Acute Exacerbation of Idiopathic Pulmonary Fibrosis

Dong Weng,[1] Xian-Qiu Chen,[1] Hui Qiu,[1] Yuan Zhang,[1] Qiu-Hong Li,[1] Meng-Meng Zhao,[1] Qin Wu,[1] Tao Chen,[1] Yang Hu,[1] Liu-Sheng Wang,[1] Ya-Ru Wei,[1] Yu-Kui Du,[1] Shan-Shan Chen,[2] Ying Zhou,[1] Fen Zhang,[1] Li Shen,[1] Yi-Liang Su,[1] Martin Kolb,[3] and Hui-Ping Li[1]

[1]*Department of Respiratory Medicine, Shanghai Pulmonary Hospital, Tongji University, School of Medicine, Shanghai, China*
[2]*School of Medicine, Suzhou University, Suzhou, China*
[3]*McMaster University Hamilton, Department of Medicine and Pathology/Molecular Medicine, ON, Canada*

Correspondence should be addressed to Hui-Ping Li; liw2013@126.com

Received 27 June 2018; Revised 3 October 2018; Accepted 5 November 2018; Published 3 January 2019

Guest Editor: Bishi Fu

Background. Acute exacerbation of IPF (AE-IPF) is associated with high mortality. We studied changes in pathogen involvement during AE-IPF and explored a possible role of infection in AE-IPF. *Objectives*. Our purpose is to investigate the role of infection in AE-IPF. *Methods*. Overall, we recruited 170 IPF patients (48 AE-IPF, 122 stable) and 70 controls at Shanghai Pulmonary Hospital. Specific IgM against microbial pathogens and pathogens in sputum were assessed. RNA sequences of pathogens in nasopharyngeal swab of IPF patients were detected by PathChip. A panel of serum parameters reflecting immune function were assessed. *Results*. Antiviral/bacterial IgM was higher in IPF vs. controls and in AE-IPF vs. stable IPF. Thirty-eight different bacterial strains were detected in IPF patient sputum. Bacteria-positive results were found in 9/48 (18.8%) of AE-IPF and in 26/122 (21.3%) stable IPF. Fifty-seven different viruses were detected in nasopharyngeal swabs of IPF patients. Virus-positive nasopharyngeal swabs were found in 18/30 (60%) of tested AE-IPF and in 13/30 (43.3%) of stable IPF. AE-IPF showed increased inflammatory cytokines (IL-6, IFN-γ, MIG, IL-17, and IL-9) vs. stable IPF and controls. Mortality of AE-IPF in one year (39.5%) was higher compared to stable IPF (28.7%).*Conclusions*. IPF patients had different colonization with pathogens in sputum and nasopharyngeal swabs; they also displayed abnormally activated immune response, which was exacerbated during AE-IPF.

1. Background

Idiopathic pulmonary fibrosis (IPF) is a fatal disease with unknown etiology, characterized by a radiographic and pathologic pattern of usual interstitial pneumonia (UIP). Patients with IPF have a median survival time of 3 years [1], following either a progressive course of worsening respiratory function, or a more rapid decline described as acute exacerbation (AE-IPF) [2]. The common criteria for AE-IPF include a diagnosis of IPF with acute worsening of dyspnea in the preceding month, new radiographic opacities or ground glass on computed tomography (CT), and exclusion of alternative causes (e.g., infection, congestive heart failure, and pulmonary embolism). AE-IPF is a dangerous condition with a high mortality (often >50%) [3–8]. In some reports, the one-year mortality of patients with AE-IPF was almost 100% [4, 5].

The previously used definition of AE-IPF [7] has proven to be unclear, and a consensus on the definition even in expert centers has been difficult [9]. Recently, an international working group had suggested that it would be important to rule out obvious infections for IPF patients with deteriorating symptoms over less than one month but had also acknowledged that AE following a triggering event might end as bad as idiopathic AE episodes [10]. Known triggers for AE-IPF include lung surgery, bronchoscopy with BAL, aspiration, pollution, and preceding infections, but the exact causes and mechanisms for AE-IPF remain unclear [3]. The fundamental to the concept of idiopathic AE-IPF is

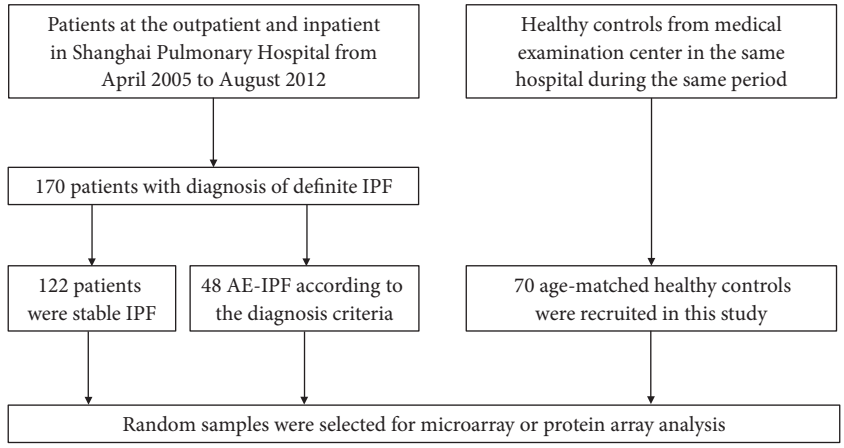

Figure 1: Flow chart of patient enrollment.

the assumption that these episodes are a distinct clinical entity and that it is important to distinguish them from acute respiratory deterioration of known cause, which was questioned by more recent data [9, 11]. Many publications do not report sufficient details to confidently exclude infections in events reported as AE-IPF. Indeed, it is almost impossible to exclude a lot of different infections, especially viral pathogens in the clinical situation due to unreliable commercial tests and inconsistent clinical testing. In our clinical observations, many patients of IPF with AE experienced common cold symptoms before their rapid decline. Typical common cold symptoms include cough, worsening dyspnea and mild fever—all of them have been included in the description of AE-IPF events [11]. Further, recent evidence points towards a potential role of an altered lung microbiome in triggering IPF progression, including AE-IPF [12–17].

In this study, we asked whether IPF patients may be particularly sensitive to common infectious triggers, some of them then developing AE-IPF. We aimed to investigate the association of AE-IPF with microbial colonization and/or latent infection.

2. Methods

2.1. Subjects and Selection Criteria. We prospectively enrolled 170 definite IPF patients (122 stable IPF without corticosteroid, immunosuppression, and antibiotic therapy and 48 AE-IPF) who were managed at the Shanghai Pulmonary Hospital between April 2005 and August 2012, either in the outpatient or inpatient department (Figure 1). The diagnosis of IPF was established according to international guidelines [6]. All patients were treated according to the IPF guidelines [6] after admission. The therapies for AE-IPF in our group were as follows: oxygen therapy (including nasal catheter, mask oxygen inhalation, and noninvasive ventilation when necessary); glucocorticoids (mainly methylprednisolone 80-320 mg/day); antibiotics (mainly broad-spectrum antibiotics, empirically covering common pathogens of respiratory tract infections, antifungal therapies for patients accompanied with fungal infection); antioxidation therapy (glutathione); immune support therapy (gamma globulin, etc.); nutritional support; and symptomatic therapy. Regarding episodes of AE-IPF [6–8], we applied the following criteria of AE-IPF: (1) established diagnosis of definite IPF; (2) progressive dyspnea within 1 month, and presented with hypoxemia at room air; (3) new bilateral radiographic opacities in CT scan; (4) absence of identifiable etiology including pulmonary embolism, pneumothorax, congestive heart failure, and pneumonia (using usual clinical criteria with presence of fever > 38.5°C, elevated WBC count > 15,000, and pulmonary infiltrates resolving with antibiotic therapies). We also recruited 70 healthy age-matched controls from the medical examination center of the same hospital during the same time period (April 2005 and August 2012). Healthy controls were admitted to our hospital for health examination and did not get diagnosed with any diseases, showing normal lung function and chest X-ray. All of the subjects in the study were followed up by telephone or outpatient appointments until Sept. 2014. Clinical data of patients and healthy controls were prospectively collected and analyzed. The ethics committee of the College of Medicine and Life Science, Tongji University, approved this study. All participants gave written informed consent.

Fasting venous blood specimens were sampled from IPF patients and healthy controls on the day after admission or on the day of medical examination. All IPF patients underwent pulmonary function tests before acute exacerbation. Arterial blood was sampled from IPF patients (at room air) on the day of admission to perform arterial blood gas analysis.

The severity of pulmonary fibrosis and lesion involvement was assessed according to the Helbich quantified HRCT scoring system [18], and ground-glass opacities (including consolidation), reticular shadow, and honeycombing were included as indicators for fibrosis assessment. HRCT scans at three levels (aortic arch, tracheal bifurcation, and at a dimension of 1 cm above the diaphragm) were used for HRCT scoring. The total HRCT score was calculated by summing the scores of all levels. A higher HRCT score indicated more severe pulmonary fibrosis (Table 1).

2.2. Serum IgM Antibody Detection. Peripheral blood was centrifuged in a procoagulant tube at 3000 rpm for 15 min, and serum was separated for determination of pathogen-specific

Table 1: HRCT scoring criteria.

HRCT imaging Ground-glass changes	Scores
No ground-glass opacities	0
Ground-glass opacity area < 5%	1
Ground-glass opacity area 6-24%	2
Ground-glass opacity area 25-49%	3
Ground-glass opacity area 50-74%	4
Ground glass opacity area > 75%	5
Reticular changes (septal thickening)	
No reticular shadow	0
Reticular shadow area < 5%	1
Reticular shadow area 6-24%	2
Reticular shadow area 25-49%	3
Reticular shadow area 50-74%	4
Reticular shadow area > 75%	5
Honeycomb-like changes	
No honeycombing	0
Honeycombing area < 5%	1
Honeycombing area 6-24%	2
Honeycombing area 25-49%	3
Honeycombing area 50-74%	4
Honeycombing area > 75%	5
Total	

The "area" indicates the percentage of lesions in the corresponding HRCT scans.

IgM. The immunofluorescence-based Pneumoslide IgM kit (Vircell, Spain) was used to detect specific IgM antibody against *Legionella*, *Mycoplasma pneumoniae*, *Q fever Rickettsia*, *Chlamydia pneumoniae*, *Adenovirus*, *respiratory syncytial virus*, *influenza A virus*, *influenza B virus*, *and parainfluenza virus*. The cytomegalovirus (CVM) IgM ELISA kit (BioAssay, USA) was used to detect the IgM antibody response to CMV.

2.3. Culture of Pathogens in Sputum. Spontaneous sputum samples were collected from all IPF patients in the early morning for 3 consecutive days after hospital admission, and samples were immediately (within 30 min) sent for sputum culturing. Qualified samples needed to meet the following criteria: (1) squamous cells < 10 cells/low magnification; (2) white blood cells (WBC) > 25 cells/low magnification; or (3) the squamous cell: WBC ratio < 1 : 2.5. Consistent results obtained more than twice of each sputum culture from the same patient were considered as a single result. If the results of the same patient were inconsistent, sputum cultures were performed again.

2.4. Viral RNA Extraction and PathoChip. Random nasopharyngeal swab samples were selected with the help of computational random number generators. RNA was extracted from nasopharyngeal swab stored in virus sampling tube using QIAamp Viral RNA Mini Kits (Qiagen Inc., Hilden, Germany: cat. no. 52906) according to the manufacturer's instructions. The RNA was stored at -80°C. The PathChip (PathGEN Dx, Singapore) can detect over 70,000 full-genome RNA sequences of pathogens (including over 50,000 viruses and 20,000 bacteria) clinically relevant to humans [19]. The RNA samples were purified, fragmented, labeled, and hybridized onto the PathChip according to the manufacturer's protocol. After hybridization, the PathChip was washed, stained, and scanned using the Affymetrix GeneChip system. The Affymetrix image file (.CEL) containing all the raw signal intensities for each PathChip was uploaded into the GIS proprietary software described previously [19], which automatically detects pathogen recognition signatures.

2.5. Serum Inflammatory Cytokines Profiling. The first step, soluble proteins from the serum samples of healthy controls ($n = 6$), stable IPF ($n = 6$), and AE-IPF ($n = 6$) were profiled using the RayBio® L-Series 507 Biotin Label-based Antibody Array system (RayBiotech, GA, USA). The next step, we designed a new array (RayBiotech QAH-CUST, RayBiotech Inc.) by using 30 different cytokines selected according to our observations and literature reports, and 60 samples (AE-IPF patients, $n = 20$; stable IPF, $n = 20$; health control, $n = 20$) were examined. The array was used by following the manufacturer's instructions to measure the following cytokines: BMP-7, EOT, Flt-3L, G-CSF, GM-CSF, ICAM-1, IFN-γ, IL-10, IL-12 p40, IL-12 p70, IL-13, IL-15, IL-17, IL-1α, IL-1β, IL-22, IL-4, IL-6, IL-7, IL-9, leptin, LIGHT, MCP-1, MCP-2, MIG, MMP-7, NT-3, PDGF-BB, TGF-β1, and TSLP. After developing, slides were scanned, and the images were processed and quantified using Axon GenePix4400A microarray scanners. Intensity was normalized to internal positive controls for comparison.

2.6. Statistical Analysis. Statistical analyses were performed using the software program SPSS 13.0. Counting data are presented as mean ± SD. The independent sample Student's t-test was used for comparisons between two groups, and one-way ANOVA followed by Tukey's post hoc test was used to compare three groups. The chi-square test was used for constituent ratio comparisons. Pearson's method was used for association analyses. Survival rates were estimated using Kaplan-Meier methods and group comparisons were tested using log-rank test. Statistical significance was defined at an alpha value of $p < 0.05$.

3. Results

3.1. Demographic Data. A total of 170 patients with IPF were enrolled from Shanghai Pulmonary Hospital. Clinical characteristics of the patients are summarized in Table 2. Controls were age matched, compared with IPF patients, and had less exposure to potential environmental triggers, cigarette smoking, and also no history of recent common cold symptoms. Patients with AE-IPF showed a significantly higher incidence (89.6%) of recent cold symptoms (including more cough, nasal obstruction, rhinorrhea, sore throat, chills, and headache 1-2 weeks before acute exacerbation) compared with stable IPF patients. Patients were followed from the time of the enrollment visit at our

Table 2: Clinical characteristics.

		AE-IPF ($n = 48$)	Stable IPF ($n = 122$)	Control ($n = 70$)
Gender	Male	48/48 (100%)	110/122 (90.2%)	63/70 (90%)
	Female	0/48	12/122 (9.8%)	7/70 (10%)
Age (yr)		65 ± 9	64 ± 8	59 ± 7
Environmental exposure[a]		8/48 (16.7%)[#]	26/122 (21.3%)[#]	6/70 (8.6%)
Surgical lung biopsy[b]		0	5	/
Smoking (%)		70.8[#]	68.9[#]	28.6
History of recent cold (%)		89.6[*,#]	13.1[#]	0
Family history		0	1	0
1-year mortality		19/48 (39.5%)[*,#]	35/122 (28.7%)	0
WBC ($\times 10^9$/L)		9.01 ± 4.61[#]	8.06 ± 2.45[#]	6.01 ± 1.46
Neutrophils (%)		67.74±12.37[*,#]	59.12 ± 9.55	60.17 ± 6.74
Lymphocytes (%)		22.62±10.38[*,#]	29.58 ± 8.45[#]	32.46 ± 4.95
Monocytes (%)		6.45 ± 2.78[#]	7.30 ± 1.85[#]	5.87 ± 2.38
pH		7.43 ± 0.31[*]	7.42 ± 0.26	NA
$PaCO_2$ (mmHg)		37.92 ± 5.39	37.89 ± 5.46	NA
PaO_2 (mmHg)		68.97 ± 16.45[*]	80.47 ± 15.9	NA
SaO_2 (%)		91.71 ± 6.98[*]	94.83 ± 3.12	NA
FVC (% predicted)		59.35 ± 10.93[*]	84.68 ± 22.62	NA
FEV1 (% predicted)		65.75 ± 10.78[*]	84.89 ± 20.01	NA
FEV1/FVC		89.14 ± 8.01[*]	80.65 ± 6.48	NA
TLC (% predicted)		66.24 ± 16.14	81.97 ± 19.26	NA
RV/TLC		43.06 ± 10.14	40.41 ± 5.68	NA
DLco (% predicted)		59.98 ± 19.50	62.88 ± 20.02	NA
HRCT scores		20.67 ± 5.98[*]	12.27 ± 3.84	NA

[*]$p < 0.05$ vs. stable IPF; [#]$p < 0.05$ vs. control. [a]Patients were engaged in mining, painting, chemical manufacturing, teaching, carpentry, welding, warehouse managing, and farming. [b]5 subjects were diagnosed with IPF by biopsy. Abbreviations: WBC: white blood cell; $PaCO_2$: carbon dioxide partial pressure; PaO_2: oxygen partial pressure; SaO_2: oxygen saturation; FVC: forced vital capacity; FEV1: 1 second forced expiratory volume; TLC: total lung capacity; DLco: diffusion capacity for carbon monoxide; HRCT: high-resolution computed tomography; NA: not available.

hospital until Sept. 2014, and survival analysis was performed. As expected, overall Kaplan-Meier survival analysis showed significantly higher mortality of AE-IPF (23/48, 47.9%) compared with stable IPF (50/122, 41.0%; log rank to compare these curves $p = 0.039$). In AE-IPF patients, 19 patients (19/48, 39.58%) died within one year after the AE episode; of them, 57.9% (11 of 19) died within one month. In stable IPF patients, the 1-year mortality was 28.7% (35/122), which was significantly lower than that of AE-IPF (Figure 2, $p = 0.041$). All deaths occurred within the follow-up period (Sept. 2014).

IPF patients had significantly higher total WBC counts and neutrophils than healthy controls (stable IPF 8.06 ± 2.45, AE-IPF 9.01 ± 4.61, control 6.01 ± 1.46; difference IPF to control $p = 0.002$). AE-IPF patients showed a slightly higher neutrophil percentage than stable IPF, which could indicate latent infections in patients developing AE-IPF. Compared with stable IPF, AE-IPF patients had significantly lower arterial oxygen pressure ($p = 0.001$) and saturation ($p < 0.0001$), while pulmonary function tests indicated that AE-IPF patients had worse FVC (% pred) ($p = 0.02$), worse FEV1 (% pred) ($p = 0.007$), and increased FEV1/FVC ratio ($p = 0.01$). The HRCT scores of AE-IPF patients were significantly higher than that of stable IPF patients ($p = 0.001$).

3.2. Antimicrobial IgM, Sputum, and Nasopharyngeal Swap Analysis

3.2.1. Serum IgM Antibodies. Detection of IgM antibody against 10 common pathogens revealed that mycoplasma was the pathogen with the highest IgM positive rate (12.2%) in the serum of AE-IPF patients, followed by legionella (7.3%), adenovirus (7.3%), and RSV (4.9%). In the serum of stable IPF patients, mycoplasma also showed the highest IgM positive rate (5.6%), followed by legionella (4.6%), RSV (3.7%), and influenza B viruses (2.8%). For healthy controls, only mycoplasma (7.1%), adenovirus (2.9%), and parainfluenza virus (1.4%) were positive (Table 3). The total positive rate of IgM antibodies was 36.6%, 19.4%, and 11.4%, respectively, in AE-IPF, stable

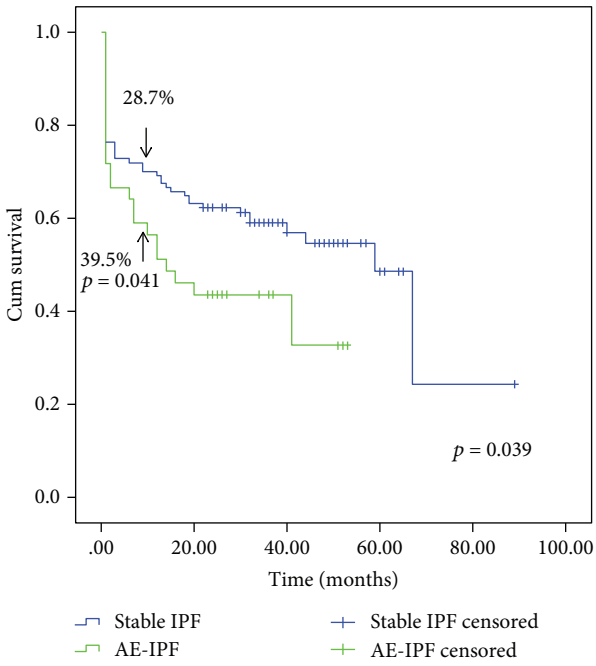

Figure 2: Kaplan-Meier survival analysis showing significantly higher mortality of AE-IPF than IPF (stable IPF) by using the log-rank test ($p = 0.039$). AE-IPF patients (39.5%) had higher one-year mortality than stable IPF (28.7%) ($p = 0.041$). In AE-IPF group (23 cases of death), 19 cases died of respiratory failure by acute exacerbation; 4 died of severe pneumonia. In stable IPF group (50 cases of death), 15 died of acute exacerbation in the period of follow-up, 10 died of pneumonia, 5 died of lung cancer, 2 died of liver cancer, 2 died of intestine cancer, 5 died of myocardial infarction, 2 died of gastrointestinal bleeding, 4 died of pulmonary embolism, 3 died of stroke, 1 died of diabetes, and 1 died of trauma.

Table 3: Specific IgM antibodies against 10 common pathogens (serum, number of positive cases, and positive rate).

IgM	AE-IPF ($n = 41$)	Stable IPF ($n = 108$)	Control ($n = 70$)
Mycoplasma	5, 12.2%	6, 5.6%	5, 7.1%
Legionella	3, 7.3%	5, 4.6%	0, 0%
Respiratory syncytial virus	2, 4.9%	4, 3.7%	0, 0%
Adenovirus	3, 7.3%	1, 0.9%	2, 2.9%
Influenza B virus	1, 2.4%	3, 2.8%	0, 0%
Cytomegalovirus	1, 2.4%	1, 0.9%	0, 0%
Chlamydia	0, 0%	1, 0.9%	0, 0%
Rickettsia	0, 0%	0, 0%	0, 0%
Parainfluenza Virus	0, 0%	0, 0%	1, 1.4%
Influenza A Virus	0, 0%	0, 0%	0, 0%
Total	15, 36.6%$^{*\#}$	21, 19.4%	8, 11.4%

After chi-square test, $^{*}p < 0.05$ vs. stable IPF; $^{\#}p < 0.05$ vs. healthy controls.

IPF, and healthy controls (Table 3). The positive rate of IgM in AE-IPF was significantly higher than that seen in both stable IPF ($p = 0.0290$) and healthy controls ($p = 0.0016$), and a nonsignificant difference in the positive rates of IgM was seen when comparing stable IPF and healthy controls.

Table 4: Pathogens in sputum of IPF patients.

Pathogens	Number of strains		
	AE-IPF ($n = 48$)	Stable IPF ($n = 122$)	Total ($n = 170$)
Gram-negative bacteria	9	25	34
Klebsiella pneumoniae	2	8	10
Acinetobacter baumannii	0	4	4
Mycobacterium tuberculosis	4	4	8
Pseudomonas aeruginosa	1	2	3
Loffi Acinetobacter	1	0	1
Serratia marcescens	0	1	1
Enterobacter cloacae	0	1	1
Raoultella	0	1	1
Other	1	4	5
Gram-positive cocci	0	4	4
Total no. of bacterial strain	9	29	38
Positive cases	9	26	35
Positive rate	9/48 (18.8%)	26/122 (21.3%)	35/170 (20.6%)

3.2.2. Culture of Pathogens in Sputum. The categories and constituent ratio of pathogens detected in the sputum of 170 IPF cases are listed in Table 4. A total of 38 bacterial strains were detected. Most prominent were Gram-negative bacteria (89.5%); Gram-positive strains only accounted for 10.5%. In terms of the Gram-negative strains, *Klebsiella pneumonia* was most abundant (26.3%), followed by *Mycobacterium tuberculosis* (21.1%), and *Acinetobacter baumannii* (10.5%). The total detection rates in AE-IPF and stable IPF patients were 18.8% and 21.3%, respectively (Table 4). There was no significant difference between AE-IPF and stable IPF.

3.2.3. Detection of Viruses in Nasopharyngeal Swab. The categories and constituent ratio of viruses detected by PathGEN® PathChip Kit in the throat swab of 30 stable IPF and 30 AE-IPF cases are listed in Table 5. A total of 57 different viruses (40 in AE-IPF and 17 in stable IPF) were detected. Virus-positive rates in AE-IPF patients were 60.0% (18/30) and 43.3% (13/30) in stable IPF. There was no significant difference between AE-IPF and stable IPF ($p = 0.1965$). In the AE-IPF group, HHV (human herpesvirus) and INF A (influenza virus A) accounted for 37.5% (15/40) and 30% (12/40), respectively. In stable IPF patients, HHV and HRV (human rhinovirus) were both accounted for 23.5%.

3.2.4. Inflammatory Cytokines. To investigate the association between AE-IPF and infections, we detected the expression levels of antimicrobial inflammatory cytokines in the serum of randomly selected healthy controls ($n = 20$), stable IPF ($n = 20$), and AE-IPF patients ($n = 20$) using RayBiotech QAH-CUST microarray. When compared with controls

Table 5: Viruses in nasopharyngeal swabs of IPF patients.

Virus[a]	Number of viruses		
	AE-IPF ($n = 30$)	Stable IPF ($n = 30$)	Total ($n = 60$)
HHV	15	4	19
INF A	12	0	12
HRV	6	4	10
Other positive viruses[b]	7	9	16
Total positive viruses[c]	40	17	57
Positive cases	18	13	31
Positive rate	18/30 (60.0%)	13/30 (43.3%)	31/60 (51.7%)

[a]HHV: human herpesvirus; INF A: influenza virus A; HRV: human rhinovirus. [b]Other positive viruses include AE-IPF: Andean potato latent virus; Mimivirus terra2; Tailam virus strain; halovirus; Emiliania huxleyi virus 86; oat dwarf virus; pepper mild mottle virus; stable IPF: Shamonda virus; Pandoravirus dulcis; pestivirus Giraffe-1; alfalfa mosaic virus; Megavirus chiliensis; murine osteosarcoma virus; Rous sarcoma virus; Y73 sarcoma virus; and hepatitis G virus. [c]Some patients were positive for two kinds of virus

and stable IPF patients, AE-IPF patients showed significant increases in the levels of IL-6, IFN-γ, MIG, IL-17, and IL-9 (Figures 3(a) and 3(e)). These cytokines had critical roles in anti-infection responses. These results suggested infections might play a role in the initiation and development of AE-IPF.

4. Discussion

IPF is a disease of unknown etiology that is usually progressive, either in a linear or stepwise manner [1]. In this study, the patients were all diagnosed definite IPF with UIP pattern in HRCT prior to acute exacerbation. There are no changes in diagnostic criteria of definite IPF between 2011 [6] and 2018 [20] guidelines. AE-IPF is an episode of exacerbation that develops rapidly within a few weeks and often occurs unexpectedly during the stable phase of IPF. All of the patients were treated according to the IPF guidelines [6] after admission (data not shown). AE-IPF is associated with high mortality and poor prognosis [3]. The one-year mortality is variable between 40–100% [4]. In our study, AE-IPF patients had a one-year mortality of almost 40% after the episode; 58% (11 of 19) died within the first month. Moua et al. just published a large cohort of patients with IPF and other fibrotic lung disease from the United States who were admitted to the hospital with acute respiratory worsening, having a one-year mortality of almost 80% [5]. The cohort in the report of Moua et al. had an average lower FVC (62% pred.) than our stable IPF group (FVC 84% pred.), but their average FVC was similar to our AE-IPF group (FVC 59% pred.). This could be explained by differences in the study population (ours was only IPF) and also differences in the health care systems (hospitalizations for diagnostic purposes and milder respiratory problems are much more common in China compared to the US). While we do not have follow-up lung function data from all AE-IPF patients except the information about their death, our follow-up data of stable IPF patients show a one-year decline in FVC (270 ± 206 ml) similar to recent studies [21, 22]. The stable IPF patients in our study showed a relatively high mortality (50/122, 41.0%) during follow-up; half of them (25/50) died due to nonrespiratory reasons (different cancers, myocardial infarction, gastrointestinal bleeding, pulmonary embolism, stroke, and others), 15/50 died due to AE in the period of follow-up, and 10/50 died of pneumonia. In stable IPF patients, the one-year mortality was 28.7% (35/122), which was significantly lower than that of AE-IPF ($p = 0.041$).

The earlier definition of AE-IPF warranted exclusion of acute infections of the lower respiratory tract, ideally by tracheobronchial aspirate or bronchoscopy. This is not always and consistently done across centers, not even within the rigid setting of clinical trials in which AE-IPF were used as endpoint [22]. Our clinical observations suggest that rapid worsening or AE of IPF are often preceded by "cold-like" symptoms without clearly establishing an acute infectious respiratory disease. Recently, several studies suggested that progression of IPF seems to be associated with bacterial or viral infection and/or abnormal composition of the lung microbiome, which is a good reason to revisit the definition of AE-IPF [3, 12–17]. Afarwal and Jindal [4] have shown that infections are able to induce an inflammatory cascade in the lung of IPF patients, thus leading to a rapid deterioration of stable IPF. The recent study by Moua and colleagues suggested that the prognosis of AE-IPF is equally poor, regardless of them being idiopathic or triggered by infections [5]. These issues were addressed by an international working group of IPF experts proposing that AE can be triggered events (through occult or detectable infections, lung surgery, or aspiration) or can be idiopathic with similar outcomes [10]. While true pneumonias should not be termed AE according to this document, it is acknowledged that definite exclusion of potential triggers is no longer required for the definition of an AE-IPF episode.

In our study, we basically used the AE-IPF definition proposed in the 2016 document [10], even if we started to enroll subject ten years earlier. We aimed to investigate whether abnormal bacterial, viral, or antimicrobial immune responses were related to the development of AE-IPF. Our data show that AE-IPF patients had significantly higher rates of antimicrobial IgM in their serum compared to stable IPF and significantly more neutrophils. This indicates that infectious pathogens, particularly cold-causing viral and bacterial pathogens, might be an important triggering factor in a substantial number of AE-IPF. Similar findings have been reported before in smaller studies [23]. We also investigated virus sequences in nasopharyngeal swabs of IPF patients. Our data (Table 5) showed that virus-positive samples were highest in the AE-IPF group (60.0%) but also considerable in stable IPF (43.3%). In the AE-IPF group, human herpesvirus and influenza A were the most prominent viruses. Of note, it has been shown before that herpes virus is associated with IPF [24] and can cause exacerbation of pulmonary fibrosis in animal models [25, 26]. Further, acute exacerbation of IPF has been reported after influenza A vaccination [27]. The presence of influenza A in AE-IPF patients supports the notion that cold-associated infections are able to trigger these events. In

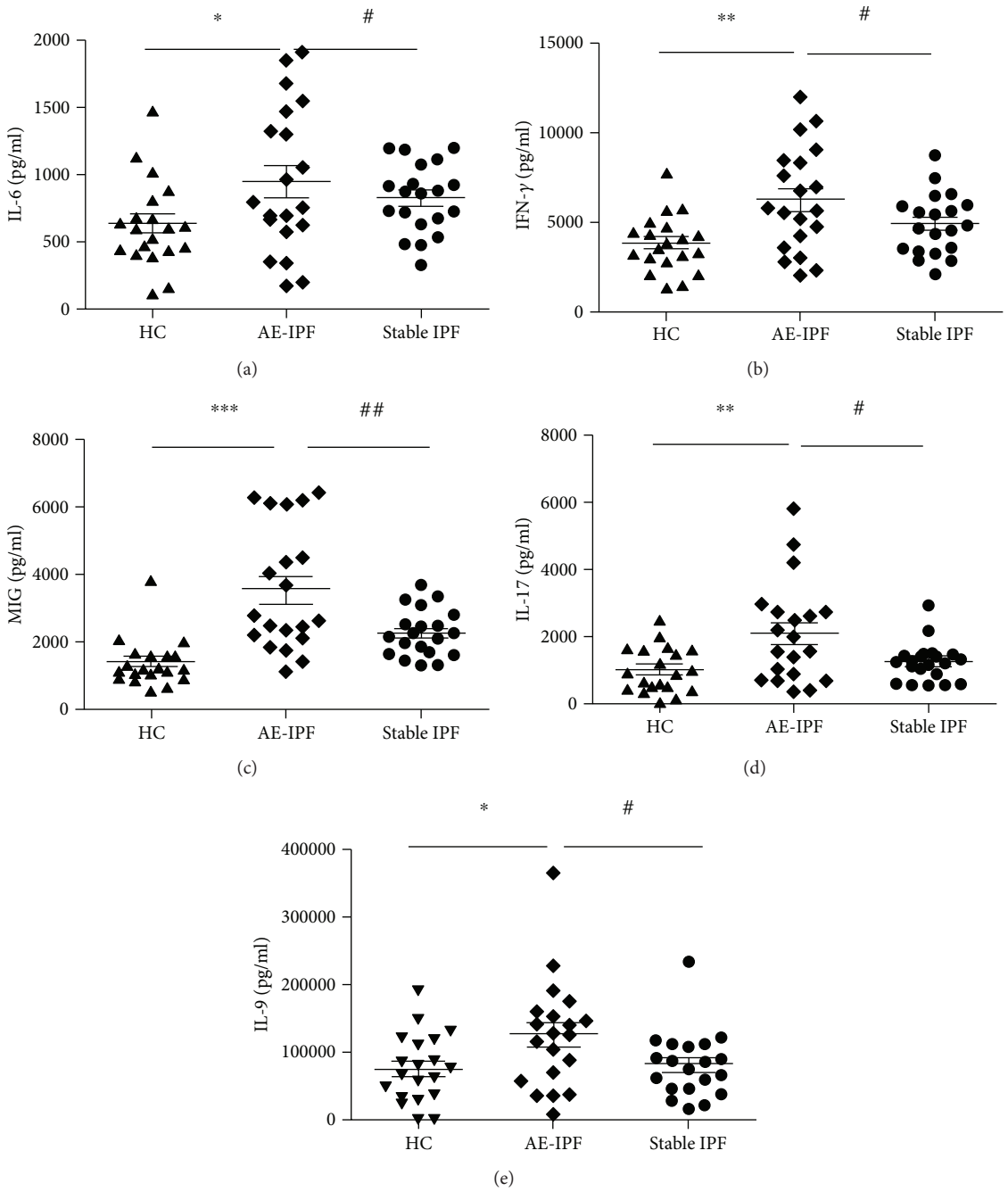

Figure 3: Antimicrobial inflammatory cytokines in AE-IPF. Serum of 40 IPF patients (20 AE-IPF and 20 stable IPF) and 20 controls was examined with protein microarray analysis. When compared with controls and stable IPF patients, AE-IPF patients showed significant increases in the levels of IL-6, IFN-γ, MIG, IL-17, and IL-9. One-way ANOVA followed by Tukey's post hoc test was used to compare three groups. $^{*}p < 0.05$, $^{**}p < 0.01$, $^{***}p < 0.001$ AE IPF vs. controls. $^{\#}p < 0.05$, $^{\#\#}p < 0.01$, $^{\#\#\#}p < 0.001$ AE IPF vs. stable IPF.

contrast, Wootton et al did not find evidence for viruses in AE of IPF in a rather large study where they used bronchoscopies and molecular analysis for viral particles [28]. However, even with such a sophisticated approach, it is not possible to rule out a relationship between acute viral infection and subsequent development of AE-IPF because the time between the onset of symptoms and the sampling of bronchial fluid may be too long to detect viral particles [29]. In our study, we also found significantly increased inflammatory cytokines in AE-IPF patients that may indicate a biological process against an infection. IL-6, IFN-γ, MIG, IL-17, and IL-9 are important inflammatory cytokines in the anti-infection immune response [30–44] and were all increased in the blood of patients with AE-IPF in our cohort. The changes of cytokines mainly reflect the inflammation cascade amplification effect of AE-IPF. Pathogen infection might be a trigger or a secondary infection in later stage. This also provides supporting evidence for glucocorticoid therapy

in AE-IPF. Our data also shows that the antimicrobial IgM serum response against respiratory pathogens and positive sputum cultures tended to be higher in stable IPF patients compared to healthy subjects, suggesting a certain level of latent infection in stable IPF patients. Positive rate of MTB in our study was relatively high. This might be in keeping with the local prevalence. MTB was a long-term infection, while other pathogens might be removed by effective therapies in short time. This meant the detective rate of MTB might be higher than other pathogens in sputum. However, it may be an area of further interest for future work.

Our study has several limitations. The data is observational and even with the significant increase in the anti-infectious cytokines, we have no clear evidence to support that the infections caused AE-IPF through this immune response. However, our group had reported the relationship between virus infection and AE-IPF using animal model [26] recently. The single-center design is always somewhat problematic as certain findings may be influenced by local practice and also local differences in the incidence and prevalence of certain infections. Further, our study would be stronger if we had an independent cohort to validate the finding. Nevertheless, this is one of the largest studies of AE-IPF where the role of infections and anti-infection immune response was explored with advanced diagnostic tools.

5. Conclusion

Taken together, our data suggest that latent infections and/or abnormal colonization in the lungs of IPF patients and "common cold"-associated virus infections together with a significantly elevated anti-infection immune response might be a common triggering factor for AE-IPF.

Abbreviations

IPF: Idiopathic pulmonary fibrosis
UIP: Usual interstitial pneumonia
AE-IPF: Acute exacerbation of IPF
CT: Computed tomography
WBC: White blood cell
PaCO2: Carbon dioxide partial pressure
PaO2: Oxygen partial pressure
SaO2: Oxygen saturation
FVC: Forced vital capacity
FEV1: 1 second forced expiratory volume
TLC: Total lung capacity
DLco: Diffusion capacity for carbon monoxide
HRCT: High-resolution computed tomography.

Data Availability

All data used to support the findings of this study are available from the corresponding author upon request.

Ethical Approval

The studies were performed in accordance with the Declaration of Helsinki and Good Clinical Practice guidelines. Ethical approval for the study was granted by Research Ethics Committee of School of Medicine, Tongji University, and research and development approval was obtained for Shanghai Pulmonary Hospital (reference number: 2014fk04).

Consent

Written informed consent was received from participants prior to inclusion in the study.

Conflicts of Interest

No potential conflicts of interest were disclosed.

Authors' Contributions

HPL, DW, MK, Y. Zang, and HQ are involved in the conception, hypothesis, and design of the study. XQC, HPL, DW, Q. H. Li, YH, YRW, HQ, LSW, QW, PZ, YKD, SSC, ZF, MMZ, Y. Zhou, FZ, LS, and YLS are responsible for the selection of patients and acquisition of samples. DW, XQC, YRW, HPL, YH, MMZ, LSW, PZ, YKD, Y. Zang, HQ, and SSC are responsible for the acquisition of the data. DW, XQC, Y. Zang, HQ, and HPL are responsible for the analysis and interpretation of the data. DW, XQC, MK, and HPL are responsible for the substantial involvement in the writing and/or revision of the article. MK is responsible for the English edition of the manuscript. Dong Weng, Xian-Qiu Chen, Hui Qiu and Yuan Zhang contributed equally to this work.

Acknowledgments

The authors would like to acknowledge the patients who consented to the study. The authors also would like to acknowledge the ATS2018 conference for accepting this manuscript as a conference abstract in A42. ILD SCIENTIFIC ABSTRACTS: TREATMENT AND ACUTE EXACERBATION. This research is supported by grants from the National Science Foundation of China (nos. 81730002, 81670055, 81670056, 91442103, 81500052, and 81570057), Ministry of Science and Technology of the People's Republic of China (2016YFC1100200, 2016YFC1100204), Shanghai Hospital Development Center (16CR3054A), and Fundamental Research Funds for the Central Universities (22120180020).

References

[1] B. Ley, H. R. Collard, and T. E. King Jr., "Clinical course and prediction of survival in idiopathic pulmonary fibrosis," *American Journal of Respiratory and Critical Care Medicine*, vol. 183, no. 4, pp. 431–440, 2011.

[2] S. K. Frankel and M. I. Schwarz, "Update in idiopathic pulmonary fibrosis," *Current Opinion in Pulmonary Medicine*, vol. 15, no. 5, pp. 463–469, 2009.

[3] C. J. Ryerson and H. R. Collard, "Acute exacerbations complicating interstitial lung disease," *Current Opinion in Pulmonary Medicine*, vol. 20, no. 5, pp. 436–441, 2014.

[4] R. Agarwal and S. K. Jindal, "Acute exacerbation of idiopathic pulmonary fibrosis: a systematic review," *European Journal of Internal Medicine*, vol. 19, no. 4, pp. 227–235, 2008.

[5] T. Moua, B. D. Westerly, M. M. Dulohery, C. E. Daniels, J. H. Ryu, and K. G. Lim, "Patients with fibrotic interstitial lung disease hospitalized for acute respiratory worsening: a large cohort analysis," *Chest*, vol. 149, no. 5, pp. 1205–1214, 2016.

[6] G. Raghu, H. R. Collard, J. J. Egan et al., "An official ATS/ERS/JRS/ALAT statement: idiopathic pulmonary fibrosis: evidence-based guidelines for diagnosis and management," *American Journal of Respiratory and Critical Care Medicine*, vol. 183, no. 6, pp. 788–824, 2011.

[7] H. R. Collard, B. B. Moore, K. R. Flaherty et al., "Acute exacerbations of idiopathic pulmonary fibrosis," *American Journal of Respiratory and Critical Care Medicine*, vol. 176, no. 7, pp. 636–643, 2007.

[8] W. D. Travis, U. Costabel, D. M. Hansell et al., "An official American Thoracic Society/European Respiratory Society statement: update of the international multidisciplinary classification of the idiopathic interstitial pneumonias," *American Journal of Respiratory and Critical Care Medicine*, vol. 188, no. 6, pp. 733–748, 2013.

[9] C. J. Ryerson, V. Cottin, K. K. Brown, and H. R. Collard, "Acute exacerbation of idiopathic pulmonary fibrosis: shifting the paradigm," *The European Respiratory Journal*, vol. 46, no. 2, pp. 512–520, 2015.

[10] H. R. Collard, C. J. Ryerson, T. J. Corte et al., "Acute exacerbation of idiopathic pulmonary fibrosis. An international working group report," *American Journal of Respiratory and Critical Care Medicine*, vol. 194, no. 3, pp. 265–275, 2016.

[11] K. A. Johannson and H. R. Collard, "Acute exacerbation of idiopathic pulmonary fibrosis: a proposal," *Current Respiratory Care Reports*, vol. 2, no. 4, pp. 233–240, 2013.

[12] M. K. Han, Y. Zhou, S. Murray et al., "Lung microbiome and disease progression in idiopathic pulmonary fibrosis: an analysis of the COMET study," *The Lancet Respiratory Medicine*, vol. 2, no. 7, pp. 548–556, 2014.

[13] P. L. Molyneaux and T. M. Maher, "The role of infection in the pathogenesis of idiopathic pulmonary fibrosis," *European Respiratory Review*, vol. 22, no. 129, pp. 376–381, 2013.

[14] P. L. Molyneaux, M. J. Cox, A. U. Wells et al., "Changes in the respiratory microbiome during acute exacerbations of idiopathic pulmonary fibrosis," *Respiratory Research*, vol. 18, no. 1, p. 29, 2017.

[15] P. L. Molyneaux, S. A. G. Willis-Owen, M. J. Cox et al., "Host-microbial interactions in idiopathic pulmonary fibrosis," *American Journal of Respiratory and Critical Care Medicine*, vol. 195, no. 12, pp. 1640–1650, 2017.

[16] Y. Takahashi, A. Saito, H. Chiba et al., "Impaired diversity of the lung microbiome predicts progression of idiopathic pulmonary fibrosis," *Respiratory Research*, vol. 19, no. 1, p. 34, 2018.

[17] Y. Huang, S. F. Ma, M. S. Espindola et al., "Microbes are associated with host innate immune response in idiopathic pulmonary fibrosis," *American Journal of Respiratory and Critical Care Medicine*, vol. 196, no. 2, pp. 208–219, 2017.

[18] T. H. Helbich, G. Heinz-Peer, I. Eichler et al., "Cystic fibrosis: CT assessment of lung involvement in children and adults," *Radiology*, vol. 213, no. 2, pp. 537–544, 1999.

[19] E. A. F. Simões, C. Patel, W.-K. Sung et al., "Pathogen chip for respiratory tract infections," *Journal of Clinical Microbiology*, vol. 51, no. 3, pp. 945–953, 2013.

[20] G. Raghu, M. Remy-Jardin, J. L. Myers et al., "Diagnosis of idiopathic pulmonary fibrosis. An official ATS/ERS/JRS/ALAT clinical practice guideline," *American Journal of Respiratory and Critical Care Medicine*, vol. 198, no. 5, pp. e44–e68, 2018.

[21] T. E. King Jr., W. Z. Bradford, S. Castro-Bernardini et al., "A phase 3 trial of pirfenidone in patients with idiopathic pulmonary fibrosis," *The New England Journal of Medicine*, vol. 370, no. 22, pp. 2083–2092, 2014.

[22] L. Richeldi, R. M. du Bois, G. Raghu et al., "Efficacy and safety of nintedanib in idiopathic pulmonary fibrosis," *The New England Journal of Medicine*, vol. 370, no. 22, pp. 2071–2082, 2014.

[23] T. J. Huie, A. L. Olson, G. P. Cosgrove et al., "A detailed evaluation of acute respiratory decline in patients with fibrotic lung disease: aetiology and outcomes," *Respirology*, vol. 15, no. 6, pp. 909–917, 2010.

[24] F. Calabrese, A. Kipar, F. Lunardi et al., "Herpes virus infection is associated with vascular remodeling and pulmonary hypertension in idiopathic pulmonary fibrosis," *PLoS One*, vol. 8, no. 2, article e55715, 2013.

[25] T. R. McMillan, B. B. Moore, J. B. Weinberg et al., "Exacerbation of established pulmonary fibrosis in a murine model by gammaherpesvirus," *American Journal of Respiratory and Critical Care Medicine*, vol. 177, no. 7, pp. 771–780, 2008.

[26] H. Qiu, D. Weng, T. Chen et al., "Stimulator of interferon genes deficiency in acute exacerbation of idiopathic pulmonary fibrosis," *Frontiers in Immunology*, vol. 8, p. 1756, 2017.

[27] Y. Umeda, M. Morikawa, M. Anzai et al., "Acute exacerbation of idiopathic pulmonary fibrosis after pandemic influenza A (H1N1) vaccination," *Internal Medicine*, vol. 49, no. 21, pp. 2333–2336, 2010.

[28] S. C. Wootton, D. S. Kim, Y. Kondoh et al., "Viral infection in acute exacerbation of idiopathic pulmonary fibrosis," *American Journal of Respiratory and Critical Care Medicine*, vol. 183, no. 12, pp. 1698–1702, 2011.

[29] M. R. J. Kolb and L. Richeldi, "Viruses and acute exacerbations of idiopathic pulmonary fibrosis: rest in peace?," *American Journal of Respiratory and Critical Care Medicine*, vol. 183, no. 12, pp. 1583-1584, 2011.

[30] B. W. Kinder, K. K. Brown, M. I. Schwarz, J. H. Ix, A. Kervitsky, and T. E. King Jr, "Baseline BAL neutrophilia predicts early mortality in idiopathic pulmonary fibrosis," *Chest*, vol. 133, no. 1, pp. 226–232, 2008.

[31] M. S. Wilson, S. K. Madala, T. R. Ramalingam et al., "Bleomycin and IL-1beta-mediated pulmonary fibrosis is IL-17A dependent," *The Journal of Experimental Medicine*, vol. 207, no. 3, pp. 535–552, 2010.

[32] S. Mi, Z. Li, H. Z. Yang et al., "Blocking IL-17A promotes the resolution of pulmonary inflammation and fibrosis via TGF-β1–dependent and –independent mechanisms," *Journal of Immunology*, vol. 187, no. 6, pp. 3003–3014, 2011.

[33] M. M. Curtis and S. S. Way, "Interleukin-17 in host defence against bacterial, mycobacterial and fungal pathogens," *Immunology*, vol. 126, no. 2, pp. 177–185, 2009.

[34] A. Cruz, A. G. Fraga, J. J. Fountain et al., "Pathological role of interleukin 17 in mice subjected to repeated BCG vaccination after infection with Mycobacterium tuberculosis," *The Journal of Experimental Medicine*, vol. 207, no. 8, pp. 1609–1616, 2010.

[35] G. Markel, E. Bar-Haim, E. Zahavy et al., "The involvement of IL-17A in the murine response to sub-lethal inhalational infection with Francisella tularensis," *PLoS One*, vol. 5, no. 6, article e11176, 2010.

[36] C. Gonzalez-Lombana, C. Gimblet, O. Bacellar et al., "IL-17 mediates immunopathology in the absence of IL-10 following Leishmania major infection," *PLoS Pathogens*, vol. 9, no. 3, article e1003243, 2013.

[37] C. R. Crowe, K. Chen, D. A. Pociask et al., "Critical role of IL-17RA in immunopathology of influenza infection," *Journal of Immunology*, vol. 183, no. 8, pp. 5301–5310, 2009.

[38] W. Hou, H. S. Kang, and B. S. Kim, "Th17 cells enhance viral persistence and inhibit T cell cytotoxicity in a model of chronic virus infection," *The Journal of Experimental Medicine*, vol. 206, no. 2, pp. 313–328, 2009.

[39] D. Jiang, J. Liang, J. Hodge et al., "Regulation of pulmonary fibrosis by chemokine receptor CXCR3," *The Journal of Clinical Investigation*, vol. 114, no. 2, pp. 291–299, 2004.

[40] M. Zeremski, R. Dimova, Q. Brown, I. M. Jacobson, M. Markatou, and A. H. Talal, "Peripheral CXCR3-associated chemokines as biomarkers of fibrosis in chronic hepatitis C virus infection," *The Journal of Infectious Diseases*, vol. 200, no. 11, pp. 1774–1780, 2009.

[41] R. J. Noelle and E. C. Nowak, "Cellular sources and immune functions of interleukin-9," *Nature Reviews Immunology*, vol. 10, no. 10, pp. 683–687, 2010.

[42] H. C. Chang, S. Sehra, R. Goswami et al., "The transcription factor PU.1 is required for the development of IL-9-producing T cells and allergic inflammation," *Nature Immunology*, vol. 11, no. 6, pp. 527–534, 2010.

[43] W. Elyaman, E. M. Bradshaw, C. Uyttenhove et al., "IL-9 induces differentiation of TH17 cells and enhances function of FoxP3+ natural regulatory T cells," *Proceedings of the National Academy of Sciences of the United States of America*, vol. 106, no. 31, pp. 12885–12890, 2009.

[44] P. Licona-Limón, J. Henao-Mejia, A. U. Temann et al., "Th9 cells drive host immunity against gastrointestinal worm infection," *Immunity*, vol. 39, no. 4, pp. 744–757, 2013.

Hindawi
Mediators of Inflammation
Volume 2018, Article ID 6808934, 14 pages
https://doi.org/10.1155/2018/6808934

Research Article

RIG-I Signaling via MAVS Is Dispensable for Survival in Lethal Influenza Infection *In Vivo*

Wenxin Wu,[1] **Xiaoqiu Wang**,[2] **Wei Zhang**,[1] **Lili Tian**,[1] **J. Leland Booth**,[1] **Elizabeth S. Duggan**,[1] **Sunil More**,[3] **Lin Liu**,[3] **Mikhail Dozmorov**,[4] **and Jordan P. Metcalf**[1,5,6]

[1]*Pulmonary, Critical Care & Sleep Medicine, Department of Medicine, University of Oklahoma Health Sciences Center, Oklahoma City, Oklahoma, USA*
[2]*Department of Pediatric Respiratory Medicine, Pubin Children Hospital, Shanghai Children Medical Center Affiliated to Shanghai Jiao Tong University School of Medicine, Shanghai 200092, China*
[3]*The Lundberg-Kienlen Lung Biology and Toxicology Laboratory, Department of Physiological Sciences, Center for Veterinary Health Sciences, Oklahoma State University, Stillwater, Oklahoma, USA*
[4]*Department of Biostatistics, Virginia Commonwealth University, Richmond, VA 23298, USA*
[5]*Department of Microbiology and Immunology, University of Oklahoma Health Sciences Center, Oklahoma City, Oklahoma, USA*
[6]*Veterans Affairs Medical Center, Oklahoma City, Oklahoma, USA*

Correspondence should be addressed to Jordan P. Metcalf; jordan-metcalf@ouhsc.edu

Received 18 June 2018; Accepted 26 August 2018; Published 8 November 2018

Academic Editor: Bishi Fu

Retinoic acid-inducible gene I (RIG-I) is an important regulator of virus-induced antiviral interferons (IFNs) and proinflammatory cytokines. It requires interaction with an adaptor molecule, mitochondrial antiviral-signaling protein (MAVS), to activate downstream signaling pathways. To elucidate the mechanism(s) by which RIG-I-dependent recognition of IAV infection *in vivo* triggers innate immune responses, we infected mutant mice lacking RIG-I or MAVS with influenza A virus (IAV) and measured their innate immune responses. As has previously been demonstrated with isolated deletion of the virus recognition receptors TLR3, TLR7, and NOD2, RIG-I or MAVS knockout (KO) did not result in higher mortality and did not reduce IAV-induced cytokine responses in mice. Infected RIG-I KO animals displayed similar lung inflammation profiles as did WT mice, in terms of the protein concentration, total cell count, and inflammatory cell composition in the bronchoalveolar lavage fluid. RNA-Seq results demonstrated that all types of mice exhibited equivalent antiviral and inflammatory gene responses following IAV infection. Together, the results indicated that although RIG-I is important in innate cytokine responses *in vitro*, individual deletion of the genes encoding RIG-I or MAVS did not change survival or innate responses *in vivo* after IAV infection in mice.

1. Introduction

Infection with influenza A virus (IAV), a negative-sense single-strand RNA virus, is a major cause of morbidity and mortality. There are approximately 5 million clinical infections and 250,000–500,000 deaths resulting from yearly IAV epidemics around the globe, particularly in people over 65 years old who account for 90% of all influenza-associated deaths in the USA [1, 2].

Innate immunity is the first line of defense against virus infection that triggers the expression of interferon (IFN) and proinflammatory cytokines. Cells of the innate immune system detect viral infection largely through pattern recognition receptors (PRRs) present either on the cell surface or within distinct intracellular compartments. PRRs have the ability to distinguish self from nonself molecules. The innate immune system responds to influenza through three classes of PRRs. First, retinoic acid-inducible gene I (RIG-I) and melanoma differentiation-associated gene 5 (MDA5), widely expressed in various types of cells, such as myeloid dendritic cells (DC), macrophages, epithelial cells, and fibroblasts, detect intracellular ssRNAs and transcriptional intermediates

of IAV [3, 4]. After recognition of virus, RIG-I or MDA5 binds to the downstream adaptor molecule, mitochondrial antiviral-signaling protein (MAVS), activating antiviral and proinflammatory signaling. Second, endosomal Toll-like receptors (TLRs) are also involved in IAV recognition. TLR3, a double-strand RNA sensor, is used by some epithelial cells and myeloid DC to detect the viral replicative intermediate dsRNA [5]. Plasmacytoid DC use TLR7 to recognize influenza genomic RNA upon release in late endosomes [6]. Finally, the nucleotide-binding domain and leucine-rich repeat-containing proteins (NLRP), including NLRP3 and nucleotide-binding oligomerization domain 2 (NOD2), may serve as intracellular mediators of IAV initiated host-cell signaling through the formation of a biochemical complex called the inflammasome in myeloid cells and airway epithelial cells [7–9].

The innate immune response triggered by PRR activation is essential for controlling viral infection. PRR receptors are the primary modulators of proinflammatory cytokine and chemokine production that activates leukocytes and recruits them to the site of infection, ideally optimizing immune responses and enhancing recovery [10]. However, excessive inflammation caused by an uncontrolled innate immune response is harmful to the host and contributes to mortality in IAV-infected patients [11]. The acute surge of cytokine release leads to an intense infiltration and activation of inflammatory cells, which is responsible for severe inflammation that exacerbates chronic lung diseases. Highly pathogenic IAV strains, including pandemic stains and avian influenza, are usually associated with excessive cytokine responses [12, 13].

RIG-I is essential for IFN induction during RNA virus infections of non-pDC cell types, and mice that are deficient in RIG-I-like receptor signaling pathways are extremely susceptible to other RNA viruses [14–16]. Our previous work using RIG-I transgenic mice showed that RIG-I overexpression in mice protects against cigarette smoke enhanced susceptibility of these animals to influenza infection [17]. Although PRRs are important in innate cytokine response *in vitro*, the deletion of genes encoding PRRs other than RIG-I does not worsen survival during IAV infection *in vivo*. In fact, mice deficient in TLR3 had an unexpected survival advantage during influenza infection perhaps due to significantly reduced inflammatory mediator induction in the animals [18]. Deletion of NOD2 did not change the survival rates of mice during lethal influenza infection [19].

In order to determine whether RIG-I signaling was important for survival and IAV-induced cytokine responses in mice, we infected mutant mice lacking RIG-I or MAVS with IAV, measured their innate immune responses, including IFN and proinflammatory cytokine induction, and determined their mortality. The mechanism(s) by which RIG-I-dependent recognition of IAV infection *in vivo* triggers innate immune responses was also evaluated.

2. Results

2.1. RIG-I Is Not Required for Survival in Lethal IAV Infection. RIG-I$^{-/-}$ mice in a C57BL/6 background were prepared as described in Materials and Methods and, as with all other mouse strains used, were genotyped and bred under pathogen-free conditions in the animal facility at the University of Oklahoma Health Sciences Center. To confirm RIG-I disruption, we isolated lung AEC II from RIG-I knockout (KO) and wild-type (WT) mice. Isolated cells were cultured for 2 days, infected with IAV for 24 h, and stained for RIG-I. IAV-infected WT AEC express high levels of RIG-I while infected RIG-I KO AEC do not express RIG-I (Figure 1(a)). We also confirmed RIG-I KO in mouse lung by immunostaining. Mice were infected with IAV and sacrificed after 6 days. Lungs were processed for immunohistochemistry for detection of IAV nucleoprotein (NP) and RIG-I. PBS mock control KO and WT mouse lungs had minimal immunofluorescence when stained for RIG-I. As expected, RIG-I was highly induced in lungs from IAV-infected WT mice. Viral NP expression was detected in lungs from both WT and KO animals when infected with IAV (Figure 1(b)). The results demonstrate that virus replicated in mouse lungs after IAV infection with concurrent induction of RIG-I. The data demonstrate that RIG-I protein expression is deficient in RIG-I KO AEC II and in RIG-I KO mouse lung, even when infected with IAV.

In order to determine the *in vivo* role of RIG-I in survival during severe IAV infection, we inoculated RIG-I KO and littermate WT animals with a lethal dose of virus (1000 pfu). Unexpectedly, we found that RIG-I KO mice had no significant difference in survival after IAV challenge as compared to similarly exposed WT mice by Kaplan-Meier survival analysis ($p = 0.696$, $n = 13$ and 15, respectively, Figure 1(c)). Weight loss was significant in both infected groups and reached a nadir at 7 days after infection though it did not differ significantly between the groups (Figure 1(d)).

2.2. Inflammatory Responses in the Lung Are Induced during IAV Infection Even in the Absence of RIG-I. To investigate the role of RIG-I in the inflammatory response to IAV, RIG-I KO and WT C57BL/6 mice were intranasally infected with 300 pfu IAV PR8. The mock group was sham infected by inoculation with a single dose of an equal volume of PBS. Animals were sacrificed at 2, 4, and 6 days after infection, and bronchoalveolar lavage fluids (BALF) were collected to assess cellular infiltration and mediator content in the airspaces.

BAL is the most common manner to sample the components of the epithelial lining fluid and to determine the amount of total protein, an index of transudation from the vascular compartment into the lungs, and reflects lung injury. We found no significant difference in BAL protein levels in both infected mouse groups at all time points (Figure 2(a)).

In terms of total inflammatory cells, IAV inoculation not only caused a significant increase in the total viable leukocytes in BALF from day 2 but also significantly increased the percentage of neutrophils in BALF in all infected groups (Figures 2(b) and 2(c)). However, RIG-I KO did not significantly alter the composition of the inflammatory cell population during viral infection. At day 6 after infection, RIG-I KO mice appeared to have more inflammatory cell infiltration into BALF than did WT mice, but the difference was not statistically significant. Thus, the total viable cell numbers in BALF were similar in both mouse groups

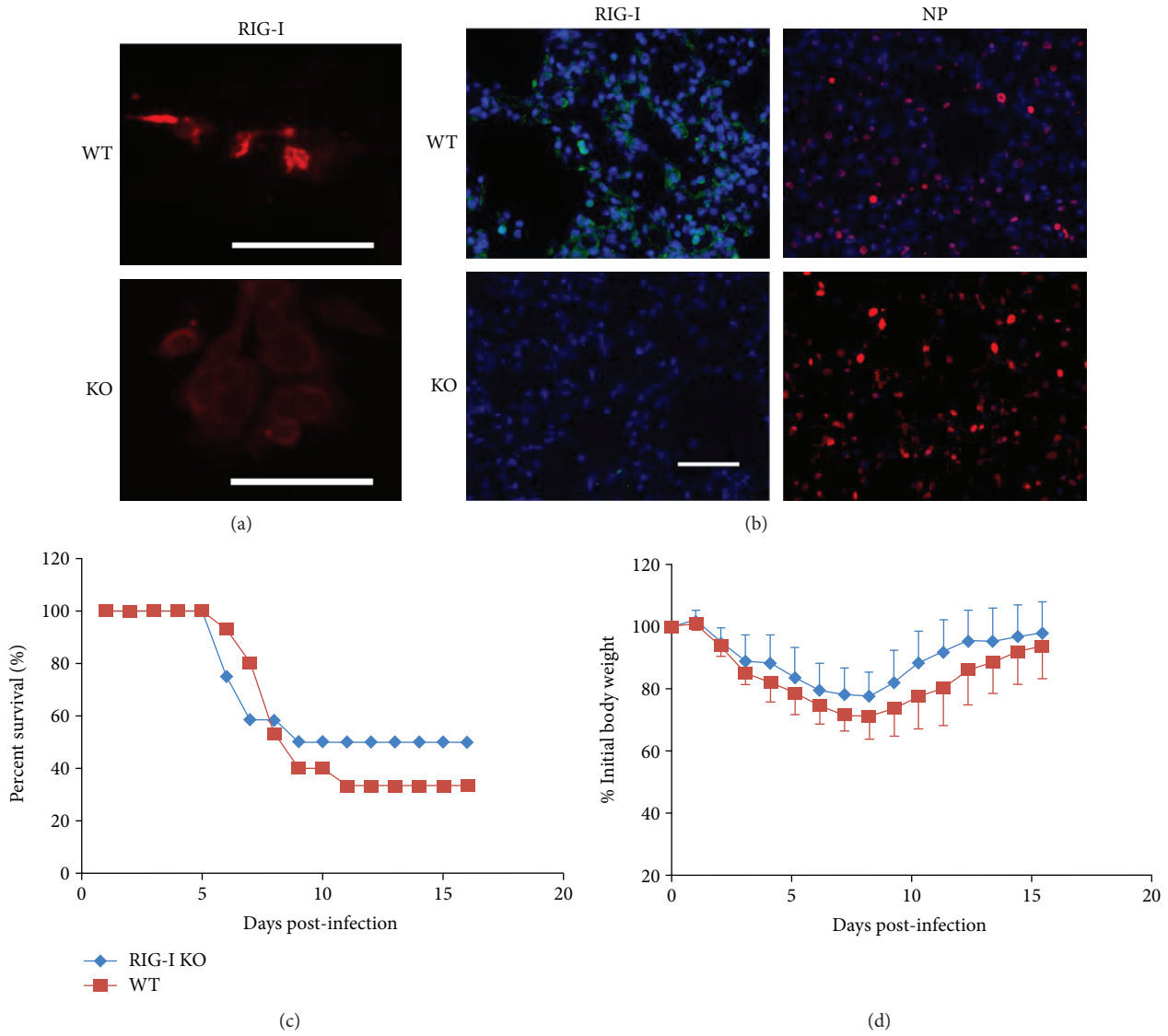

Figure 1: RIG-I is dispensable for survival and weight loss during influenza infection. (a) Wild-type (WT), but not RIG-I KO, mice express RIG-I in isolated type II alveolar epithelial cells (AEC). AEC II were infected with IAV PR8 at an MOI of 6 and incubated for an additional 24 h to stimulate RIG-I production. The cells were processed for immunohistochemistry for detection of RIG-I (red). Scale bars = 50 μm. (b) WT, but not RIG-I KO, mice infected with IAV express RIG-I in the lung. Immunohistochemical staining of RIG-I and IAV nucleoprotein (NP) in WT and RIG-I KO mice. Mice were intranasally infected with 300 pfu IAV PR8 or mock infected with PBS. Mouse lungs were processed for immunohistochemistry for detection of RIG-I protein (green) or IAV NP (red). The bar represents 100 μm. (c and d) RIG-I KO and littermate WT mice were intranasally inoculated with IAV at 1000 pfu/mouse. Mortality (c) and body weights (d) were monitored daily. Body weight data were normalized to each mouse's starting body weight. Data are expressed as mean ± standard deviation ($n = 13$ for RIG-I KO mice; $n = 15$ for WT mice).

at all time points. Plaque assays of whole lung showed that viral titers were equally elevated in WT and KO mice after 6 days of infection (Figure 2(d)). Thus, as for mortality, the viral burden in the lung was not altered by RIG-I KO.

Examination of histopathology revealed that IAV-infected lungs in both types of mice showed typical viral pneumonia with interstitial edema and inflammatory infiltration, as well as necrotizing bronchitis and bronchiolitis. IAV infection resulted in the expected neutrophilic alveolar infiltrate with some lymphocytes. However, we found little difference in terms of the severity of inflammation in RIG-I KO and WT mice (Figure 2(e)).

2.3. RIG-I Deficiency Does Not Alter Antiviral Interferon and Inflammatory Cytokine Responses to Influenza Infection. In order to determine how mice survive IAV infection in the absence of a major antiviral sensor, we assessed PRR and cytokine expression during infection of both mouse strains. Mice were inoculated intranasally with a single, nonlethal dose of the IAV PR8 strain (300 pfu). Lung tissues and BALF were collected at 2, 4, and 6 days after infection, and PRR and cytokine expression was determined by qRT-PCR or multiplex immunoassay, respectively. All tested PRR mRNAs were induced by virus in lungs from WT mice at 2 days after PR8 infection (Figure 3(a)). Specifically, pulmonary expression of

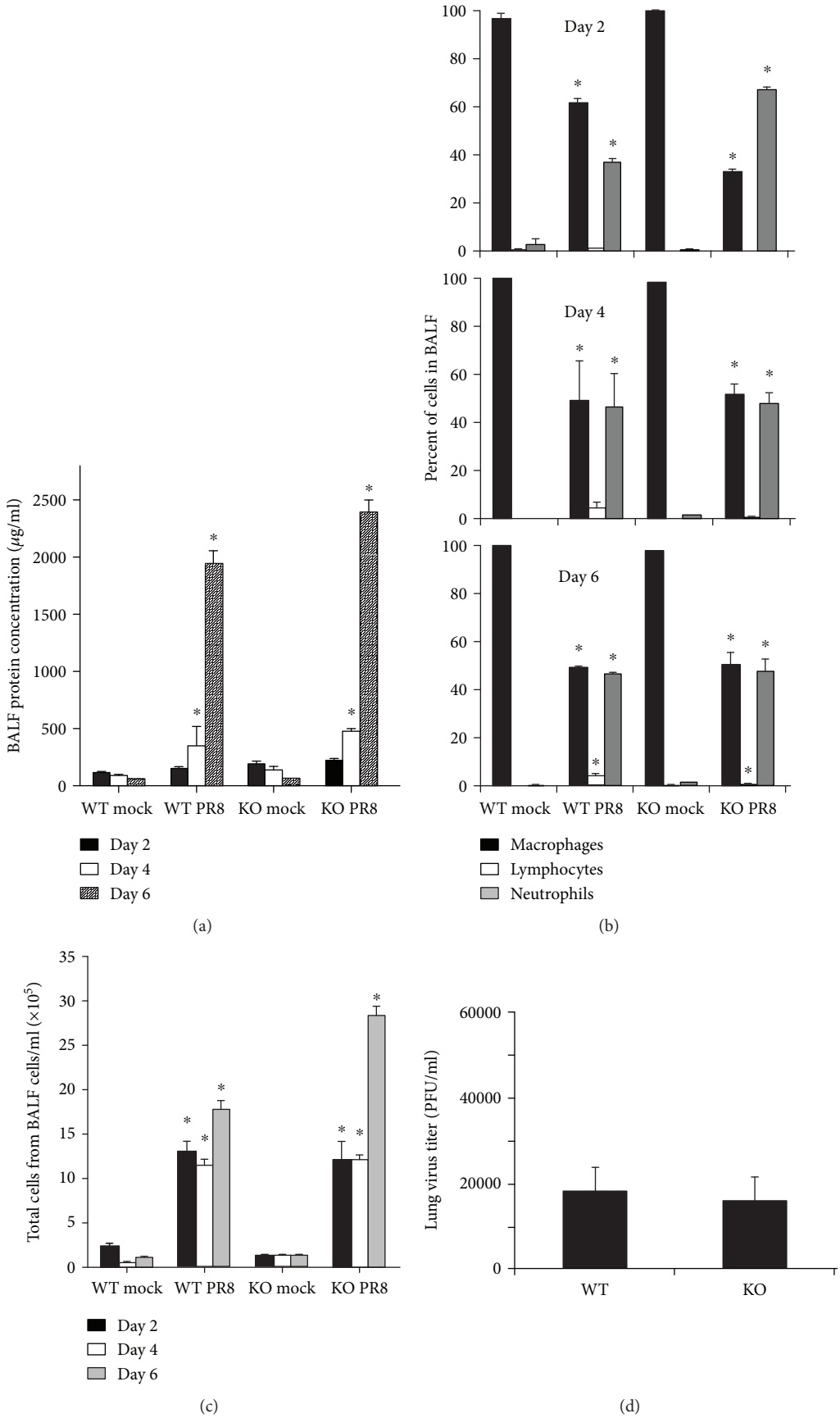

Figure 2: Continued.

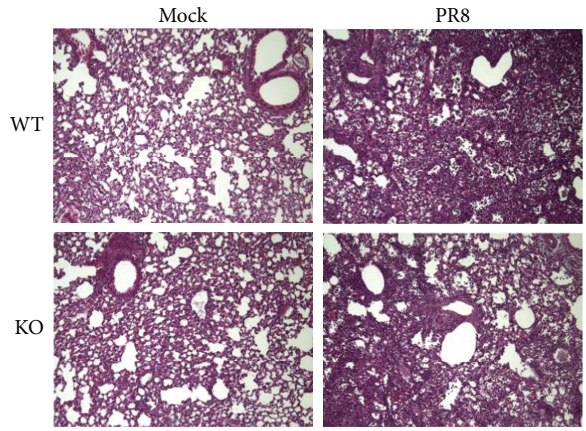

(e)

Figure 2: Inflammatory profile in the bronchoalveolar lavage fluid (BALF) and virus titer in the lung. WT and RIG-I KO mice were intranasally infected with 300 pfu of the IAV PR8 or mock infected with PBS. BALF was harvested at the indicated time points after infection. Total protein levels (a), immune cell differential (b), and total cells (c) in BALF were determined. Cytospins of the cells were prepared using a Cytopro Cytocentrifuge and stained with Diff-Quik. Differential counts were manually determined using the morphology of more than 400 cells/sample from 2 slides/mouse. Lung tissue viral titers were determined at 6 days postinfection by plaque assay on MDCK cells (d). Data are expressed as means ± SEM ($n \geq 3$/group). * denotes significant difference compared to the corresponding mock infected groups ($p < 0.05$). (e) Mouse lung tissue pathology after IAV infection. Mice were intranasally infected with 300 pfu of IAV PR8 strain. Samples were harvested after 6 days. Lung tissue sections prepared from the infected mice were fixed, processed, and stained with H&E. The lungs of 3 mice from each treatment group were processed for histology, and results shown were typical for the group (200x magnification).

RIG-I was markedly upregulated following influenza infection in WT mice. As expected, there was no RIG-I expression in RIG-I KO mice with PR8 infection. Remarkably, we found that NOD2 mRNA expression was much greater in RIG-I KO mouse lung as compared with WT mice, especially at day 6 after infection. PR8 induction of NOD2 mRNA in RIG-I KO mice (15-fold) was significantly greater than in WT mice (2-fold, Figure 3(a)). This suggests compensatory NOD2 overexpression in the absence of RIG-I. To confirm this *in vitro*, we isolated fibroblasts from the ears of RIG-I KO and WT mice. NOD2 mRNA induction by IAV was greater in cells from KO mice than in cells from WT mice (Figure 3(b)).

We also measured IFN and cytokine mRNA induction in response to IAV in these animals. The IFN-β and λ2/3 response to flu infection was similar in RIG-I KO and WT mice. Consistent with the inflammatory cell profile in BALF, mRNA expression of the proinflammatory cytokines IL-6, TNFα, and IP-10 was highly and similarly induced in both genotypes during IAV infection (Figure 4). The data suggest that RIG-I is not required for the innate antiviral and proinflammatory cytokine response to IAV in mice. Finally, to confirm that cytokine induction was reflected at the level of translation, we measured cytokine proteins in BALF and blood cytokine levels from mice exposed to IAV in both genotypes using multiplex immunoassay (Figure 5). The protein levels of IL-6, MCP-1, TNFα, IP-10, and IFN-γ in serum showed similar patterns to those seen in BALF.

2.4. MAVS Is Dispensable for Survival in IAV Infection In Vivo. In order to further examine the role of RIG-I pathway activation in the response to IAV infection, we next investigated whether depletion of MAVS, the RIG-I adaptor, affects the survival rate during IAV infection. We inoculated MAVS KO and littermate WT animals with a lethal dose of virus (1000 pfu). As we found for RIG-I KO, MAVS KO had no significant effect on survival after IAV challenge, with approximately 18% and 23% survival at 16 days in MAVS KO and WT mice ($n = 18$ and 19, respectively, Figure 6(a)). Weight loss was significant in both infected groups and reached a nadir at 7 days after infection (Figure 6(b)). The body weight data agreed with the survival data in that there was no significant difference in weight loss between IAV-infected MAVS KO and WT mice (approximately 31% vs. 28% loss for MAVS KO and their littermate WT at day 7).

We also compared PRR and cytokine expression during IAV infection of both mouse strains. Mice were inoculated intranasally with a single, nonlethal dose of the IAV PR8 strain (300 pfu). Lung tissues were collected at 6 days after infection, and PRR and cytokine expression was determined by qRT-PCR. Again, all tested PRR mRNAs were induced by virus in lungs from WT mice after PR8 infection (Figure 6(c)). Lung expression of RIG-I and MDA5 was modestly upregulated following influenza infection in MAVS KO mice as compared with WT mice, suggesting that there was attempted compensation for MAVS KO by overexpression of RIG-I and MDA5. There was also a markedly compensatory increase in TLR3 expression in MAVS KO mice. Surprisingly, we found that TLR7 mRNA expression was significantly lower in MAVS KO mice as compared with WT mice. To assess downstream effects of PRR signaling, we measured IFN-β and IL-6 cytokine mRNA induction in response to IAV in these animals. The IL-6 response to flu infection was similar in RIG-I KO and WT mice, but IFN-β

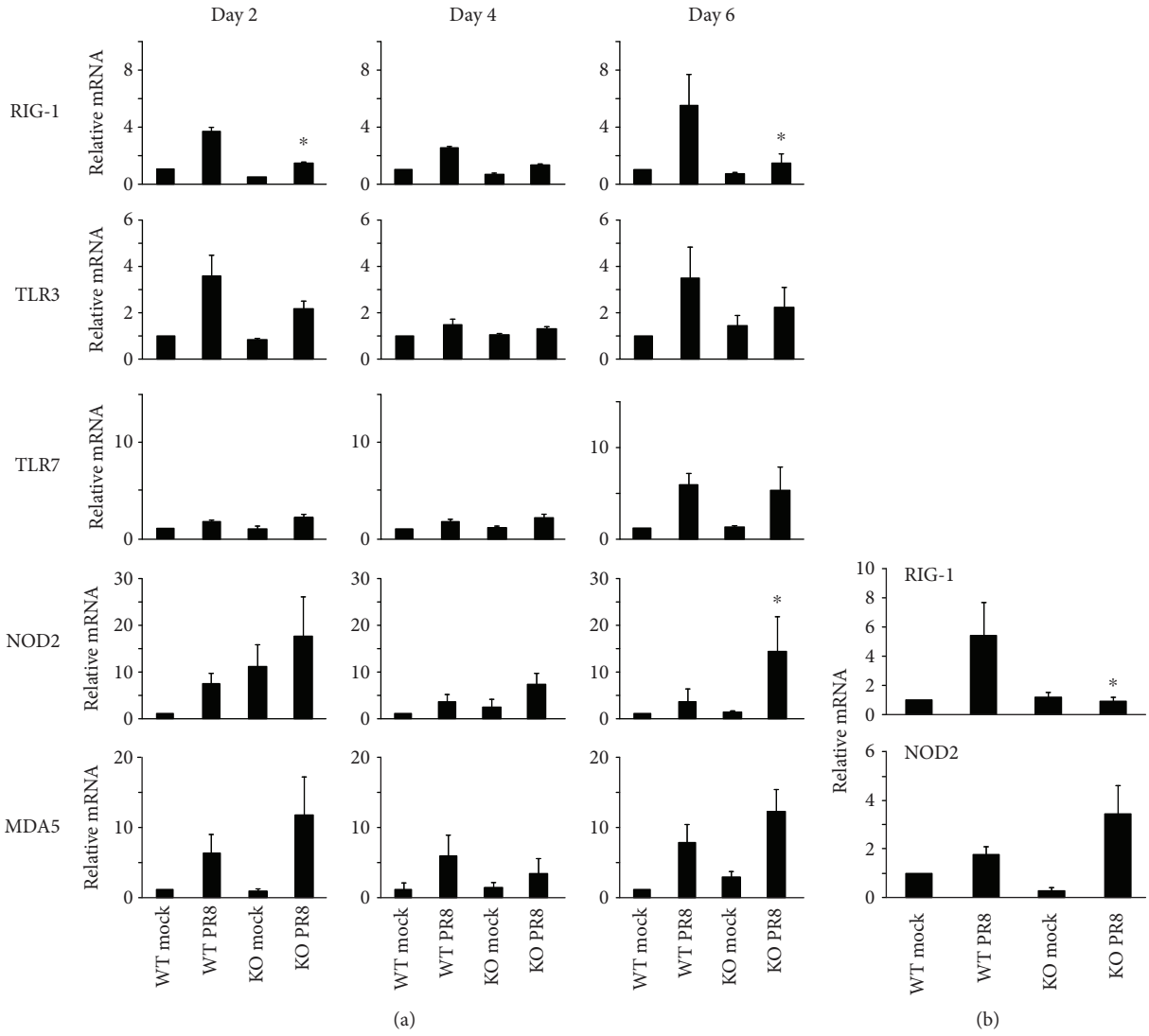

Figure 3: Virus PRR mRNA induction in RIG-I KO mice during IAV infection. (a) mRNA induction in mouse lung. Mice were infected with 300 pfu of the IAV PR8 strain. Mock-treated mice were inoculated with PBS. At the indicated time points, the mice were sacrificed and lung tissues were collected for RNA preparation. (b) mRNA induction in primary ear fibroblasts infected with IAV. Primary ear fibroblasts isolated from RIG-I WT and KO mice were infected with IAV PR8 at an MOI of 1. After 24 h, cells were collected for RNA extraction. The mRNA levels were assessed by qRT-PCR and normalized by β-actin. Data are expressed as means ± SEM of fold increase over the WT mock group ($n \geq 3$ per group). For clarity, we only show significant differences ($^*p < 0.05$) between the PR8-infected RIG-I KO group and the PR8-infected WT group. p value was calculated from the ΔΔCt values from different experimental groups.

mRNA expression was significantly reduced in MAVS KO mice as compared to that seen in WT mice. The data suggest that IFN-β expression is affected in the lung at day 6 while proinflammatory cytokine response is the same in both types of mice during IAV infection.

2.5. Interferon and Inflammatory Response Genes Are Induced during IAV Infection Even in the Absence of RIG-I or MAVS. To better understand the effect of modulation of RIG-I signaling on global gene expression, we used high-throughput RNA sequencing (RNA-Seq) technology, a powerful way to profile the transcriptome with great efficiency and higher accuracy. RNA-Seq was performed on mRNA derived from WT, RIG-I KO, and MAVS KO mouse lungs at 6 days postinfection. Using the 43,304 annotated genes in the mouse genome database, gene expression was quantified and compared between the mock and the virus-infected groups, and differentially expressed genes (DEGs) were identified using a false discovery rate (FDR) of 0.1.

All three types of mice shared 32.6% of total DEGs during infection (Figure 7(a)). The DEGs that distinctively changed in each strain only accounted for 17.7% (WT), 10.2% (RIG-I KO), and 8.9% (MAVS KO). To examine the biological roles, a Gene Ontology (GO) enrichment analysis was applied to the DEGs (Figure S1). Notably, the DEGs were mostly enriched in the regulation of innate immune reactions, such as the defense response, the antiviral response, and the inflammatory response. Nine out of 12 biological processes overlap each other between WT and RIG-I or MAVS KO mice during IAV infection.

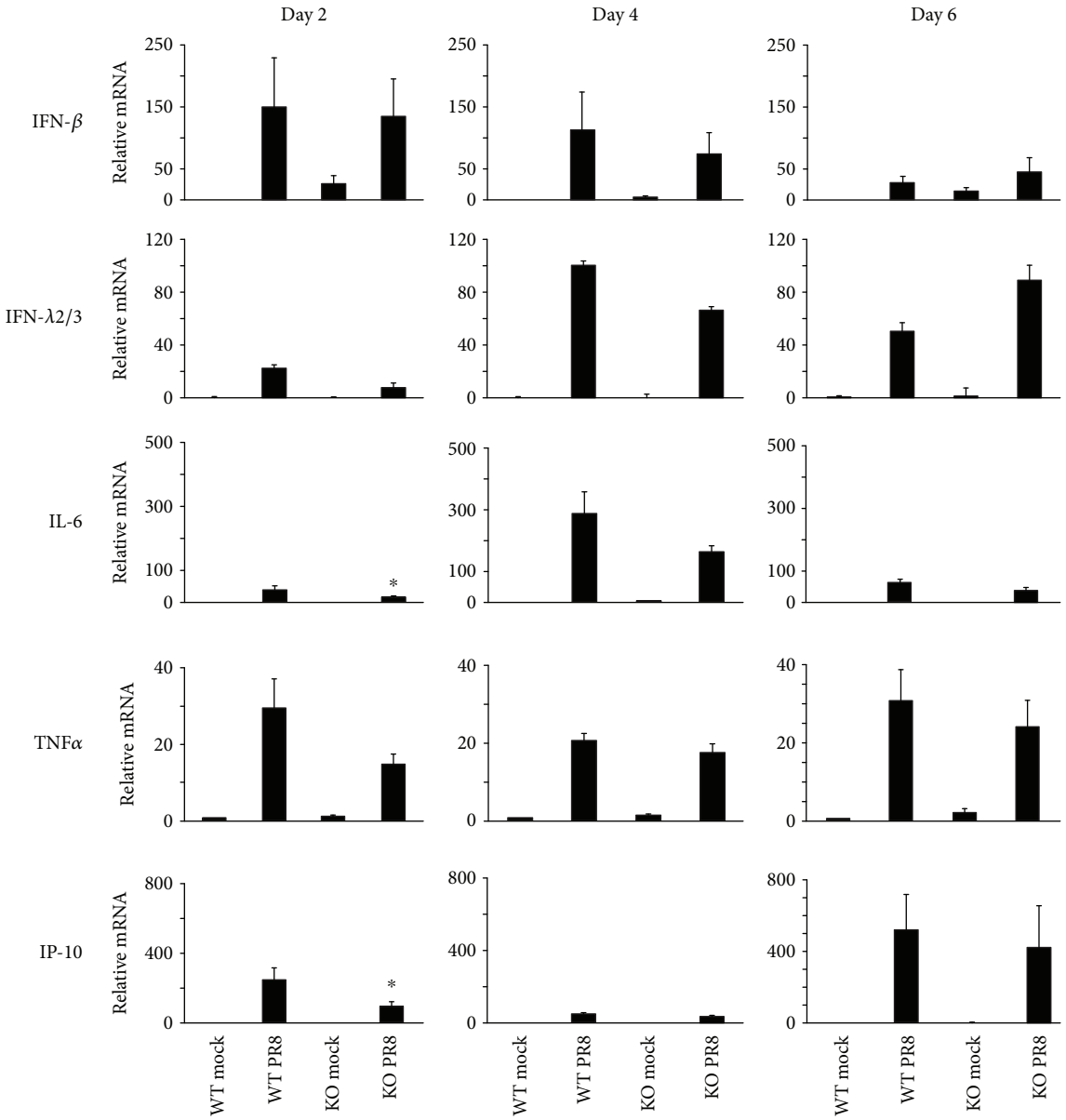

Figure 4: Antiviral and proinflammatory cytokine mRNA induction during IAV infection. Mice were intranasally infected with 300 pfu of the IAV PR8 strain. Mock-treated mice were inoculated with PBS. At the indicated time points, the mice were sacrificed and lung tissues were collected for RNA extraction. IFN and cytokine mRNA levels were assessed by qRT-PCR and normalized to β-actin. Data are expressed as means ± SEM of fold increase ($n \geq 3$ per group). * denotes significant difference compared to the PR8 infected WT group, $p < 0.05$. p value was calculated from the ΔΔCt values from different experimental groups.

Two key innate immune responses that occur during IAV infection and impact survival are interferon responses and inflammatory responses. Therefore, we focused on DEGs in these categories with an FDR of 0.1 that were upregulated by IAV exposure in the WT and KO mouse groups. The $\log_2$ counts per million for the corresponding gene sets were averaged for each group and clustered as heat maps using Euclidean distance and the Ward clustering metric. The yellow/blue gradient indicates high/low gene expression, respectively. In the first set (Figure 7(b)) are genes related to the interferon response genes, including Irf1, Ifi44, Irf7, and Oas1g. The second gene set (Figure 7(c)) included genes related to inflammatory responses, such as Ccl5, Il6, Il1b, and Tnf. The gene expression data shows that IFN response and inflammatory genes were induced by IAV in the absence of RIG-I and MAVS. As demonstrated in Figure 6, RNA-Seq also showed that IAV infection induced IFNb1 3-fold over mock in MAVS KO mice. The induction by IAV was much less than that seen in WT mice. In contrast, MAVS KO did not affect induction of downstream IFN-stimulated genes (ISGs, Ifi44, Ifi204, Ifi47, Ifit2, Ifi205, etc.) by IAV. As downstream genes are similarly activated in KO mice despite differential IFN-β induction, it is likely that other IFNs or cytokines might compensate for IFN-β in the mouse lung [20].

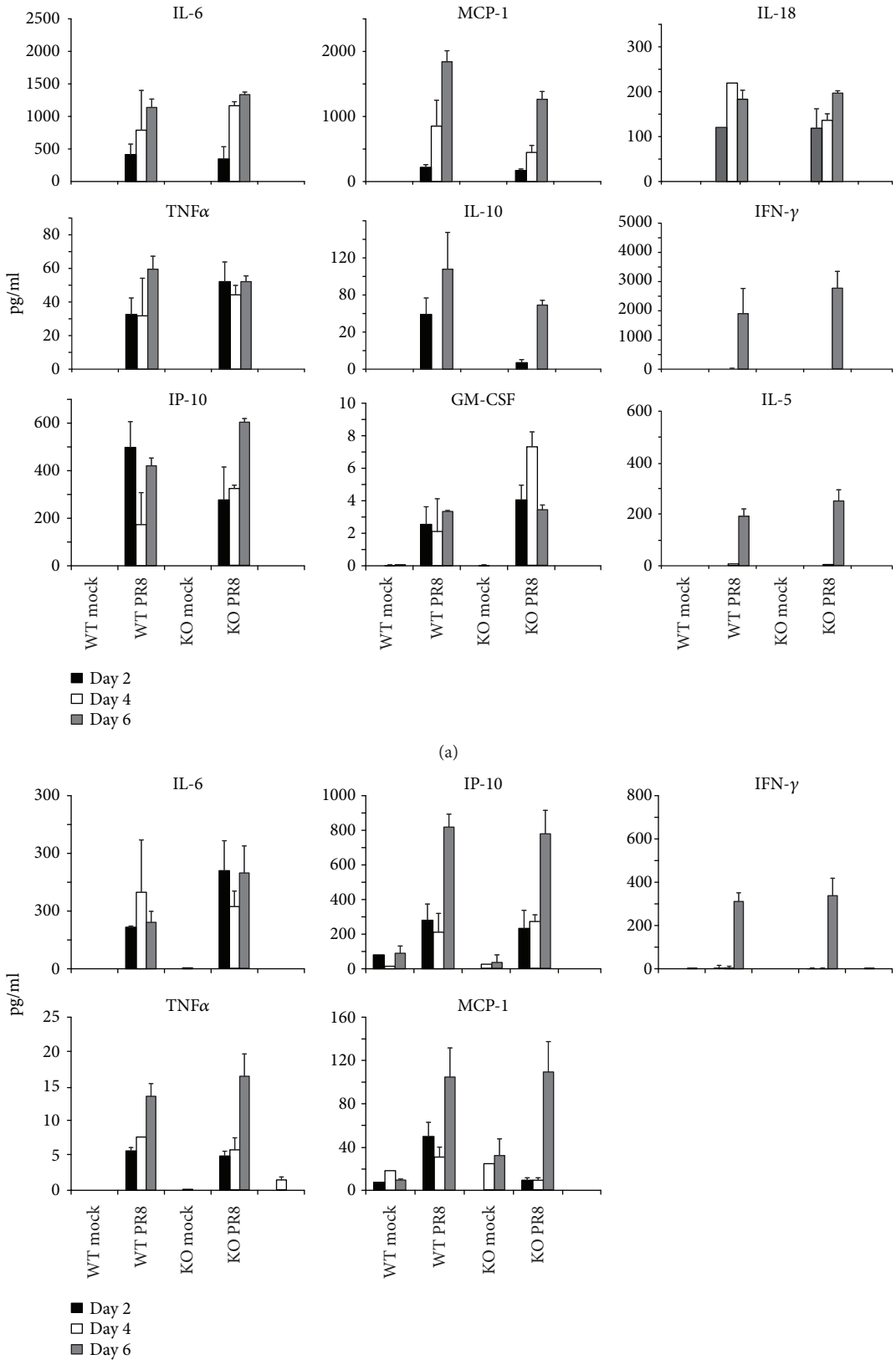

Figure 5: Antiviral and proinflammatory cytokine protein levels in BALF and serum in RIG-I KO and WT mice during IAV infection. Mice were intranasally infected with 300 pfu of the IAV PR8 strain. (a) BALF and (b) serum were harvested at the indicated time points after infection. Mock-treated mice were inoculated with PBS. Antiviral and proinflammatory cytokine protein levels were determined by multiplex immunoassay. Data are expressed as mean ± SEM ($n \geq 3$ per group).

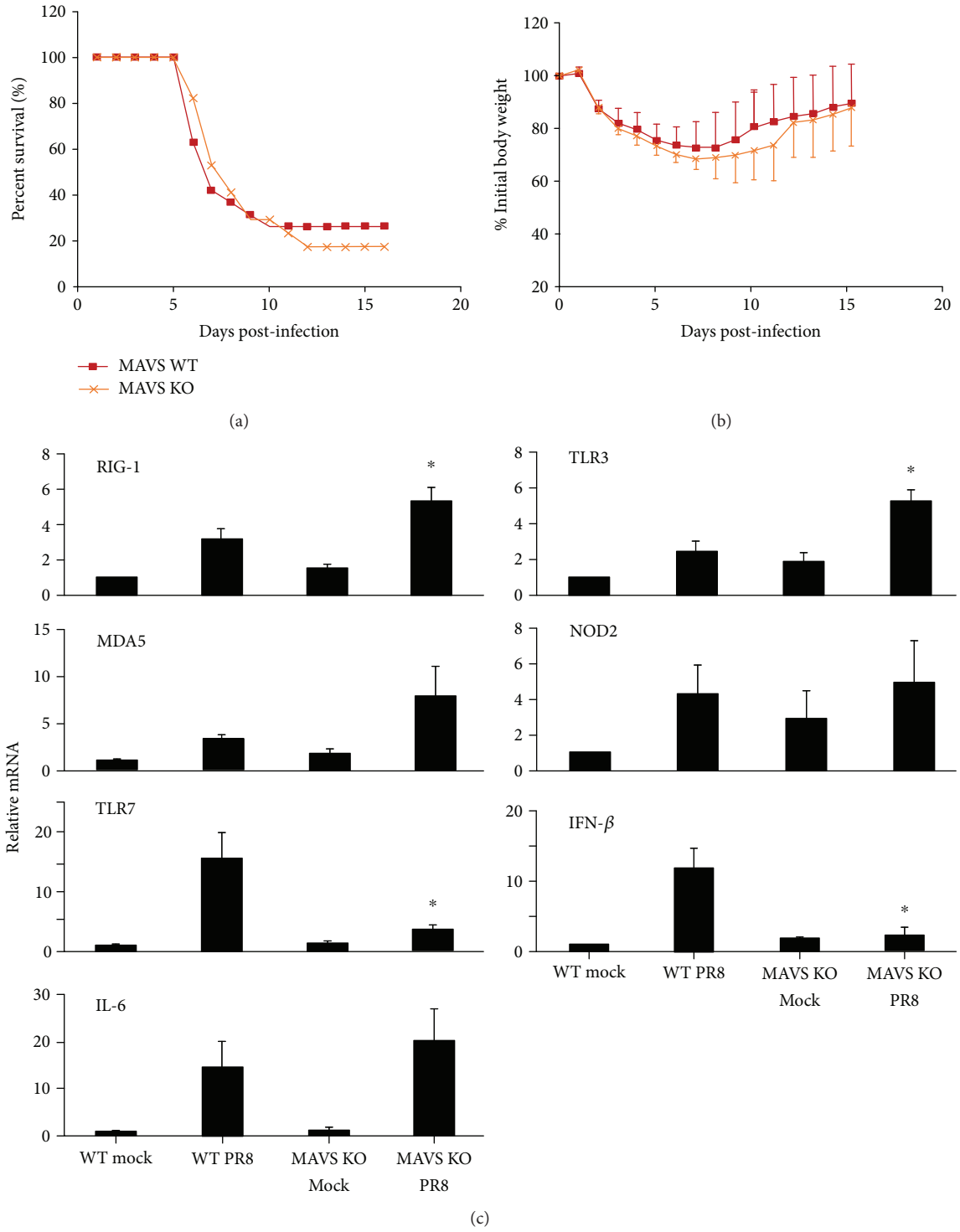

Figure 6: MAVS is dispensable for survival and cytokine induction during influenza infection. MAVS KO and littermate WT mice were intranasally inoculated with IAV at 1000 pfu/mouse. Mortality (a) and body weights (b) were monitored daily. Body weight data were normalized to each mouse's starting body weight. Data are expressed as mean ± standard deviation ($n = 18$ for MAVS KO mice; $n = 19$ for WT mice). (c) PRR and cytokine mRNA induction in mouse lung. Mice were infected with 300 pfu of the IAV PR8 strain. Mock-treated mice were inoculated with PBS. At day 6 postinfection, the mice were sacrificed and lung tissues were collected for RNA preparation. The mRNA levels were assessed by qRT-PCR and normalized β-actin. Data are expressed as mean ± SEM of fold increase ($n \geq 3$ per group). For clarity, we only show significant differences ($^*p < 0.05$) between the PR8-infected MAVS KO group and the PR8-infected WT group. p value was calculated from the ΔΔCt values from different experimental groups.

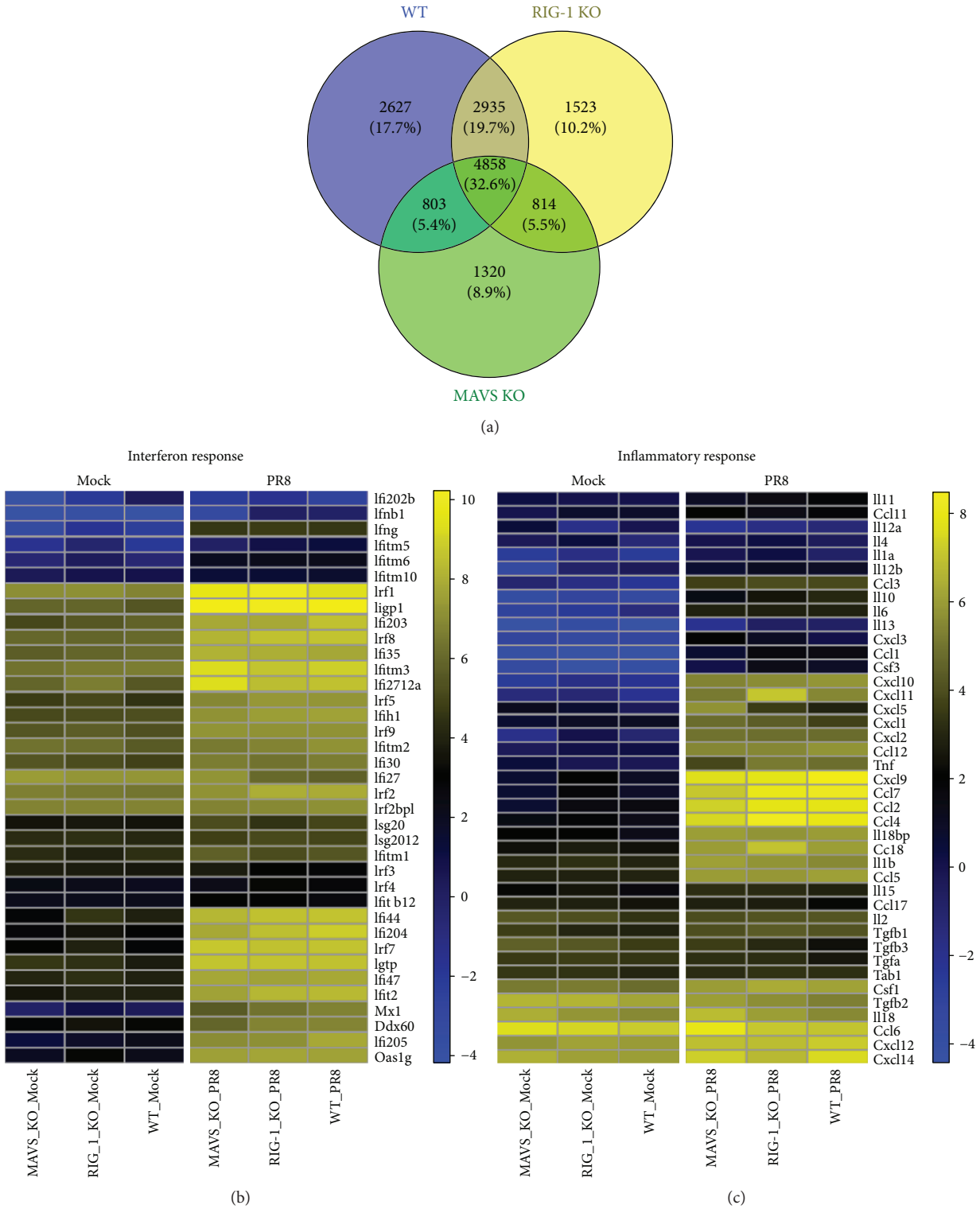

Figure 7: The absence of RIG-I or MAVS does not inhibit induction of interferon or generation of an inflammatory response during IAV infection. WT, RIG-I KO, and MAVS KO mice were mock-infected or infected with the IAV PR8 strain (300 PFU/mouse). At day 6 postinfection, lung tissue was collected, and total RNA was isolated and analyzed for RNA-Seq using 3′ inTAG next-generation sequencing ($n = 6$). (a) Venn diagram showing the distribution of shared differentially expressed genes during IAV infection. Heat map comparing the genes of interferon (b) and inflammatory responses (c). The log2 counts per million for the corresponding gene sets were averaged for each group and clustered as heat maps using the Euclidean distance and Ward clustering metric. The yellow/blue gradient indicates high/low gene expression, respectively.

3. Discussion

The critical role of the RIG-I-MAVS-dependent pathway in recognizing IAV infection and controlling pathogenesis has been established and implies an essential role for RIG-I in immunity against IAV [3, 4, 21]. To further investigate the impact of RIG-I specifically *in vivo*, it would be ideal to examine IAV pneumonia in RIG-I-deficient mice. Two groups previously reported that RIG-I-deficient C57BL/6 mice had developmental defects and have high mortality during embryogenesis [3] or within 3 weeks after birth as a result of extensive hepatocellular apoptosis [22]. A successful approach to generate viable RIG-I$^{-/-}$ mice has been to generate them in a complex background involving 129Sv, C57BL/6, and ICR mice and repeatedly backcross the mice into C57BL/6. We obtained early generation founders of these mice (a kind gift from Dr. Michael Gale, University of Washington) and backcrossed them into a C57BL/6 background to the F4 generation. Similar viable mice containing MDA5$^{-/-}$ in addition to RIG-I$^{-/-}$ in this background have been developed by his group in this manner [23]. The RIG-I$^{-/-}$ mouse line developed in our laboratory described herein has an approximately 94% C57BL/6 genetic background, as determined by microsatellite DNA analysis (see Materials and Methods).

Here, our work showed that RIG-I$^{-/-}$ mice had similar survival and body weight loss compared to WT mice following IAV infection. Infected RIG-I$^{-/-}$ animals displayed a similar pattern of lung inflammation as did WT mice. RNA-Seq results showed that RIG-I KO, MAVS KO, and WT mice exhibited similar induction of antiviral and inflammatory genes following intranasal challenge with IAV. The data suggest that RIG-I's role in the recognition and inhibition of IAV can be replaced by other PRRs in mice. Investigations by other groups demonstrating similar inflammatory responses to IAV in the absence of other PRRs provide additional evidence for the existence of compensatory or complementary *in vivo* mechanisms of PRR induction. For example, TLR7 deficiency does not alter survival and viral clearance following IAV infection but exacerbates body weight loss [24]. Also, lung mRNA expression of IFNs and chemokines from mice infected with IAV is not affected by isolated knockout of the MyD88 or MAVS pathway. This suggests that either the MyD88 or MAVS signaling pathway is sufficient for initial antiviral responses to IAV *in vivo* [25]. Our group has also reported that neither RIG-I nor TLR3 siRNA alone completely blocked IFN induction in human lung epithelial cells. Only double knockdown of RIG-I and TLR3 completely inhibited IFN induction by influenza. This shows that signaling compensation of RIG-I for TLR3, or vice versa, preserving IFN induction by IAV occurs in human lung [26]. Our results combined with other reports strongly suggest that innate immune responses to IAV are not regulated by a single receptor or intracellular signaling pathway. In fact, the response appears to be a well-orchestrated process, which involves multiple complementary PRRs and signaling pathways in different cells and tissues of the body.

Notably, we found that NOD2 or TLR3 mRNA expression was greatly increased in IAV-infected RIG-I or MAVS KO mice, respectively. Thus, activation of NOD2 following IAV infection of mice could compensate for the absence of functional RIG-I. Morosky et al. have shown that RIG-I and NOD2 not only are colocalized to cellular ruffles and cell-cell junctions but also interact directly [27]. Moreover, RIG-I negatively regulates ligand-induced NF-κB signaling mediated by NOD2, and NOD2 negatively regulates type I IFN induction by RIG-I. At the cellular level, it seems likely that RIG-I expression negatively regulates NOD2 signaling and expression, and *vice versa*. In the absence of inhibition of NOD2 signaling by RIG-I in RIG-I$^{-/-}$ mice, unrestrained NOD2 might optimize innate immune responses to viral infections and improve survival. Recently, RNAi screening has implicated the other RIG-I-like receptor, MDA5, as a significant contributor to the cellular defense against IAV [28].

Our current model is that RIG-I serves as the primary PRR for IAV-mediated cytokine induction in the primary IAV infection sites, lung epithelia and macrophages, and that TLR3, NOD2, MDA5, and TLR7 in epithelia and other immune cells serve as important alternate PRRs for generating an innate response to IAV. Our findings show that host recognition of IAV by PRR *in vivo* and initiation of innate immunity are more complex than currently appreciated in that two or three pathways compensate for one another in upregulating antiviral responses. There might be extensive cooperative and/or competitive interactions among different PRRs that support and regulate antiviral sensing and induction of innate immune responses. Our previous publication demonstrated that RIG-I overexpression in the lung improves survival of cigarette smoke-exposed mice during IAV infection [17]. This suggests that, although solitary PRR deficiency might be dispensable in innate response to IAV, overexpression of one major PRR is sufficient to restore the innate response to IAV infection in an immunosuppressed cohort.

Together, our results demonstrate that RIG-I is dispensable for the innate cytokine response to IAV. These results, together with our earlier report showing that overexpression of RIG-I in the lung improves survival during viral infection in smoke-exposed mice, provide new insight into the mechanisms on how the host immune system maintains homeostasis during influenza infections. More studies are required to elucidate the underlying mechanisms of control of viral infection and virus-mediated excessive inflammation by the innate immune response.

4. Materials and Methods

4.1. Ethics Statement. The Institutional Animal Care and Use Committee (IACUC) of the University of Oklahoma Health Sciences Center approved all of the protocols for the animal experiments (protocol number: 17-106-HI). The facility where this research was conducted is accredited by AAALAC. The facility operates according to the Guide for the Care and Use of Laboratory Animals and the requirements of the Animal Welfare Act and Regulations and the Public Health Service Policy on Humane Care and Use of

Laboratory Animals. All procedures were performed by personnel trained in the techniques according to IACUC guidelines. All invasive clinical procedures were performed while animals were anesthetized.

4.2. Preparation of Influenza Virus Stock and Plaque Assays. H1N1 influenza virus, A/PR/34/8 (PR8), was passaged in Madin-Darby canine kidney (MDCK, ATCC, #CCL-34™, Manassas, VA) cells. Virus was grown in MDCK cells in DMEM/F12 with ITS+ (BD Biosciences, Franklin Lakes, NJ) exposed to trypsin, harvested at 72 hours postinfection, and titered by plaque assay in MDCK cells. There was no detectable endotoxin in the final viral preparations used in the experiments as determined by limulus amebocyte lysate assay (Cambrex, Walkersville, MD). The lower limit of detection of this assay is 0.1 EU/ml or approximately 20 pg/ml LPS. For determination of viral titers in infected mice, whole mouse lungs were collected and homogenized in 1 ml of ice-cold PBS. Solid debris was pelleted by centrifugation, and viral titer was determined using a standard plaque assay on MDCK cells.

4.3. Animals. Specific pathogen-free MAVS KO mice with mixed C57BL/6 and 129SvEv genetic background were purchased from the Jackson Laboratory (Bar Harbor, ME). RIG-I$^{-/-}$ mice were generated by Dr. S. Akira's group on a mixed ICR × 129Sv × C57BL/6 genetic background. The RIG-I$^{-/-}$ mice were backcrossed into a C57BL/6 background through the F4 generation and had no developmental defects. The F4 mice were 90–94% C57BL/6 background as determined by JAX using genome scanning (Table 1).

All mice were genotyped and bred under pathogen-free conditions in the animal facility at the University of Oklahoma Health Sciences Center. Mice were housed at 20°C on a 12-hour light/dark cycle in sterile microisolator cages and fed *ad libitum* with sterile chow and water.

4.4. Influenza Virus Infection. IAV infection was performed under isoflurane anesthesia. IAV PR8 stock was diluted in PBS to make lethal and sublethal doses of virus. These virus doses (50 μL solution) were administered by intranasal instillation as the animal was held in a vertical position while being sedated. Control animals received PBS. Mice were monitored daily for 16 days for clinical symptoms (shaking, tiredness, and piloerection), and their weight was recorded daily.

4.5. Bronchoalveolar Lavage (BAL). Mice were sacrificed using isoflurane. BAL was performed using a closed thorax technique by exposing the trachea, nicking the bottom of the larynx, and inserting a 3/4-inch 22-gauge cannula into the proximal trachea. The proximal end of the trachea was tied off, and 0.6 ml of sterile PBS was gently introduced into the lungs and recovered. This was repeated 3 times for a total volume of 1.8 ml. Return volume varied by <10% between samples. BALF was centrifuged to remove cells. Cells obtained were placed on slides for determination of cell populations using a Cytopro Cytocentrifuge (Wescor, Logan, UT) and stained with Diff-Quik (Dade Behring, Newark, DE). Differential counts were made with ≥400 cells/sample from 2 slides/mouse. The BALF was pooled and frozen.

Table 1: Genome scanning to determine C57BL/6 background of the RIG-I$^{-/-}$ mice.

Sample	129S1/SvImJ	C57BL/6J
1	8.84%	91.16%
2	9.52%	90.48%
3	6.46%	93.54%
4	7.19%	92.81%
5	5.10%	94.90%
6	6.42%	93.58%
7	8.50%	91.50%
8	7.82%	92.18%
9	5.44%	94.56%
10	6.51%	93.49%
B6J	0.00%	100.00%
129S	100.00%	0.00%
Heterozygous	50.00%	50.00%

4.6. Multiplex Immunoassay. Cytokine protein levels in the BALF and serum were determined by multiplex immunoassay (Affymetrix, Santa Clara, CA). The assay was run on a Bio-Plex 200 multiplex system (Bio-Rad, Hercules, CA).

4.7. Measurement of mRNA Expression by Quantitative Real-Time PCR (qRT-PCR). Total RNA from lung was extracted using a modified TRIzol (Invitrogen, Carlsbad, CA) protocol and spectrophometrically quantitated. The integrity of RNA was verified by formaldehyde agarose gel electrophoresis. Equal amounts (1 μg) of RNA from each sample were reverse-transcripted into cDNA with oligo (dT) SuperScript II First-Strand Synthesis System for RT-PCR (Invitrogen, Carlsbad, CA). Gene-specific primers for mouse PRRs, cytokines, and the β-actin housekeeping genes were used. The primers' sequences were the same as in our earlier publication [17]. qRT-PCR was performed using 100 ng sample RNA and SYBR Green (Quanta Biosciences, Gaithersburg, MD) in a Bio-Rad CFX96™ Touch Real-Time PCR Detection System. Results were calculated and graphed from the ΔCT of target gene and normalizer, β-actin.

4.8. Isolation of Primary Ear Fibroblast from Mice. Mice were euthanized using isoflurane. The left and right pinna were removed and minced using sterile scissors in growth media (DMEM, 10% FBS, 1x nonessential amino acids [Gibco, Cat. #11140-050], 1x Pen-Strep from Gibco) supplied with collagenase (4 mg/ml; Worthington, Lakewood, NJ) and protease (Dispase II, 4 mg/ml; Roche) to enhance cell extraction. The resultant suspension was cultured overnight in a 37°C incubator. A single-cell suspension of this preparation was obtained by passage through a cell strainer twice to remove remaining debris. Cells were pelleted by centrifugation at 1020 × g for 5 minutes. Cells were pooled from both pinna and resuspended in 5 ml of growth media and brought up to 25 ml with growth media. Cells were plated on a round

150 mm plate and allowed to adhere overnight in a 37°C incubator. Following the overnight incubation, media were replaced and cells were grown to confluence prior to infection with IAV.

4.9. Histological and Immunohistochemical Analysis of Mouse Lung Tissue and Alveolar Epithelial Cells (AEC) II. At day 6 after IAV infection, mice were sacrificed and lungs were fixed in 4% paraformaldehyde in PBS at room temperature for 30 minutes and were then embedded in paraffin. Fixed tissue was hematoxylin and eosin- (H&E-) stained to assess inflammation and fibrosis. Sections (3–5 μm) were mounted on glass slides and immunoprobed with a rabbit anti-mouse polyclonal antibody for RIG-I (Abcam) or an anti-NP polyclonal antibody [29]. AEC II were purified and plated on collagen-coated glass slides and cultured [30]. After 1 day, the cells were infected with IAV PR8 at an MOI of 1 and incubated for an additional 24 h to stimulate RIG-I production. The cells were probed with a rabbit anti-mouse polyclonal antibody for RIG-I (Santa Cruz Biotechnology). Nuclei were stained with DAPI (blue). After washing, the sections were probed with a donkey anti-rabbit secondary antibody conjugated to Alexa Fluor 546 (BD/Molecular Probes). Transmitted light and fluorescent microscopy images were obtained using an Olympus BX51 microscope running cellSens imaging software (Olympus, Center Valley, PA).

4.10. RNA-Seq Analysis. Mouse lung total RNA was collected as described earlier. Library preparation and sequencing were conducted using 3′ inTAG next-generation sequencing by the Clinical Genomics Center Core Facility of the Oklahoma Medical Research Foundation (Oklahoma City, OK). Differential gene expression for day 6 post-IAV infection was determined relative to mock inoculated mice.

All sequencing reads were quality-controlled using FastQC v0.11.2. Illumina adapters were trimmed using Cutadapt v1.9.dev2; replicates were merged and aligned with their reference genome (UCSC mouse genome build mm10) using Subread-align v1.4.6-p4. The BAM files from alignment were processed using featureCounts v1.4.6-p4 to obtain the counts per gene in all samples. Mus_musculus.GRCm38.83.gtf gene definition file was used. The differential expression analysis was performed using edgeR v3.18.1. Genes having counts per million less than 2 in all samples were excluded. Differentially expressed genes were defined using p value <0.01 and FDR-corrected p value <0.1 cutoffs. All bioinformatics analyses were conducted in the R/Bioconductor computing environment v3.4.0.

4.11. Statistical Analysis. Where applicable, for data other than that related to RNA-Seq, the data was expressed as mean ± standard error of the mean (SEM). Statistical significance was determined by one-way ANOVA with Student-Newman-Keuls post hoc correction for multiple comparisons. Significance was considered as $p < 0.05$. For RT-PCR results, the p value was calculated from the ΔΔCt values from different experimental groups.

Data Availability

All RNA-Seq files are available from the GEO database (accession number GSE114232), https://www.ncbi.nlm.nih.gov/geo/query/acc.cgi?acc=GSE114232.

Disclosure

The contents of this publication are solely the responsibility of the authors and do not necessarily represent the official view of NCRR or NIH.

Conflicts of Interest

The authors have no conflicts of interest.

Acknowledgments

The research described in this work was partially supported by a Clinical Innovator Award from the Flight Attendant Medical Research Institute, by the Merit Review Program of the Department of Veterans Affairs, the National Institutes of Health (1 I01 BX001937), and by the National Institutes of Health (U19AI62629 and GM103648 to J.P.M. and R21AI121591, R01HL116876, and GM103648 to L.L.). The OUHSC Rodent Barrier Facility was supported in part (Grant Number C06RR017598) by the National Center for Research Resources (NCRR), a component of the National Institutes of Health (NIH). We want to thank Dr. Shizuo Akira for generating the initial RIG-I$^{-/-}$ mice. We also thank Dr. Michael Gale, Jr., for providing us with the early complex background RIG-I$^{-/-}$ C57BL/6 backcrossed founders. We acknowledge the assistance of the Oklahoma Medical Research Foundation Imaging Analysis and Clinical Genomics Center core facilities.

Supplementary Materials

Figure S1: Gene Ontology (GO) enrichment analysis of RNA-Seq. Only the top 12 enrichment of GO terms from the "biological process" category are listed here. Gene Set Enrichment Analysis was performed on differentially expressed genes ranked by p value using clusterProfiler v.3.4.4. 10^6 permutations were performed to estimate permutation-based enrichment p value. *(Supplementary Materials)*

References

[1] W. W. Thompson, D. K. Shay, E. Weintraub et al., "Mortality associated with influenza and respiratory syncytial virus in the United States," *JAMA*, vol. 289, no. 2, pp. 179–186, 2003.

[2] W. W. Thompson, D. K. Shay, E. Weintraub et al., "Influenza-associated hospitalizations in the United States," *JAMA*, vol. 292, no. 11, pp. 1333–1340, 2004.

[3] H. Kato, S. Sato, M. Yoneyama et al., "Cell type-specific involvement of RIG-I in antiviral response," *Immunity*, vol. 23, no. 1, pp. 19–28, 2005.

[4] T. Kawai and S. Akira, "Toll-like receptors and their crosstalk with other innate receptors in infection and immunity," *Immunity*, vol. 34, no. 5, pp. 637–650, 2011.

[5] L. Guillot, R. le Goffic, S. Bloch et al., "Involvement of Toll-like receptor 3 in the immune response of lung epithelial cells to double-stranded RNA and influenza A virus," *Journal of Biological Chemistry*, vol. 280, no. 7, pp. 5571–5580, 2005.

[6] J. M. Lund, L. Alexopoulou, A. Sato et al., "Recognition of single-stranded RNA viruses by Toll-like receptor 7," *Proceedings of the National Academy of Sciences of the United States of America*, vol. 101, no. 15, pp. 5598–5603, 2004, Epub 2004 Mar 19.

[7] P. G. Thomas, P. Dash, J. R. Aldridge Jr. et al., "The intracellular sensor NLRP3 mediates key innate and healing responses to influenza A virus via the regulation of caspase-1," *Immunity*, vol. 30, no. 4, pp. 566–575, 2009.

[8] I. C. Allen, M. A. Scull, C. B. Moore et al., "The NLRP3 inflammasome mediates in vivo innate immunity to influenza A virus through recognition of viral RNA," *Immunity*, vol. 30, no. 4, pp. 556–565, 2009, Epub 2009 Apr 9.

[9] A. Sabbah, T. H. Chang, R. Harnack et al., "Activation of innate immune antiviral responses by Nod2," *Nature Immunology*, vol. 10, no. 10, pp. 1073–1080, 2009, Epub 2009 Aug 23.

[10] P. Michael, D. Brabant, F. Bleiblo et al., "Influenza A induced cellular signal transduction pathways," *J Thorac Dis*, vol. 5, Supplement 2, pp. S132–S141, 2013.

[11] D. Kobasa, S. M. Jones, K. Shinya et al., "Aberrant innate immune response in lethal infection of macaques with the 1918 influenza virus," *Nature*, vol. 445, no. 7125, pp. 319–323, 2007.

[12] J. C. Kash, T. M. Tumpey, S. C. Proll et al., "Genomic analysis of increased host immune and cell death responses induced by 1918 influenza virus," *Nature*, vol. 443, no. 7111, pp. 578–581, 2006.

[13] C. R. Baskin, H. Bielefeldt-Ohmann, T. M. Tumpey et al., "Early and sustained innate immune response defines pathology and death in nonhuman primates infected by highly pathogenic influenza virus," *Proceedings of the National Academy of Sciences of the United States of America*, vol. 106, no. 9, pp. 3455–3460, 2009.

[14] H. Kumar, T. Kawai, H. Kato et al., "Essential role of IPS-1 in innate immune responses against RNA viruses," *Journal of Experimental Medicine*, vol. 203, no. 7, pp. 1795–1803, 2006.

[15] H. Kato, O. Takeuchi, S. Sato et al., "Differential roles of MDA5 and RIG-I helicases in the recognition of RNA viruses," *Nature*, vol. 441, no. 7089, pp. 101–105, 2006.

[16] M. J. Killip, E. Fodor, and R. E. Randall, "Influenza virus activation of the interferon system," *Virus Research*, vol. 209, pp. 11–22, 2015.

[17] X. Wang, W. Wu, W. Zhang et al., "RIG-I overexpression decreases mortality of cigarette smoke exposed mice during influenza A virus infection," *Respiratory Research*, vol. 18, no. 1, p. 166, 2017.

[18] R. L. Goffic, V. Balloy, M. Lagranderie et al., "Detrimental contribution of the Toll-like receptor (TLR)3 to influenza A virus–induced acute pneumonia," *PLoS Pathogens*, vol. 2, no. 6, article e53, 2006.

[19] F. Coulombe, S. Fiola, S. Akira, Y. Cormier, and J. Gosselin, "Muramyl dipeptide induces NOD2-dependent $Ly6C^{high}$ monocyte recruitment to the lungs and protects against influenza virus infection," *PLoS One*, vol. 7, no. 5, article e36734, 2012.

[20] N. A. Jewell, T. Cline, S. E. Mertz et al., "Lambda interferon is the predominant interferon induced by influenza A virus infection in vivo," *Journal of Virology*, vol. 84, no. 21, pp. 11515–11522, 2010.

[21] M. Weber, H. Sediri, U. Felgenhauer et al., "Influenza virus adaptation PB2-627K modulates nucleocapsid inhibition by the pathogen sensor RIG-I," *Cell Host & Microbe*, vol. 17, no. 3, pp. 309–319, 2015.

[22] Y. Wang, H. X. Zhang, Y. P. Sun et al., "*Rig*-$I^{-/-}$ mice develop colitis associated with downregulation of Gαi2," *Cell Research*, vol. 17, no. 10, pp. 858–868, 2007.

[23] J. S. Errett, M. S. Suthar, A. McMillan, M. S. Diamond, and M. Gale, "The essential, nonredundant roles of RIG-I and MDA5 in detecting and controlling West Nile virus infection," *Journal of Virology*, vol. 87, no. 21, pp. 11416–11425, 2013.

[24] S. Stegemann-Koniszewski, M. Gereke, S. Orrskog et al., "TLR7 contributes to the rapid progression but not to the overall fatal outcome of secondary pneumococcal disease following influenza A virus infection," *Journal of Innate Immunity*, vol. 5, no. 1, pp. 84–96, 2013.

[25] S. Koyama, K. J. Ishii, H. Kumar et al., "Differential role of TLR- and RLR-signaling in the immune responses to influenza A virus infection and vaccination," *The Journal of Immunology*, vol. 179, no. 7, pp. 4711–4720, 2007.

[26] W. Wu, W. Zhang, E. S. Duggan, J. L. Booth, M. H. Zou, and J. P. Metcalf, "RIG-I and TLR3 are both required for maximum interferon induction by influenza virus in human lung alveolar epithelial cells," *Virology*, vol. 482, pp. 181–188, 2015.

[27] S. A. Morosky, J. Zhu, A. Mukherjee, S. N. Sarkar, and C. B. Coyne, "Retinoic acid-induced gene-I (RIG-I) associates with nucleotide-binding oligomerization domain-2 (NOD2) to negatively regulate inflammatory signaling," *Journal of Biological Chemistry*, vol. 286, no. 32, pp. 28574–28583, 2011.

[28] A. A. Benitez, M. Panis, J. Xue et al., "In vivo RNAi screening identifies MDA5 as a significant contributor to the cellular defense against influenza A virus," *Cell Reports*, vol. 11, no. 11, pp. 1714–1726, 2015.

[29] H. Zhang and G. M. Air, "Expression of functional influenza virus A polymerase proteins and template from cloned cDNAS in recombinant vaccinia virus infected cells," *Biochemical and Biophysical Research Communications*, vol. 200, no. 1, pp. 95–101, 1994.

[30] A. Mishra, Y. Guo, L. Zhang et al., "A critical role for $P2X_7$ receptor–induced VCAM-1 shedding and neutrophil infiltration during acute lung injury," *The Journal of Immunology*, vol. 197, no. 7, pp. 2828–2837, 2016.

Hindawi
Mediators of Inflammation
Volume 2018, Article ID 2320640, 11 pages
https://doi.org/10.1155/2018/2320640

Research Article

MicroRNA Expression Profile of Whole Blood Is Altered in Adenovirus-Infected Pneumonia Children

Feng Huang,[1,2] Junsong Zhang,[2] Diyuan Yang,[1] Yuelan Zhang,[3] Jinxiang Huang,[3] Yaochang Yuan,[2] Xuefeng Li,[3] and Gen Lu[1]

[1]*Guangzhou Women and Children's Medical Center, Guangzhou Medical University, Guangzhou, 510120 Guangdong, China*
[2]*Institute of Human Virology, Zhongshan School of Medicine, Sun Yat-sen University, Guangzhou, 510080 Guangdong, China*
[3]*The Second Affiliated Hospital of Guangzhou Medical University, the State Key Laboratory of Respiratory Disease, Guangdong Provincial Key Laboratory of Allergy & Clinical Immunology, The Sixth Affiliated Hospital of Guangzhou Medical University, Qingyuan People's hospital, Sino-French Hoffmann Institute, School of Basic Medical Sciences, Guangzhou Medical University, Guangzhou, 511436 Guangdong, China*

Correspondence should be addressed to Xuefeng Li; xuefengli@gzhmu.edu.cn and Gen Lu; lugen@gzhmu.edu.cn

Received 22 May 2018; Revised 2 August 2018; Accepted 19 August 2018; Published 14 October 2018

Academic Editor: Chetan Meshram

Human adenovirus (Adv) infection is responsible for most community-acquired pneumonia in infants and children, which results in significant morbidity and mortality in children every year. MicroRNAs (miRNAs) are associated with viral replication and host immune response. Knowing the miRNA expression profile will help understand the role of miRNAs in modulating the host response to adenovirus infection and possibly improve the diagnosis of adenovirus-infected pneumonia. In our study, total RNA extracted from whole blood of adenovirus-infected pneumonia children and healthy controls were analyzed by small RNA deep sequencing. Expression profiles of whole blood microRNAs were altered and distinctly different in adenovirus-infected children. The top 3 upregulated miRNA (hsa-miR-127-3p, hsa-miR-493-5p, and hsa-miR-409-3p) were identified in adenovirus-infected children and provided a clear distinction between infected and healthy individuals. Potential host target genes were predicated and validated by qRT-PCR to study the impact of microRNAs on the host genes. Most of the target genes were involved in the MAPK signaling pathway and innate immune response. These highly upregulated microRNAs may have crucial roles in Adv pathogenesis and are potential biomarkers for adenovirus-infected pneumonia.

1. Introduction

Human adenovirus (Adv) infection is responsible for most community-acquired pneumonia in infants and children [1, 2]. Adv causes infections for 5–10% of upper and lower respiratory tract infections in children, which results in pneumonia and nearly 1.3 million deaths of children every year [3, 4]. The fatality rates for untreated severe pneumonia or disseminated disease caused by Adv may even exceed to 50% [5, 6]. There are no efficacious antiviral drugs for Adv treatment until now. Also, the traditional diagnosis of Adv infection is limited. Therefore, to discover the interaction between the virus and its host will help us to find novel treatment and diagnosis for Adv infection.

Human Advs are nonenveloped double-stranded DNA viruses and belong to the Adenoviridae family [7, 8]. Human Advs are divided into seven subgroups including 53 serotypes based on immunologic and biological characteristics. Adv replicates efficiently in human cells and triggers an innate immune response such as inflammatory response in the host cells. Also, viral infection has proved to have a great impact on cellular small RNA expression and gene expression [9–11]. Adv infects the host cells through binding to different cellular receptors such as coxsackievirus and adenovirus receptor (CAR) [12]. During Adv DNA replication, host cellular proteins such as nuclear factor I and POU2F1 are used by Adv [13, 14]. In turn, the host will trigger an innate immune response against Adv infection. However,

the details of Adv and host interaction still remains poorly defined.

Small RNAs are important regulators that modulate development, proliferation, differentiation, and apoptosis of organisms [15, 16]. Small RNAs include microRNA (miRNA), siRNA, tRFs, piRNA, and rasiRNAs, which regulate gene expression in a wide range of processes such as viral replication and host immune response. miRNAs are the most well-studied small RNAs during the latest decades. miRNAs are very important regulators that modulate transcriptome changes [17]. miRNAs regulate gene expression in a wide range of physiological and pathological processes such as in immune response and viral replication [18]. Although miRNAs have been examined in Adv type 3-infected human laryngeal epithelial cells and Adv type 2-infected human lung fibroblast cells [19, 20], there is no research about small RNA profiling in whole blood of Adv-infected pneumonia children. In our study, we sought to present the different miRNA profiles between Adv-infected pneumonia children and healthy controls, identify candidate diagnostic biomarkers for pneumonia with Adv infection in children, and examine the role of miRNAs in host defense response in Adv-infected children.

2. Materials and Methods

2.1. Patients. The whole blood samples used in the study were obtained from Guangzhou Women and Children's Medical Center. Children diagnosed with human Adv pneumonia were included in the study. The diagnosis of human Adv pneumonia was considered certain when it was associated with the following criteria: (1) lower respiratory and/or systemic symptoms, (2) lung infiltration on chest radiography or computed tomography (CT) scan, and (3) positive results for human Adv IgM antibody in sera and/or human Adv DNA by PCR in throat swabs and/or bronchoalveolar lavage (BAL) fluid. A total of 33 samples from patients and 33 samples from healthy volunteers were used in the study. The ages of all patients (male or female) and healthy volunteers (male or female) range from one year to three years. The study was approved by the Ethics Committee at Guangzhou Women and Children's Medical Center (number 2014121815), and written informed consent was obtained from all guardians.

2.2. RNA Extraction and Small RNA Sequencing. The blood samples of the patients and volunteers were collected in anticoagulant tubes. The total RNA was isolated using RiboPure™ Blood RNA Isolation Kit (Ambion, USA) according to the manufacturer's protocol. The extracted small RNAs were treated with DNase before deep sequencing. RNA concentration was determined using a NanoDrop ND1000 system (Thermo Fisher Scientific, South San Francisco, CA), and their integrity was verified using an Agilent 2100 Bioanalyzer (Agilent Technologies, USA). Small RNA deep sequencing was performed as previously described [21]. A total of 3 samples from patients and 3 samples from healthy volunteers were used for small RNA deep sequencing in the study. The clinical characteristics of the 3 patients and 3 healthy volunteers are summarized in Table 1.

2.3. Cell and Virus Culture. Human primary lung fibroblasts (IMR-90) and human 293T cells were grown in Dulbecco's modified Eagle's medium (DMEM) (HyClone) supplemented with 10% fetal bovine serum (Invitrogen), streptomycin, and penicillin (Invitrogen). All virus infections were carried out in serum-free medium for 1 h, followed by addition of saved complete medium.

2.4. Transfection. miRNA inhibitors (GenePharma Co., China) were transfected into IMR-90 cells with Lipofectamine RNAiMAX (Invitrogen) at final concentrations of 100 nM according to the manufacturer's protocol.

2.5. Virus Growth Assay. IMR-90 cells transfected with miRNA inhibitors were infected with HAdV5 (isolated from patients) at an MOI of 10 in serum-free medium. Virus titers were determined 72 h after infection by plaque assays performed on 293T cells [22, 23].

2.6. Quantitative Real-Time PCR (qRT-PCR) Analysis. A qRT-PCR experiment was performed using the Power SYBR Green PCR Master Mix. Each reaction was performed in a 10 μL volume system containing 0.5 μL of cDNA, 0.5 μL of each primer, 5 μL of Power SYBR Green PCR Master Mix, and 3.5 μL of ddH_2O. The reactions were incubated in a 96-well plate at 95°C for 10 minutes, followed by 39 cycles of 95°C for 15 seconds and 62°C for 1 minute. For miRNA quantitation, 10 ng of total RNA was reverse-transcribed using specific stem-loop primers. U6 was used as an endogenous control.

2.7. Data Analysis. miRNA cluster and family information from miRBase (miRBase 20, http://www.mirbase.org/) was used to annotate the cluster of miRNAs. miRNA target genes were predicted based on two software: miRDB software (http://mirdb.org/) and TargetScan software (http://www.targetscan.org/).

2.8. Statistical Analysis. Data were analyzed using GraphPad Prism 6.0 software (La Jolla, CA, USA). The two-tailed Student's t-test was used to determine the significance of statistical data between two experimental groups. Data were considered significant at $^{*}P < 0.05$, $^{**}P < 0.01$, and $^{***}P < 0.001$.

3. Results

3.1. Different Expressions of MicroRNAs in Adv-Infected Children vs. Healthy Children. To study the impact of Adv infection on cellular small RNA expression in pneumonia children, deep sequencing of small RNAs was performed in our study. Accordingly, we found an apparent small RNA peak at 21–24 nt for miRNAs (Figure 1(a)). When we analyzed the differently expressed small RNAs, 118 miRNAs were found differently expressed in Adv-infected children vs. healthy children in a volcano plot (Figure 1(b)). We mapped the clean reads from each group to the known miRNA sequences and identified 908 miRNAs in Adv-infected children versus healthy controls (Figure 1(c)).

Table 1: Clinical features of healthy volunteers and patients.

Volunteer or patient	Age	Gender	Fever duration[a] (days)	Laboratory characteristics[b]					Radiology[e]
				WBC ($\times 10^9$/L) (5–12)	HsCRP (mg/L)(<5)	Specific IgM[c] (IU/mL)	HAdV DNA[d] (throat swabs/BALF)	LDH (U/L) (159–322)	Consolidation
V1	1y9m	male	–	8.6	–	–	–	–	–
V2	2y8m	female	–	9.0	–	–	–	–	–
V3	2y3m	male	–	5.7	–	–	–	–	–
A1	2y1m	male	13	10.2	26.5	+	+/+	919	+
A2	1y9m	female	16	8.3	51.14	+	+/+	812	+
A3	2y8m	female	22	2.8	10.98	+	+/+	948	+

[a]Fever duration from onset to normothermia. [b]Data extracted from the first test for the children on admission. [c]Specific IgM antibodies against HAdV pneumoniae were detected in 2 mL of acute phase (on admission) patient serum using a commercial ELISA kit. [d]HAdV pneumonia DNA was detected by real-time PCR in throat swabs or bronchoalveolar lavage fluid (BALF). [e]Judged by chest radiograph or CT scan in whole course of the patients.

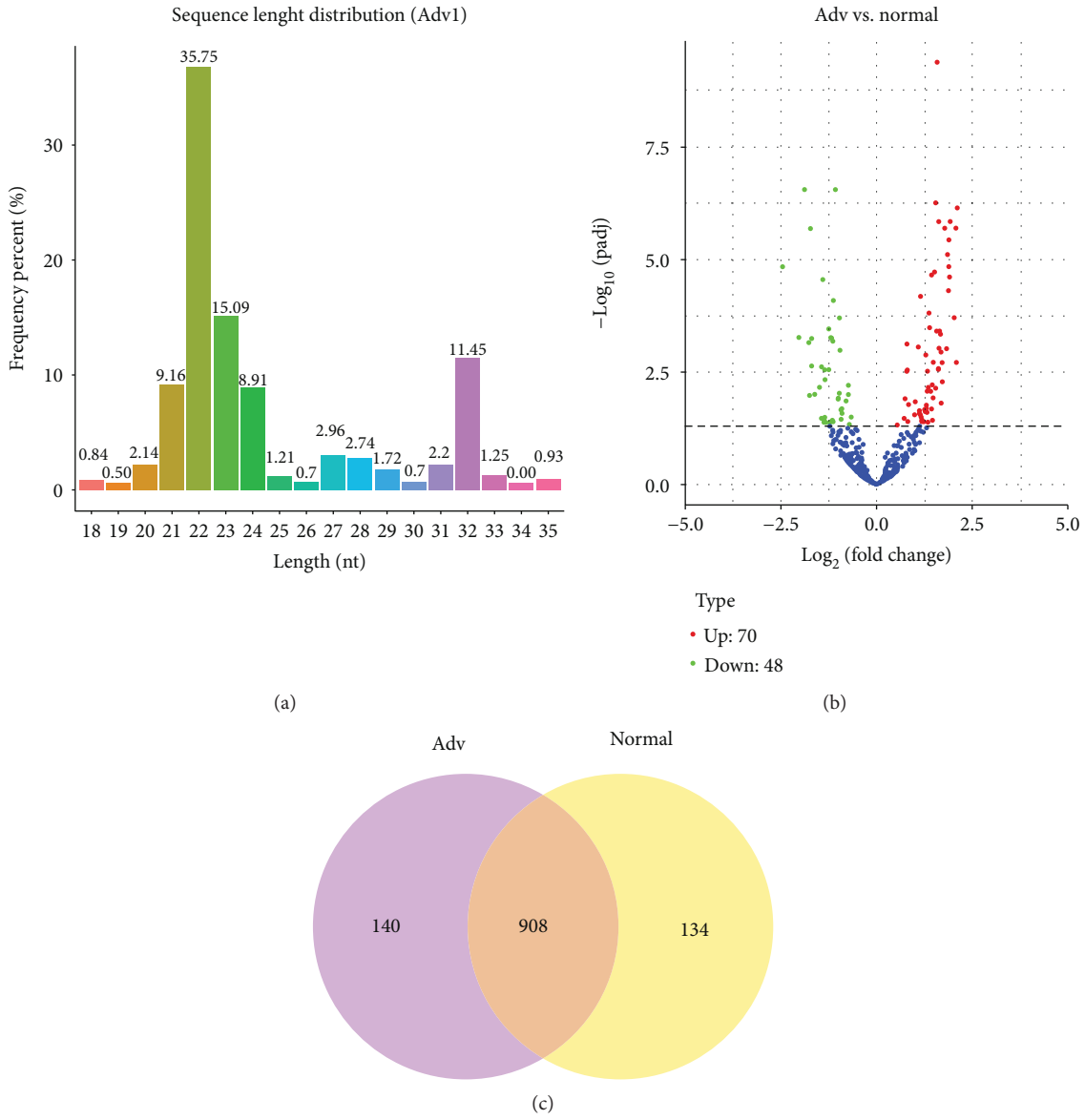

Figure 1: miRNA expression profile of whole blood from adenovirus-infected pneumonia children. (a) Deep sequencing shows the distribution of small RNAs of whole blood from adenovirus-infected pneumonia children. The miRNA peaks appear around 22 nt. (b) Volcano plot of differently expressed miRNAs between Adv-infected children and healthy controls. (c) Venn diagram of differently expressed miRNAs between Adv-infected children and healthy controls.

Furthermore, hierarchical cluster analysis of differentially expressed miRNA is shown in Figure 2. Specially, 77 differentially expressed miRNAs in the 6 samples passed our fold-change filter (log2 fold change > 1.0), among which 20 miRNAs that have high expression (reads up to 1000 in Adv samples) and showed significant different expressions were selected for further analysis (Table 2).

3.2. Validation of Differentially Expressed miRNAs. To confirm the differential expression of miRNAs in Adv patients vs. healthy controls, we performed qRT-PCR assays in our study. The result showed that hsa-miR-127-3p, hsa-miR-379-5p, hsa-miR-493-5p, hsa-miR-409-3p, hsa-miR-99b-5p, hsa-miR-370-3p, and hsa-miR-381-3p were upregulated in whole blood samples from 5 Adv-infected children vs. 5 healthy controls (Figure 3(a)), while hsa-miR-101-3p, hsa-miR-150-5p, hsa-miR-29a-3p, and hsa-miR-342-3p were downregulated in whole blood samples from 5 Adv-infected children vs. 5 healthy controls (Figure 3(a)), which was comparable with our sequencing data. To identify candidate diagnostic miRNA biomarkers, we focused on the upregulated miRNAs. More samples (15 Adv-infected children vs. 15 healthy controls) were collected to verify the expression of the upregulated miRNAs (Figure 3(b)). From the result, we found that hsa-miR-127-3p, hsa-miR-493-5p, and hsa-miR-409-3p were significantly increased. Also, after depleting these miRNAs with miRNA inhibitors, the viral replications were significantly decreased (Figure 3(c)). These findings

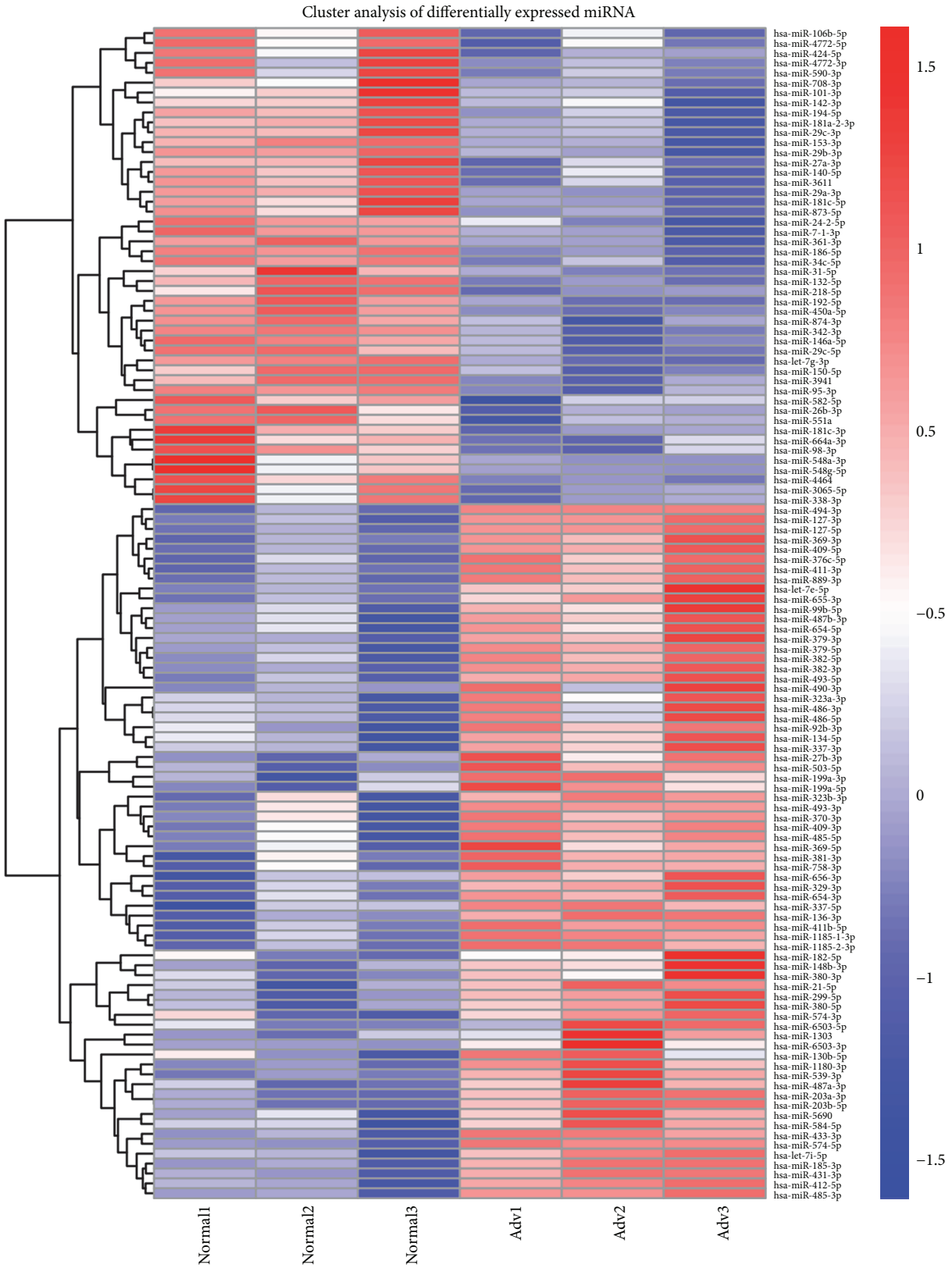

Figure 2: Hierarchical cluster analysis of differentially expressed miRNAs.

Table 2: Top 20 different expressed miRNAs.

miRNA name	Reads in ADV	Reads in control	Log2 fold change	*P* value
has-miR-381-3p	9358	3507	1.17	0.00511
has-miR-486-5p	5480	2240	1.12	0.00434
has-miR-409-3p	4916	1223	1.61	0.00023
has-miR-486-3p	4745	1922	1.12	0.00402
has-miR-127-3p	3950	753	2.10	$6.35E-09$
has-miR-182-5p	2396	870	1.17	0.00762
has-miR-99b-5p	2241	650	1.46	0.00066
has-miR-379-5p	1687	378	1.88	$3.31E-07$
has-miR-370-3p	1682	617	1.18	0.00621
has-let-7e-5p	1239	429	1.33	0.00030
has-miR-493-5p	1089	237	1.87	$1.63E-06$
has-miR-494-3p	1070	342	1.54	$3.94E-09$
has-miR-101-3p	57,893	150,004	−1.12	0.00825
has-miR-142-3p	24,616	77,702	−1.25	0.00841
has-miR-150-5p	15,854	41,850	−1.25	0.00025
has-miR-29a-3p	6679	18,944	−1.40	$9.01E-07$
has-miR-186-5p	6093	13,066	−1.07	$1.49E-09$
has-miR-27a-3p	5558	11,953	−1.00	0.00170
has-miR-342-3p	3373	13,980	−1.87	$1.37E-09$
has-miR-29b-3p	1339	3404	−1.25	$1.60E-05$

imply that our selected miRNAs may reflect the infection of Adv, and such miRNAs can likely serve as biomarker candidates for Adv-infected patients.

3.3. Predict Target Genes of Differentially Expressed miRNAs. To study the biological significance of miRNAs, we then predicted the computational target genes of miRNAs. We focused on the targets of verified miRNAs with distinct expression profiles. Go enrichment of the predicted target genes of the miRNAs showed that the target genes were mainly involved in cellular process and molecular function (Figure 4(a)). In particular, most of the target genes participated in the MAPK signaling pathway and Ras signaling pathway (Figure 4(b)). The top five predicted target genes of hsa-miR-127-3p, hsa-miR-493-5p, or hsa-miR-409-3p are listed in Table 3 by the highest miRNA target score from two miRNA predictive software.

The target genes were selected for further validation with qRT-PCR, and we found that the mRNA expression of 8 genes (PSMB5, ITGA6, MYCBP2, TCF7L2, UBE2V2, HIPK1, UBE2D2, and KANSL1) were downregulated in Adv-infected patients compared to healthy controls (Figure 5). Most of them are transcription factors or factors involved in the ubiquitin pathway. The downregulated mRNAs may indicate the mechanism of Adv infection and Adv-induced pneumonia.

4. Discussion

Human Advs are common causative pathogens of acute respiratory infections in children. The treatment of human Adv infections is limited because prospective, randomized therapeutic trials have not been done. Therefore, it is very important to discover the mechanism of Adv-infected pneumonia and search the biomarkers for Adv-infected pneumonia in children. The regulatory potential of miRNA is well defined, and the different profiles of miRNA expression are the result of diverse diseases including viral infections. In our study, we found that the miRNA profile in whole blood of Adv-infected children was different from that of healthy children. Blood samples of Adv-infected children reflect the associated pathology of Adv infection and thus provide a better understanding of the disease.

Profiling of miRNA expression from Adv-infected blood samples identified a cluster of 118 miRNAs significantly altered. The altered blood miRNA profile was similar to cells infected with Adv reported previously [19, 20], indicating that the different expressed miRNAs identified in our study could be taken as the candidate diagnostic biomarkers for pneumonia with Adv infection in children. Among these different expressed miRNAs, hsa-let-7e-5p was reported to involve in the replication of influenza infection [24]. hsa-miR-127-3p was reported to affect the Epstein-Barr virus-associated lymphoma through targeting the PTEN-AKT-mTOR pathway [25]. Altogether, these miRNAs play important roles in innate immune response or viral replication, thus affecting the outcome of the disease.

Through miRNA target gene GO analysis, we found that most target genes of different expressions of miRNAs were involved in the MAPK signaling pathway. The MAPK signaling pathway is activated by Toll-like receptors [26], which play important roles in innate immune response against viral infection. Also, the activation of the MAPK pathway will result in the activation of the NF-κB signal pathway, which

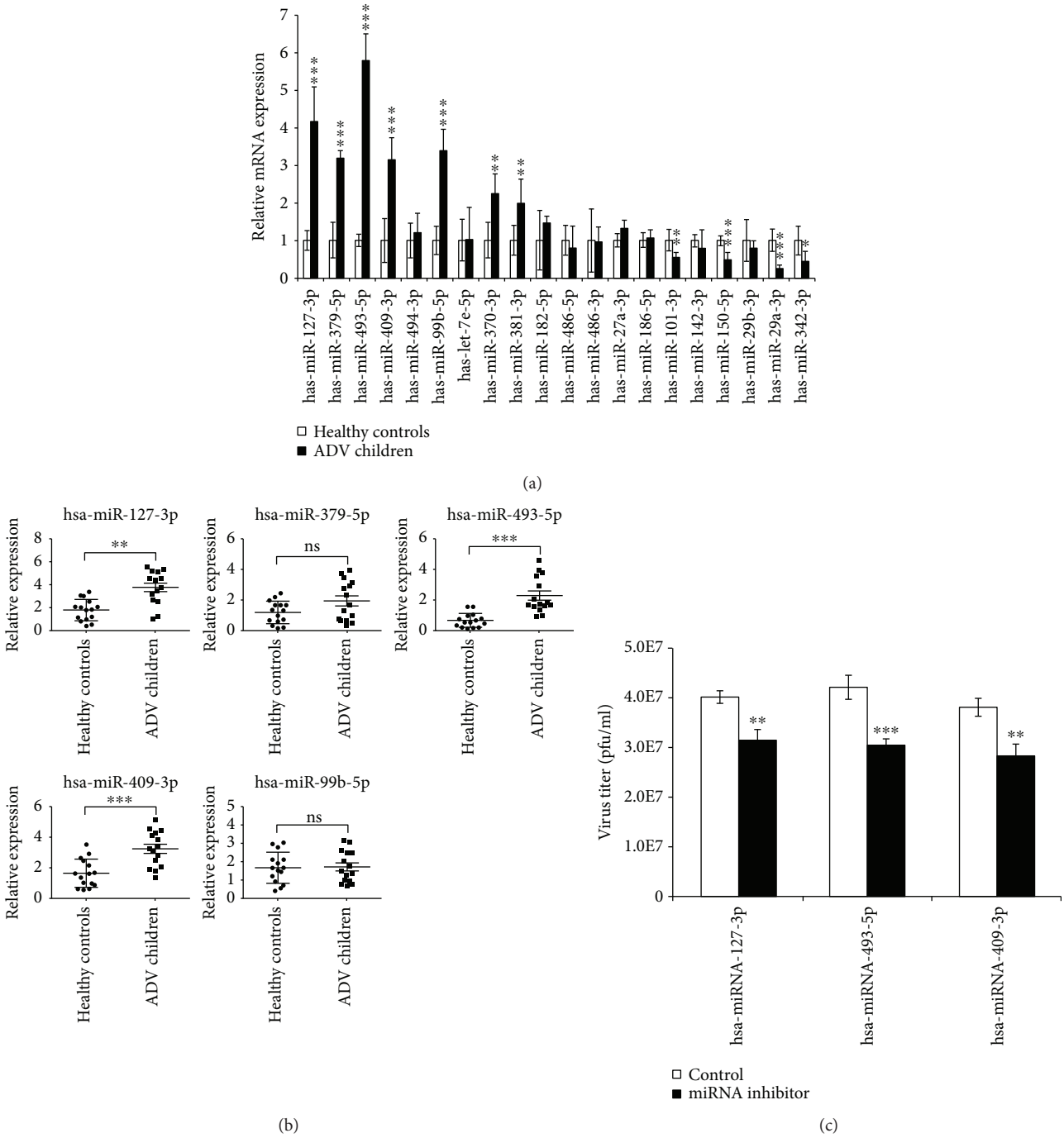

Figure 3: Quantification of miRNA expression levels by qRT-PCR. (a) Quantification of top 20 differently expressed miRNAs, including upregulated and downregulated miRNAs. Five samples from Adv-infected children and 5 from healthy controls were used in the experiment. (b) Quantification of top 5 upregulated miRNAs. 15 samples from Adv-infected children and 15 from healthy controls were used in the experiment. (c) The effect of miRNA inhibitors on the replication of Adv. After transfection with miRNA inhibitors, cells were infected with HAdV5 at an MOI of 10. Virus was harvested, and the titer was determined on 293T cells at the indicated time points. Data are shown as means ± SD from three independent experiments. $^{**}P < 0.01$ and $^{***}P < 0.001$ (Student t test).

will stimulate the production of inflammatory cytokines and MMPs [27] and finally lead to pneumonia. Thus, the altered miRNA expression profile of whole blood from Adv-infected children partly reflected the mechanism of Adv-infected pneumonia.

With a developmental framework or disease process, miRNAs exhibit dynamic expression patterns. In our study, we characterized the miRNA expression profile of Adv-infected children using deep sequencing analysis and identified that many miRNAs were differently expressed in

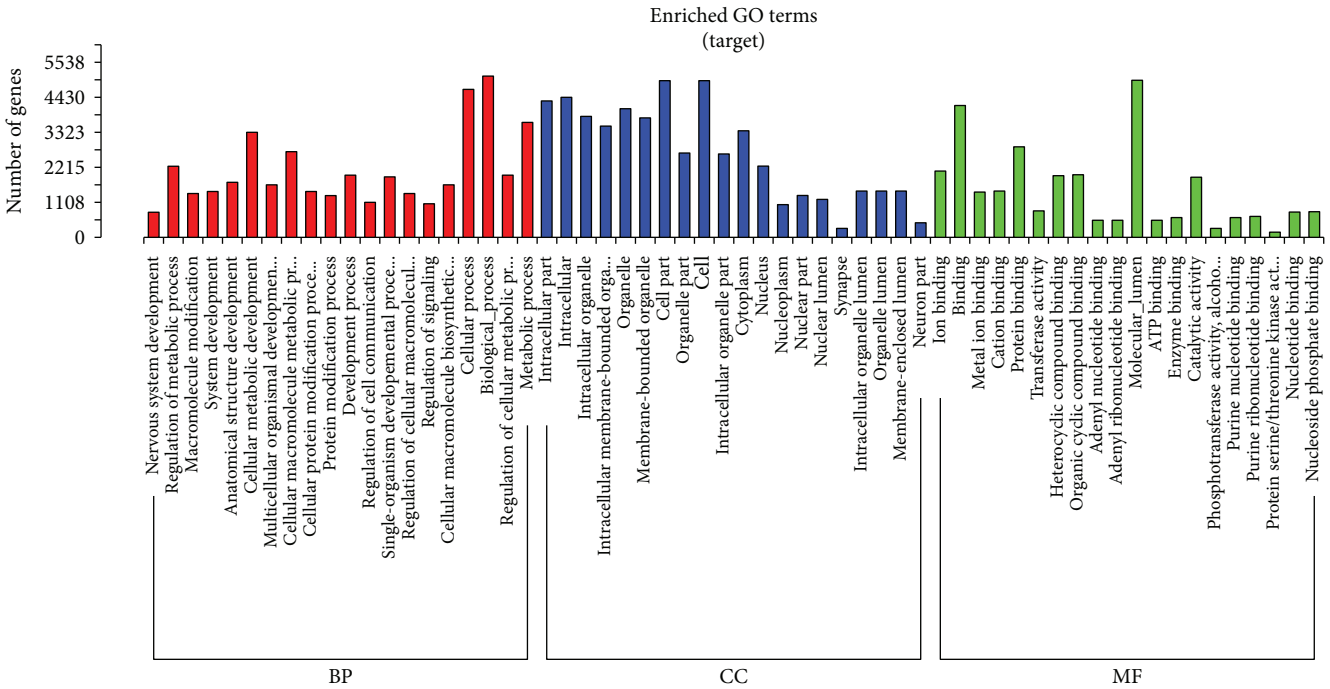

(a)

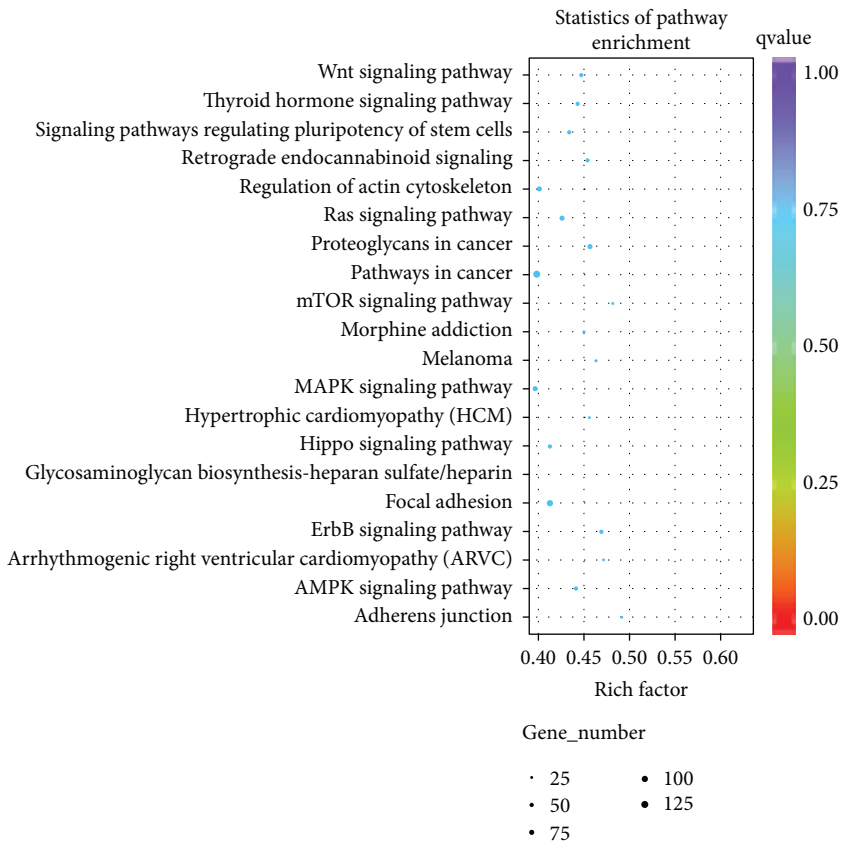

(b)

Figure 4: Go enrichment of predicted target genes. (a) The GO classification enrichment of target genes. (b) The KEGG pathway scatterplot of target genes.

Table 3: Top 5 predicted target genes.

miRNAs	Target	Gene description
hsa-miR-127-3p	PSMB5	Proteasome (prosome, macropain) subunit, beta type 5
	KIF3B	Kinesin family member 3B
	ITGA6	Integrin, alpha 6
	BCAS3	Breast carcinoma-amplified sequence 3
	MTSS1L	Metastasis suppressor 1-like
hsa-miR-493-5p	SP3	Sp3 transcription factor
	MYCBP2	MYC-binding protein 2, E3 ubiquitin protein ligase
	TCF7L2	Transcription factor 7-like 2 (T-cell specific, HMG box)
	UBE2V2	Ubiquitin-conjugating enzyme E2 variant 2
	HIPK1	Homeodomain-interacting protein kinase 1
hsa-miR-409-3p	RAB10	RAB10, member RAS oncogene family
	UBE2D2	Ubiquitin-conjugating enzyme E2D 2
	KANSL1	KAT8 regulatory NSL complex subunit 1
	MTF2	Metal response element binding transcription factor 2
	ELF2	E74-like factor 2 (ETS domain transcription factor)

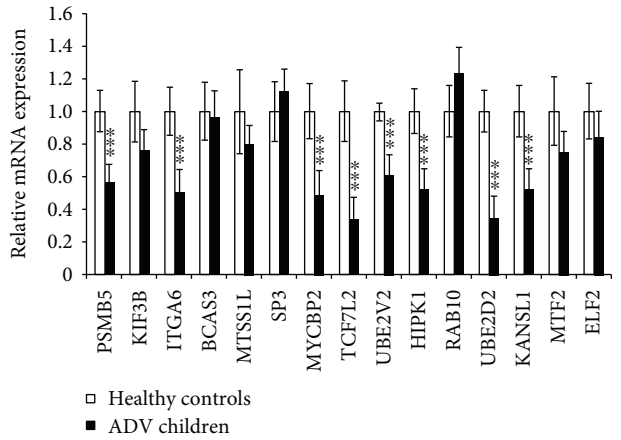

Figure 5: Validation of the expression of top 5 predicated target genes by qRT-PCR. Relative mRNA expression between 10 samples from Adv-infected children and 10 samples from healthy controls. Data are shown as means ± SD from three independent experiments. $^{***}P < 0.001$ (Student t test).

Adv-infected children when compared with healthy children. Those with the greatest differences were chosen for further verification. In particular, the expressions of hsa-miR-127-3p, hsa-miR-493-5p, and hsa-miR-409-3p from 20 Adv-infected children were significantly higher than those from 20 healthy controls, indicating that these miRNAs could be taken as good diagnostic biomarkers for Adv-infected pneumonia.

To further explore the possible molecular mechanisms of the differently expressed miRNAs in Adv-infected children, we predicted the possible target genes of hsa-miR-127-3p, hsa-miR-493-5p, and hsa-miR-409-3p and found that most of them are transcription factors or factors involved in the ubiquitin pathway. Especially, after verifying the predicted target genes with qRT-PCR, 8 genes (PSMB5, ITGA6, MYCBP2, TCF7L2, UBE2V2, HIPK1, UBE2D2, and KANSL1) were found significantly downregulated in samples from Adv-infected children. In particular, MYCBP2 is an E3 ubiquitin protein ligase [28, 29], which regulated the cAMP and mTOR signaling pathway. The mTOR signaling pathway plays a critical role in effector T cell function, the downregulation of which will result in impaired cell cytolysis and incapability of virus elimination. UBE2V2 is an ubiquitin-conjugating enzyme and is involved in the differentiation of monocytes, which can produce proinflammatory cytokines like MIP-1β [30, 31]. Thus, the downregulated UBE2V2 will result in abnormal differentiation of monocytes and more proinflammatory will be produced, which in turn aggravates pneumonia. UBE2D2 is essential for the activation of MAVS and RIG-I in response to viral infection [32–34]. The downregulation of UBE2D2 will result in abnormal activation of MAVS and RIG-I signal and virus clearance. These findings imply that the miRNA expression profile changed in Adv-infected children resulting in different transcriptome profiles, which reflects the mechanism of Adv replication and the formation Adv-infected pneumonia.

5. Conclusions

In summary, we identified the 3 most markedly differently expressed miRNAs in whole blood from Adv-infected children, which can be taken as biomarkers for Adv-infected pneumonia. Simultaneously, based on target gene prediction and qRT-PCR analysis, we found that genes MYCBP2, UBE2V2, and UBE2D2 may play important roles in viral replication and Adv-induced pneumonia. However, additional studies are necessary to clarify their roles in these processes, which will provide a physiological basis for the treatment of Adv-infected pneumonia.

Data Availability

The data used to support the findings of this study are included within the article.

Conflicts of Interest

The authors declare no conflict of interest.

Authors' Contributions

Feng Huang and Junsong Zhang contributed equally to this work.

Acknowledgments

This study was supported by the National Natural Science Foundation of China (81701990, 81702327, and 81601759), the National Science and Technology Major Project (2018ZX10101004003001), and the General Projects of Guangzhou Scientific Research (201707010183).

References

[1] C. M. Nascimento-Carvalho, "Etiology of childhood community acquired pneumonia and its implications for vaccination," *The Brazilian Journal of Infectious Diseases*, vol. 5, no. 2, pp. 87–97, 2001.

[2] S. J. Kim, K. Kim, S. B. Park, D. J. Hong, and B. W. Jhun, "Outcomes of early administration of cidofovir in non-immunocompromised patients with severe adenovirus pneumonia," *PLoS One*, vol. 10, no. 4, article e0122642, 2015.

[3] Z. A. Bhutta, J. K. Das, N. Walker et al., "Interventions to address deaths from childhood pneumonia and diarrhoea equitably: what works and at what cost?," *The Lancet*, vol. 381, no. 9875, pp. 1417–1429, 2013.

[4] A. Agweyu, M. Kibore, L. Digolo et al., "Prevalence and correlates of treatment failure among Kenyan children hospitalised with severe community-acquired pneumonia: a prospective study of the clinical effectiveness of WHO pneumonia case management guidelines," *Tropical Medicine & International Health*, vol. 19, no. 11, pp. 1310–1320, 2014.

[5] J. P. Lynch III and A. E. Kajon, "Adenovirus: epidemiology, global spread of novel serotypes, and advances in treatment and prevention," *Seminars in Respiratory and Critical Care Medicine*, vol. 37, no. 4, pp. 586–602, 2016.

[6] U. Sandkovsky, L. Vargas, and D. F. Florescu, "Adenovirus: current epidemiology and emerging approaches to prevention and treatment," *Current Infectious Disease Reports*, vol. 16, no. 8, p. 416, 2014.

[7] M. G. Ison and R. T. Hayden, "Adenovirus," *Microbiology Spectrum*, vol. 4, 2016.

[8] J. P. Lynch, M. Fishbein, and M. Echavarria, "Adenovirus," *Seminars in Respiratory and Critical Care Medicine*, vol. 32, no. 4, pp. 494–511, 2011.

[9] K. L. Wu, X. Zhang, J. Zhang et al., "Inhibition of hepatitis B virus gene expression by single and dual small interfering RNA treatment," *Virus Research*, vol. 112, no. 1-2, pp. 100–107, 2005.

[10] J. Yuan, P. K. M. Cheung, H. M. Zhang, D. Chau, and D. Yang, "Inhibition of coxsackievirus B3 replication by small interfering RNAs requires perfect sequence match in the central region of the viral positive strand," *Journal of Virology*, vol. 79, no. 4, pp. 2151–2159, 2005.

[11] J. Huang, F. Wang, E. Argyris et al., "Cellular microRNAs contribute to HIV-1 latency in resting primary $CD4^+$ T lymphocytes," *Nature Medicine*, vol. 13, no. 10, pp. 1241–1247, 2007.

[12] N. Arnberg, "Adenovirus receptors: implications for targeting of viral vectors," *Trends in Pharmacological Sciences*, vol. 33, no. 8, pp. 442–448, 2012.

[13] Z. C. Hartman, E. P. Black, and A. Amalfitano, "Adenoviral infection induces a multi-faceted innate cellular immune response that is mediated by the toll-like receptor pathway in A549 cells," *Virology*, vol. 358, no. 2, pp. 357–372, 2007.

[14] J. S. Yoon, H. H. Kim, Y. Lee, and J. S. Lee, "Cytokine induction by respiratory syncytial virus and adenovirus in bronchial epithelial cells," *Pediatric Pulmonology*, vol. 42, no. 3, pp. 277–282, 2007.

[15] A. Heintz-Buschart, D. Yusuf, A. Kaysen et al., "Small RNA profiling of low biomass samples: identification and removal of contaminants," *BMC Biology*, vol. 16, no. 1, p. 52, 2018.

[16] W. Ahmed and M. Razzaq, "RETRACTED: A small non-coding RNA AbcR2 regulate gntR transcription factor that modulate the intracellular survival of *Brucella melitensis*," *Microbial Pathogenesis*, vol. 118, pp. 118–125, 2018.

[17] D. P. Bartel, "MicroRNAs: genomics, biogenesis, mechanism, and function," *Cell*, vol. 116, no. 2, pp. 281–297, 2004.

[18] D. Piedade and J. M. Azevedo-Pereira, "MicroRNAs as important players in host-adenovirus interactions," *Frontiers in Microbiology*, vol. 8, article 1324, 2017.

[19] Y. Qi, J. Tu, L. Cui et al., "High-throughput sequencing of microRNAs in adenovirus type 3 infected human laryngeal epithelial cells," *Journal of Biomedicine & Biotechnology*, vol. 2010, Article ID 915980, 8 pages, 2010.

[20] H. Zhao, M. Chen, C. Tellgren-Roth, and U. Pettersson, "Fluctuating expression of microRNAs in adenovirus infected cells," *Virology*, vol. 478, pp. 99–111, 2015.

[21] F. Zhong, N. Zhou, K. Wu et al., "A SnoRNA-derived piRNA interacts with human interleukin-4 pre-mRNA and induces its decay in nuclear exosomes," *Nucleic Acids Research*, vol. 43, no. 21, pp. 10474–10491, 2015.

[22] J. R. Frost, M. Mendez, A. M. Soriano et al., "Adenovirus 5 E1A-mediated suppression of p 53 via FUBP1," *Journal of Virology*, vol. 92, no. 14, 2018.

[23] J. Zhang, F. Huang, L. Tan et al., "Host protein Moloney leukemia virus 10 (MOV10) acts as a restriction factor of influenza a virus by inhibiting the nuclear import of the viral nucleoprotein," *Journal of Virology*, vol. 90, no. 8, pp. 3966–3980, 2016.

[24] P. A. Tambyah, S. Sepramaniam, J. Mohamed Ali et al., "MicroRNAs in circulation are altered in response to influenza a virus infection in humans," *PLoS One*, vol. 8, no. 10, article e76811, 2013.

[25] A. Onnis, M. Navari, G. Antonicelli et al., "Epstein-Barr nuclear antigen 1 induces expression of the cellular microRNA hsa-miR-127 and impairing B-cell differentiation in EBV-infected memory B cells. New insights into the pathogenesis of Burkitt lymphoma," *Blood Cancer Journal*, vol. 2, no. 8, p. e84, 2012.

[26] Q.-W. Wang, Y. Su, J.-T. Sheng et al., "Anti-influenza A virus activity of rhein through regulating oxidative stress, TLR4,

Akt, MAPK, and NF-κB signal pathways," *PLoS One*, vol. 13, no. 1, article e0191793, 2018.

[27] W. Kang, L. Shang, T. Wang, H. Liu, and S. Ge, "Rho-kinase inhibitor Y-27632 downregulates LPS-induced IL-6 and IL-8 production via blocking p38 MAPK and NF-κB pathways in human gingival fibroblasts," *Journal of Periodontology*, vol. 89, no. 7, pp. 883–893, 2018.

[28] G. James, B. Key, and A. Beverdam, "The E3 ubiquitin ligase Mycbp 2 genetically interacts with Robo 2 to modulate axon guidance in the mouse olfactory system," *Brain Structure & Function*, vol. 219, no. 3, pp. 861–874, 2014.

[29] S. Holland and K. Scholich, "Regulation of neuronal functions by the E3-ubiquitinligase protein associated with MYC (MYCBP2)," *Communicative & Integrative Biology*, vol. 4, no. 5, pp. 513–515, 2014.

[30] Y. Zhao, M. J. C. Long, Y. Wang, S. Zhang, and Y. Aye, "Ube2V2 is a Rosetta stone bridging redox and ubiquitin codes, coordinating DNA damage responses," *ACS Central Science*, vol. 4, no. 2, pp. 246–259, 2018.

[31] L. J. Simpson and J. E. Sale, "UBE2V2 (MMS2) is not required for effective immunoglobulin gene conversion or DNA damage tolerance in DT40," *DNA Repair (Amst)*, vol. 4, no. 4, pp. 503–510, 2005.

[32] C. Polge, N. Koulmann, A. Claustre et al., "UBE2D2 is not involved in MuRF1-dependent muscle wasting during hindlimb suspension," *The International Journal of Biochemistry & Cell Biology*, vol. 79, pp. 488–493, 2016.

[33] S. Geisler, S. Vollmer, S. Golombek, and P. J. Kahle, "The ubiquitin-conjugating enzymes UBE2N, UBE2L3 and UBE2D2/3 are essential for Parkin-dependent mitophagy," *Journal of Cell Science*, vol. 127, no. 15, pp. 3280–3293, 2014.

[34] M.-H. Chiang, L.-F. Chen, and H. Chen, "Ubiquitin-conjugating enzyme UBE2D2 is responsible for FBXW2 (F-box and WD repeat domain containing 2)-mediated human GCM1 (glial cell missing homolog 1) ubiquitination and degradation," *Biology of Reproduction*, vol. 79, no. 5, pp. 914–920, 2008.